From materials to management: The expanding role of design of experiments in advanced battery technologies

Energy Storage Materials 85 (2026) 104890

Contents lists available at ScienceDirect

Energy Storage Materials

journal homepage: www.elsevier.com/locate/ensm

From materials to management: The expanding role of design of experiments in advanced battery technologies

Diego Pugliese [a,*], Roberto Staffieri [b], Federico Bella [b,*]

[a] National Institute of Metrological Research (INRiM), Strada delle Cacce 91, Turin, 10135, Italy
[b] Department of Applied Science and Technology, Politecnico di Torino, Turin, 10129, Italy

ARTICLE INFO

Keywords:
Design of experiments
Battery optimization
Electrochemical energy storage
Battery performance and aging
Recycling and circular economy
Thermal management and safety

ABSTRACT

The transition toward sustainable and high-performance batteries requires not only advances in materials and architectures, but also the adoption of systematic approaches to experimental design. This review highlights the role of design of experiments (DoE) as a versatile and powerful methodology to accelerate innovation in the battery field. By replacing trial-and-error strategies with statistically sound frameworks, DoE enables the exploration of multiple variables and their interactions, offering deeper insights into complex phenomena that govern synthesis, performance, safety, recycling, and lifetime of batteries. Applications reviewed span from the optimization of electrode formulations and cathode synthesis to advanced thermal management strategies and recycling processes of end-of-life batteries. Across these domains, DoE has proven to reduce experimental redundancy, enhance reproducibility, and guide the identification of optimal operating conditions. The review also illustrates how DoE can act as a bridge between laboratory-scale research and industrial scalability, providing tools that are essential for the development of next-generation energy storage technologies. By presenting a comprehensive overview of its impact, this article aims to inspire researchers to embrace DoE as a cornerstone for systematic innovation, fostering both scientific progress and sustainable deployment of electrochemical energy storage.

List of abbreviations

AC	Alternating current
AM	Active material
ANN	Artificial neural network
ANOVA	Analysis of variance
BBD	Box-Behnken design
BMS	Battery management system
BoL	Beginning of life
BTMS	Battery thermal management system
CA	Conductive additive
CB	Carbon black
CCCV	Constant current constant voltage
CCD	Central composite design
CD	Charge depleting
CFD	Computational fluid dynamics
CNC	Carbon nano-coat
COOL	CO_2 leaching
CR	Charging rate
CS	Charge sustaining
DC	Direct current
DoD	Depth of discharge
DoE	Design of experiments
ECM	Equivalent circuit model
EIS	Electrochemical impedance spectroscopy
EKF	Extended Kalman filter
EM	Electrochemical model
EoL	End-of-life
ESS	Energy storage system
EV	Electric vehicle
FFD	Full factorial design
FIM	Fisher information matrix
FLAB	Flooded lead acid battery
HESS	Hybrid energy storage system
HPD	Hydrogen peroxide dosage
KF	Kalman filter
LFP	Lithium iron phosphate
LIB	Lithium-ion battery
LiPB	Lithium polymer battery
LLM	Local linear model
LOF	Lack-of-fit

(continued on next column)

(continued)

(continued on next page)

* Corresponding authors.
E-mail addresses: d.pugliese@inrim.it (D. Pugliese), federico.bella@polito.it (F. Bella).

https://doi.org/10.1016/j.ensm.2026.104890
Received 31 October 2025; Received in revised form 7 January 2026; Accepted 8 January 2026
Available online 9 January 2026

(*continued*)

L/S	Liquid-to-solid ratio
ML	Machine learning
NCA	Nickel cobalt aluminum
NMC	Nickel manganese cobalt
NT	Nanotube
OA	Orthogonal array
OCV	Open circuit voltage
OFAT	One-factor-at-a-time
PB	Plackett-Burman
PCM	Phase change material
PD	Pulp density
PDCS	Power distribution control strategy
PHEV	Plug-in hybrid electric vehicle
PQRSM	Progressive quadratic response surface method
PVDF	Poly(vinylidene difluoride)
RFB	Redox flow battery
RMS	Root mean square
RMSE	Root mean square error
RSM	Response surface methodology
RTE	Round-trip efficiency
SEI	Solid electrolyte interphase
SIB	Sodium-ion battery
SLIB	Spent lithium-ion battery
S/N	Signal-to-noise ratio
SoC	State of charge
SoH	State of health
SSB	Solid-state battery
TM	Taguchi method
TR	Temperature raise
UC	Ultracapacitor

1. Introduction

Energy storage technologies are at the heart of the ongoing transition toward a sustainable, electrified, and digital society. Batteries today underpin applications ranging from portable electronics to electric vehicles (EVs), stationary energy storage systems (ESSs) and smart grids, playing a central role in decarbonization and energy transition [1–3]. Alongside performance, the sustainability and reliability of their life cycle has become a strategic priority, spanning materials design, operando safety, recycling, and second-life applications [4–6]. The push for higher energy density, faster charging, improved durability, and enhanced safety is not limited to lithium-ion batteries (LIBs), but also extends to post-lithium technologies (*e.g.*, sodium- [7–13], potassium- [14], and multivalent-ion batteries like zinc ones [15–24]). Despite their diversity, all these technologies share the need for systematic and efficient experimental strategies supporting optimization and performance assessment [25,26]. In this complex landscape, where chemistry, physics, and engineering converge, rigorous and statistically grounded experimental planning emerges as a key enabler for accelerating innovation, reducing uncertainty, and ensuring reproducibility across laboratories and scales.

The performance of LIBs depends on energy storage, power output, capacity retention, cycle life, and charging speed, which are governed by interconnected chemical, physical, and manufacturing parameters. These parameters arise from a multiscale interplay among components (anode, cathode, electrolyte, separator, binder) and processing conditions, highlighting the need for tools that capture interactions rather than single-factor effects [27–36]. Historically, understanding such relationships has relied on trial-and-error or one-factor-at-a-time (OFAT) strategies, which are not only time- and resource-intensive, but also statistically inefficient and unable to resolve interactions or nonlinearities. Coupling experiments with modeling has improved predictive capability, but the demand for efficiency and robustness has grown exponentially. In this context, statistical design of experiments (DoE) represents a powerful and systematic methodology to extract reliable information from a limited testing, supporting not only parameter screening, but also model building, optimization, and uncertainty quantification.

DoE revolves around the identification of independent variables (factors) and dependent variables (responses), exploring their interactions to establish empirical models of the studied system [37–39]. Common factorial designs, such as 2^k (for screening) and 3^k (to capture quadratic relationships), provide the foundation, while response surface methodology (RSM) enables intuitive visualization of factor/response relationships via 3D and contour plots [40,41]. More sophisticated approaches include Taguchi designs, which account for uncontrollable noise factors through the signal-to-noise ratio (S/N), and simplex centroid designs, where experimental points are distributed across vertices and centroids of the design space. Optimal designs become essential when resources are limited or when constraints dictate unique experimental conditions. Statistical validation – through residual analysis, analysis of variance (ANOVA), lack-of-fit (LOF) tests, and independent confirmation runs – is crucial to avoid overfitting and ensure model robustness, a point particularly emphasized in modern DoE practice. A scheme of the DoE methodology is represented in Fig. 1. The methodology is now consolidated across numerous fields, including photovoltaics [42–51], membranes-based technologies [52–61], electrochromic devices [62–71], materials engineering [72–81], etc.

In the field of LIBs and beyond, DoE has demonstrated its value in multiple directions [83]: from the synthesis of electrode materials – where the ratio of active material (AM), conductive additive (CA), and binder (B) critically defines energy and power density – to the optimization of cell manufacturing, where electrode coating, drying, and calendering conditions dictate quality and reproducibility. Further applications include electrolyte formulation, separator design, and the optimization of thermal management strategies, where DoE helps to identify the most relevant parameters controlling temperature rise (TR) and coolant efficiency. In operational terms, DoE has also been successfully applied to identify optimal charging protocols, such as pulse charging and multi-stage constant current, enabling shorter charging times, enhanced cycle life, and suppression of dendrite growth.

Crucially, the strength of DoE lies in its versatility and transferability across scales and technologies. At the material discovery stage, DoE has been employed to accelerate the exploration of novel electrode chemistries, such as high-nickel cathodes or silicon-based anodes, where multiple compositional and processing parameters must be optimized simultaneously. In industrial manufacturing, DoE supports process robustness by quantifying variability and identifying sensitive factors in slurry rheology, coating uniformity, drying rates, and calendering pressures. At the system level, DoE contributes to thermal management and safety by guiding the design of battery packs with optimized coolant flow rates, reduced temperature gradients, and minimized risks of thermal runaway. This multiscale applicability underscores the need for a unified statistical framework capable of informing decisions across the entire battery value chain, not merely optimizing individual unit operations.

Moreover, DoE has proven to be a transversal methodology beyond LIBs, with expanding relevance for next-generation chemistries. In sodium-ion batteries (SIBs), DoE has been used to tune electrolyte formulations for improved cycling stability. In solid-state batteries (SSBs) [84–93], it enables the identification of processing windows for ceramic electrolytes and polymer-ceramic composites [94–103], where sintering temperature, pressure, and dopant levels critically affect ionic conductivity. Even in hydrogen storage systems and fuel cells [104], DoE has guided the optimization of catalysts, membranes, and operating conditions, ensuring efficient performance under real-world constraints. This breadth of applications highlights the role of DoE not merely as a statistical tool, but as a methodological bridge between laboratory exploration and industrial implementation. By reducing experimental redundancy, quantifying uncertainty, and enabling structured comparison across studies, DoE supports reproducible and accelerated innovation.

Perhaps most importantly, DoE provides a systematic framework to

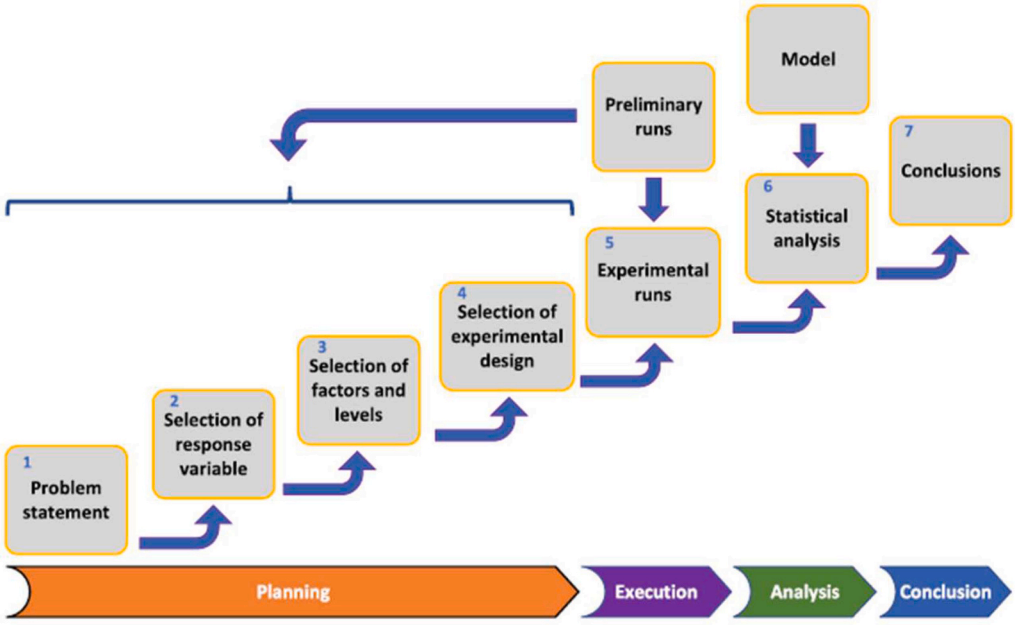

Fig. 1. DoE methodology. The process typically involves: i) Problem definition and goal setting: the problem and objectives of the experiment are clearly defined, and the relevant responses, factors, and their appropriate settings based on these objectives are chosen; ii) Experimental design selection: an appropriate experimental setup, which includes the number of factors, levels, repetitions, blocks, randomization, and the creation of a practical model, is selected; iii) Conducting experiments: experiments are carried out according to the chosen design. In some cases, especially in preliminary stages or screening, conducting a few initial experiments may help to determine suitable factor ranges; iv) Data analysis: statistical methods, such as ANOVA, and graphical tools to process the collected data are utilized; v) Objective conclusions: the results of the statistical analysis provide the basis for forming objective conclusions. Adapted and reprinted with permission from [82].

accelerate the discovery, development, and deployment pipeline in battery research. By rigorously identifying significant trends, interactions, and optimal operating windows, DoE supports the rational design of experiments in areas as diverse as recycling, aging studies, materials synthesis, thermal management, and safety engineering. In this review, the rapidly growing DoE literature is classified into four main domains – materials and synthesis, performance and aging, safety and thermal management, and recycling – and methodological practices, highlighting both opportunities and limitations of the current approaches, are critically evaluated.

2. A methodological framework for DoE in battery research

DoE plays a growing and increasingly strategic role in battery science and engineering, yet its adoption across the literature remains heterogeneous in both methodological rigor and reporting clarity. While many studies successfully employ DoE to accelerate materials optimization, manufacturing process tuning, and performance evaluation, a critical cross-analysis reveals recurring patterns, strengths, and limitations. This section provides a unified framework that contextualizes the diverse DoE strategies observed in battery research, outlining key methodological principles that will serve as a reference for the application-specific sections that follow.

DoE strategies applied in battery studies can be broadly categorized into five families, as detailed in Table 1.

A critical analysis of the existing DoE literature in battery research reveals that the quality of empirical models – and ultimately the reliability of the conclusions drawn from them – depends strongly on three interconnected elements: appropriate model selection, rigorous validation, and assessment of the practical robustness of the identified optima. Although these aspects are central to the DoE philosophy, they are implemented unevenly across studies, often limiting the predictive strength and transferability of published results.

One recurrent challenge is the alignment between design size and model complexity. Several studies employ quadratic response surface models even when the number of experimental runs provides limited

Table 1
DoE strategies applied in battery studies.

DoE family	Typical goal	Number of factors	Model capability	Typical battery applications	Strengths	Limitations
Screening designs (FFD, fractional, PB)	Identify dominant factors	High (≥6)	Linear + interactions (limited)	Electrolyte screening, recycling pre-treatment, aging factor ranking	Minimal experiments, fast insight	No curvature, no optimization
Response surface designs (CCD, BBD, 3^k)	Optimization & modeling	Medium (2–5)	Quadratic	Slurry formulation, calendering, leaching kinetics, thermal management	Predictive surfaces, interpretable optima	Higher experimental cost
Mixture designs	Composition optimization	Medium-high	Polynomial constrained	Electrolytes, AM-binder-CA ratios, solid-state composites	Handles compositional constraints	Not suitable for process variables
Taguchi / robust designs	Noise-insensitive optimization	Medium	Main effects (limited interactions)	Charging protocols, thermal robustness, degradation mitigation	Simple, robust to variability	Interaction oversimplification
Optimal designs (D-, I-optimal)	Parameter identifiability	Variable	Model-dependent	Aging models, ECM/EM identification, EIS-based models	Max info per experiment	Less intuitive, model-dependent

statistical power, creating an unfavorable ratio between parameters and degrees of freedom. This issue becomes particularly acute in systems characterized by strong nonlinearities – such as slurry rheology, solid-state electrolyte sintering, hydrometallurgical leaching, or multi-stress aging protocols – where curvature is expected, but the experimental design does not always include enough information to resolve it. When center points or replicated runs are absent, curvature detection becomes impossible, and the fitted model risks capturing noise rather than genuine trends. Conversely, some studies adopt screening models (*e.g.*, first-order factorials) even when the targeted responses exhibit well-known nonlinear behaviors. These mismatches highlight a general need for hierarchical model-building strategies, in which linear, interaction, and quadratic terms are added only when justified by data and supported by adequate experimental resolution.

Closely tied to model formulation is the issue of validation, which remains the most heterogeneous component across the battery DoE literature. Many studies rely predominantly on global goodness-of-fit metrics such as R^2, which, although informative, are insufficient to judge the adequacy of a multi-parameter regression. More robust approaches – including ANOVA decomposition, residual diagnostics, LOF tests, and significance evaluation of individual model terms – are reported only in a fraction of publications. Replicate points, especially at the design center, are essential for quantifying pure experimental error, yet they are frequently absent. Even more rarely do studies include confirmation runs at predicted optima or external validation tests under conditions not used for model building. The lack of these steps reduces confidence in model extrapolation and may obscure overfitting, especially in experiments performed under tightly controlled laboratory conditions that do not reflect real-world variability. In contrast, the most rigorous studies adopt a multi-layered validation approach, combining statistical diagnostics with independent confirmation tests, thereby demonstrating the reliability and reproducibility of their conclusions.

Beyond statistical soundness, DoE models must also be evaluated for their practical significance, an aspect often overlooked in the literature. Even when an optimum is statistically significant, its engineering relevance may be limited if the predicted conditions lie at the edge of the explored factor space, conflict with industrial constraints (*e.g.*, maximum allowed drying temperature, feasible calendering pressure, realistic electrolyte viscosity), or exhibit high sensitivity to small factor perturbations. In several cases, optimized conditions involve extreme parameter values that maximize the mathematical objective, but are unlikely to be robust under scale-up or field operation. The scarcity of robustness analyses – such as sensitivity maps, contour stability regions, or multi-objective trade-offs – further limits the generalizability of many DoE outcomes. Addressing these gaps would allow DoE to serve not only as an optimization tool but as a framework for engineering decision-making, integrating constraints, uncertainty and tolerance windows directly into the design process.

Taken together, these considerations show that the value of DoE in battery research extends far beyond reducing experimental effort: its real strength lies in generating reliable, validated, and practically meaningful models. Achieving this goal requires coherent alignment between design structure and model order, the adoption of rigorous validation protocols, and critical evaluation of whether statistically optimal conditions are also robust and industrially relevant. As the following sections will illustrate, differences in how these principles are applied across the four major battery domains – materials synthesis, performance and aging, safety and thermal management, and recycling – strongly influence the quality and utility of the reported results.

3. DoE for recycling and recovery of battery materials

Battery materials recycling and recovery are pivotal for building a sustainable and resilient battery value chain. In the context of rapidly expanding battery production capacity, closing the loop of critical raw materials is essential to reduce reliance on mining, mitigate environmental impact, and secure long-term supply. Advanced process design and optimization, supported by DoE, are therefore crucial to maximize metal yields, purity, and energy efficiency. Several studies demonstrate that DoE can significantly improve recycling strategies by enhancing the separation and recovery of valuable elements, thereby supporting more sustainable lifecycle management. Particularly promising are bioleaching approaches optimized through DoE, which combine high recovery rates with lower environmental burdens, offering a viable pathway for eco-friendly battery end-of-life (EoL) treatment. The proposed approach is transversal in several technologies, like sunlight conversion [105–114], chemical synthesis [115–124], and (super) capacitors [125–134].

Among the efforts to reduce waste, prevent environmental degradation and provide beneficial secondary raw materials, it is worthwhile mentioning the recycling of used alkaline and zinc-carbon batteries. These batteries are no longer classified as hazardous waste, but the recycling of spent batteries is mandatory (in accordance with the European Union Directives, 2006/66/EC). In this context, Calin *et al.* used DoE to optimize a corona-electrostatic separation process for recovering zinc and brass from the coarse fraction of shredded alkaline and Zn-C batteries. The process performance depends on a balance of gravitational, electrostatic, and drag forces acting on charged particles, which in turn is controlled by the separator voltage (V) and the angle (α) of the inclined feed plane. A full 3-level factorial design was carried out on these two factors, and a quadratic model was fitted to describe the dependence of metal recovery and purity on V and α. With the support of the software MODDE (Umetrics), it was possible to determine two statistical measures, *i.e.*, "goodness of fit" (R^2) and "goodness of prediction" (Q^2). The authors explicitly used R^2 and Q^2 to evaluate model adequacy, requiring small separation between them to avoid overfitting. Replicates at the center point allowed for the estimation of pure error and assessment of curvature. The results were processed by the software to determine the values of the coefficients of the polynomial model excluding those for which the uncertainties were greater than their value. Results indicate that the most important factor is the angle α. By increasing the angle, a greater metal recovery rate was obtained, but also a smaller metal purity fraction. With the help of the software, it was possible to determine the optimal values of α and V to maximize both the recovery and purity of metal and plastic fraction. The values were $V = 88$ kV and $\alpha = 31°$, corresponding to a metal recovery rate of 99.08 % and a metal purity of 91.93 %, with 52 % of non-metallic fraction recovery rate. This study illustrated a good practice in recycling-oriented DoE: a compact design, explicit model-validation metrics (R^2, Q^2), and an optimization step that quantifies trade-offs between recovery and purity.

In recent years, climate change has led the theme of recycling to assume ever greater importance [135]. Most battery models contain heavy metals that are toxic to both humans and environment. Hydrometallurgical and biometallurgical routes have emerged as promising alternatives to pyrometallurgy, enabling more selective metal recovery with lower energy input, but at the cost of increased process-complexity and multidimensional parameter spaces [136-145]. To optimize bioleaching of heavy metals from spent Ni-Cd and nickel-metal hydride batteries, Bajestani *et al.* implemented a Box-Behnken DoE on three factors: initial Fe^{3+} concentration, initial pH of Acidithiobacillus ferrooxidans culture, and initial particle size of the battery powder [136]. The 17-run design enabled estimation of main effects, interactions and curvature, with metal recoveries monitored by atomic absorption spectroscopy. Results indicated that minimizing initial powder size resulted in higher recovery efficiency for nickel and cobalt, while cadmium reached its maximum recovery efficiency at the larger mesh size. Lower pH and higher Fe^{3+} favored Ni and Co dissolution, whereas Cd leaching was maximized under opposite conditions, highlighting the intrinsic multi-objective nature of the problem. The target was to optimize the synchronous extraction of the three metals, so the initial values

of the factors were defined as follows: lowest initial pH (1), maximum initial Fe^{3+} concentration (9.7 g L^{-1}), and a mean particle size (62 μm). This setting made possible optimizing the simultaneous extraction of the three metals from the bioleaching of solid waste made of metal compounds with the resulting percentage of 87 % for the nickel recovery, 93.7 % for cobalt, and 67 % for cadmium. This example illustrated how RSM-based DoE can be used not only to locate single-metal optima, but to compromise between conflicting extraction trends, although explicit robustness or scale-up analyses were not reported.

Due to the increasingly widespread use of LIBs and, contextually, the difficulty in processing the raw materials, recycling lithium, cobalt, manganese, copper, and nickel from decommissioned batteries has become of great interest. Three main approaches are commonly adopted: i) pyrometallurgy; ii) hydrometallurgy; iii) direct recycling. Among these, pyrometallurgy is the simplest, but also the least in terms of quantity and quality of the recycled metals. Hydrometallurgy, consisting of leaching, solution purification, and metal recovery, is better in terms of final yield, but demands prior physical separation and sorting phases of the battery components. Direct recycling is the most complex, with several techniques to be applied, but it has the advantage of recovering fully functional AMs ready to be used in new battery production [146]. Within direct recycling, Wolf *et al.* used DoE to optimize centrifugation-based separation of lithium iron phosphate (LFP) and carbon black (C65) from aqueous dispersions, exploiting density and size differences between the two solids [147]. DoE was applied to investigate the dependencies on the working parameters of the three output values: T_{carbon}, $T_{LFP(LECO)}$, and $T_{LFP(XRF)}$, which represented the separation efficiency of carbon and LFP analyzed by LECO analysis and X-rays fluorescence, respectively. Fig. 2**A** represents the parameter space investigated via DoE. A reduced factorial design allowed for mapping the effect of rotation speed and volumetric flow rate on these responses, identifying conditions (54 000 rpm, 50 mL min^{-1}) that maximized LFP retention while transferring most carbon to the centrate. Structural and electrochemical characterization confirmed that LFP recovered under DoE-optimized conditions retained ~98 % of the capacity of commercial LFP, directly linking the statistical optimization to functional performance.

The recycling of cobalt, nickel, and manganese constituting LIBs is actively performed, while lithium – which is present with a percentage of 4–7 % in battery content – is sometimes not recovered for economic reasons. Indeed, lithium is recovered only after the recovery process of the other metals. Selective lithium leaching process, often based on prior roasting, can avoid this drawback enabling Li recovery as Li_2CO_3 or related phases before or alongside transition-metal recovery. Jung *et al.* focused on the study of the optimal roasting conditions and on the selection of the liquid-to-solid ratio (L/S) with the use of an experimental

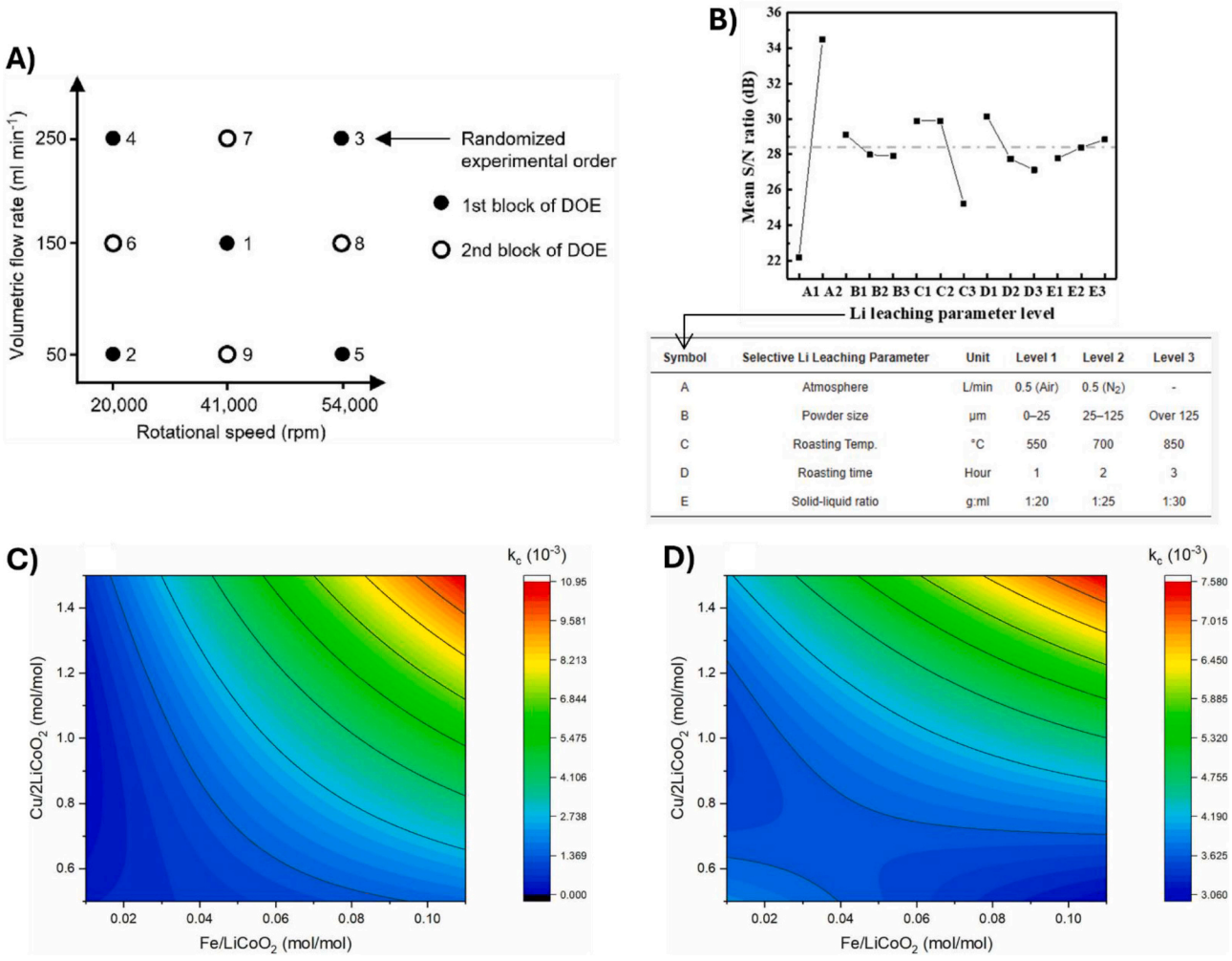

Fig. 2. A) DoE-investigated parameter space for centrifugation-based separation of LFP and carbon black (CB) for LIB recycling. Three rotational speeds and volumetric flow rates were chosen and a total of 9 experiments were conducted in randomized order. **B)** S/N graph for the optimization of selective lithium leaching of cathodic AMs from spent LIBs based on the Taguchi method (TM). X-axis labels refer to the explored parameters listed below the plot. Contour plots related to LIB AM dissolution kinetics in Fe(II)/Fe(III) catalyzed Cu-H_2SO_4 leaching system: **C)** model 2 predicting the reaction rate constant past the 30 min point, $1-(1-x)^{1/3} = k_c \cdot t$. **D)** Model 1 shows that the source of noise is the lower part ($k_c < 3.625$). Adapted and reprinted with permission from [148–150].

design based on the Taguchi method (TM) [148]. Using a Taguchi orthogonal array (OA) (L18, 2×3^4), they screened the influence of heat treatment atmosphere, powder size, roasting temperature, roasting time and L/S ratio on lithium leaching, with S/N analysis and ANOVA used to quantify factor effects. The heat treatment was identified as the parameter with the greatest impact on lithium leaching, followed by L/S ratio and, to a lesser extent, residence time. Confirmation experiments at the predicted optimum (1 h at 700°C under N_2, L/S = 1:30) yielded lithium leaching ratios close to those predicted by the Taguchi model (65.73 % *vs* 67.13 %), supporting the validity of the approach (Fig. 2**B**). This is one of the few Taguchi-based recycling studies that explicitly report both S/N optimization and a successful confirmation step, although, again, robustness to feedstock variability remains unexplored.

According to the hydrometallurgical recycling of LIBs, a wide range of lixiviants are used, but only few of them are interesting in terms of price and technology. H_2SO_4 remains one of the most viable because of its low cost and chemical stability. To obtain excellent cobalt extractions, the cathode AMs in LIBs require a reducing species due to the stability of the present higher-valence oxides. In this context, Porvali *et al.* investigated an H_2O_2-free leaching system in which dissolved Fe (II)/Fe(III) and copper participate in the reduction of $LiCoO_2$ in H_2SO_4. CCD was used to study the effect of $FeSO_4{\cdot}7H_2O$ and metallic copper loadings on the reaction rate constant (k_c) over two time windows (<30 and >30 min). Two regression models were created from k_c: i) model 1 for < 30 min; ii) model 2 for > 30 min, assuming a cubic rate law:

$$1 - (1 - x)^{\frac{1}{3}} = k_c \cdot t \quad \text{(Eq. 1)}$$

Backward elimination was used to remove statistically insignificant terms, and ANOVA indicated that Fe(II) and the Fe-Cu combined effect strongly influenced the $LiCoO_2$ dissolution rate, while copper alone did not significantly enhance cobalt extraction (Fig. 2**C and D**). This study was exemplary in its use of CCD to couple kinetic modeling with factor screening, although the design is limited to two factors and does not explicitly explore robustness with respect to temperature or solid loading.

Kahl *et al.* proposed a method to recover lithium from production waste as a lithium salt [149]. The method consisted in the thermal oxidation of pure lithium to Li_2O at a temperature between 300 and 400°C. After the oxidation, the product was dissolved in deionized water, filtrated, and eventually crystallized as $LiOH{\bullet}H_2O$, with purity >99.5 %. To make the process industrially viable, a 3^3 BBD was used to optimize temperature, residence time, and lithium sheet thickness (Fig. 3**A**). According to ANOVA, temperature and its quadratic term were dominant, with thickness as the second most influential factor and residence time having a smaller effect. The resulting regression model identified an optimum at 400°C, 2 mm thickness, and 2.5 h residence time, which was validated by two confirmation experiments yielding lithium conversion of 96.9 ± 2.6 %. This is a clear example of how DoE can efficiently map parameter space and identify near-complete

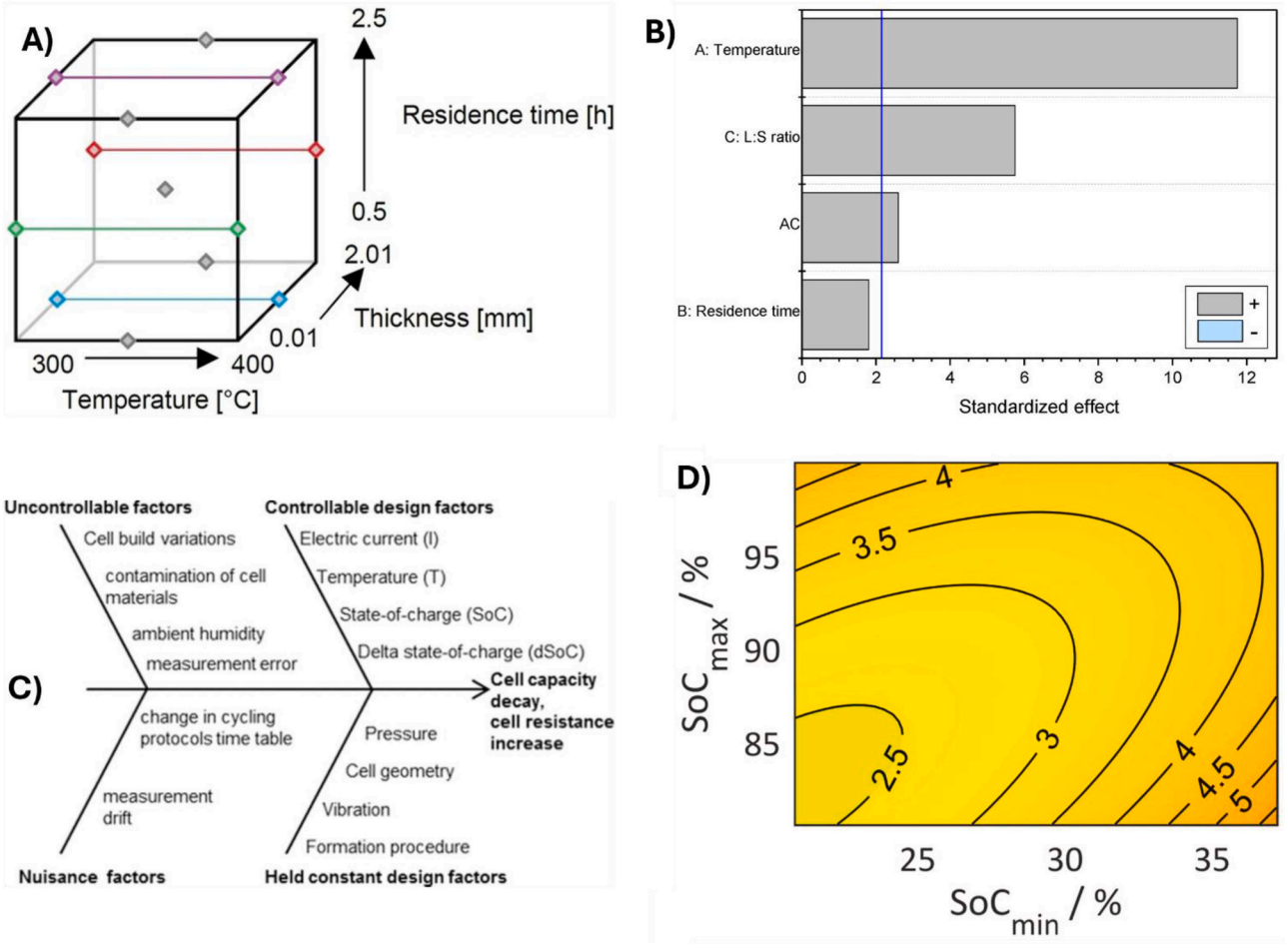

Fig. 3. A) Box-Behnken experimental design for a recycling process of primary LIBs production residues. **B)** Pareto diagram with significant effects on lithium yield coming from a CO_2 leaching (COOL) process. **C)** Fishbone-diagram of the identified causes effecting aging and the measurement thereof when large scale aging experiment for two popular lithium-ion cell chemistries is carried out. **D)** Cyclic capacity loss in % relative to beginning of life (BoL) capacity after 175 kAh as a function of two factors, shown on x and y axes, related to cyclic aging of automotive grade lithium-ion cells. Adapted and reprinted with permission from [151,152, 222,225].

conversion conditions with limited experiments, though again the variability of feed composition is not explicitly addressed.

The COOL process is a selective direct carbonization process to recover lithium from LIBs by the use of selective leaching properties of supercritical CO_2/water. According to the fact that all LIBs have the same basic structure, it is really promising because it is applicable to all kinds of LIBs and constitutes an alternative to conventional pyrometallurgical and hydrometallurgical methods. Moreover, supercritical fluids are interesting alternatives to traditional solvents used for metal extraction. Pavón *et al.* investigated the digestion of black mass at high pressure (100 bar) and varying temperature, residence time, and water: black mass ratio, using a 3^3 BBD to optimize lithium yield [150]. Statistical analysis (Pareto charts, ANOVA) showed that temperature and L/S had the strongest effects on lithium yield, including their interaction, while residence time had a minor influence (Fig. 3**B**). The optimized conditions predicted a lithium yield of 98.8 wt %, with experimental validation yielding 94.5 ± 0.3 wt %, indicating good, though not perfect, predictive performance and pointing to additional sources of variability not captured by the model.

Disposing of spent LIBs (SLIBs) in landfills can cause environmental and ecological problems, so effective management of SLIBs is crucial. The metal values in SLIBs can be recovered as a secondary resource. Both mineral and organic acids were used for metal dissolution of SLIBs; in this contest, Chabhadiya *et al.* investigated a new hybrid approach consisting in sequential leaching with both organic ($H_2C_2O_4$, named as OR) and mineral (H_2SO_4, SA) acids [151]. The study used a Taguchi OA DoE to optimize the following parameters: i) acid concentration (OR, SA); ii) pulp density (PD); iii) hydrogen peroxide dosage (HPD); iv) temperature (T); v) time (t). More in detail, Taguchi OA DoE technique was used to optimize the conditions for leaching in two sequential steps: first with oxalic acid to dissolve Cu and Li, then with sulfuric acid to dissolve Ni, Co and Mn. The TM included an objective function η called S/N, expressed in logarithmic form to reduce the effect of noise factors during experimentation, and analysis of means/ANOVA to quantify the contribution of each factor. According to the results for the first step, the most influential factors for Li and Cu leaching were time and HPD, followed by acid concentration and temperature. Under optimal conditions ($OR = 0.25$ M, $PD_1 = 10$ %, $HPD_1 = 0.5$ %, $T_1 = 80°C$, $t_1 = 90$ min), >99 % dissolution of Li and Cu was achieved. For the second step, optimal conditions ($SA = 3$ M, $PD_2 = 6$ %, $HPD_2 = 2$ %, $T_2 = 60°C$, $t_2 = 120$ min) yielded ≈99 % leaching efficiency for Co, Ni, and Mn. This work demonstrates how Taguchi designs can efficiently screen multiple process parameters in multi-step hydrometallurgical flowsheets, but, as in most recycling studies, long-term robustness, impurity tolerance, and feed variability are not systematically explored.

Overall, the studies discussed above highlight the transformative role that statistical DoE can play in advancing recycling and recovery strategies for EoL batteries. Across diverse technologies – including corona-electrostatic separation, hydrometallurgical leaching, bioleaching, centrifugation, and thermal treatments – DoE has consistently proven its ability to reduce experimental redundancy, quantify the relative importance of multiple factors, and identify optimal operating conditions. Particularly significant is its contribution to bridging laboratory studies and industrial applications, ensuring that complex recycling processes can be both efficient and reproducible. Looking ahead, and also inspired by other fields (*e.g.*, energy conversion [152–160], photocatalysis [161–170], electrocatalysis [171–180], environmental technologies [181–186], materials design [187–196], and advanced synthesis [197–205]), several directions appear especially promising.

From a methodological viewpoint, several common patterns emerge across these recycling-oriented DoE studies. Most works adopt well-established RSM or Taguchi designs with a relatively small number of factors, achieving substantial gains in yield or purity with limited experimental effort. However, validation practices are uneven: while some contributions explicitly report R^2–Q^2 pairs, ANOVA and confirmation runs, others rely on fitted models without systematic assessment of LOF or predictive error. In addition, virtually all optimizations are performed on nominal compositions and operating conditions, with little or no exploration of robustness to realistic feedstock variability, impurity levels, or scale-up constraints. Future work would benefit from integrating DoE with robustness analysis and multi-objective criteria (*e.g.*, yield, purity, energy consumption and environmental impact), thereby turning DoE from a tool for laboratory optimization into a framework for designing industrially viable and sustainable recycling processes.

4. Battery performance and aging

The ability of rechargeable batteries to deliver stable performance over time remains one of the central scientific and engineering challenges for electrified mobility and renewable energy storage, where reliability, cost, and safety must be ensured over thousands of cycles. Performance and lifetime are jointly governed by interacting stress factors – charge/discharge rates, operating temperature, depth-of-discharge windows, duty cycles, electrode composition – whose combined effects are rarely linear and often exhibit strong cross-dependencies. This complexity becomes even more pronounced in EVs and stationary ESSs [206-2015], where performance variability directly affects warranties, grid stability, and total cost of ownership. In this context, DoE provides a structured and statistically defensible framework to disentangle multi-factor interactions, quantify their significance, and reveal degradation pathways that traditional OFAT approaches systematically miss. By integrating DoE into performance and aging studies, experiments become not only more efficient, but also more informative, enabling the construction of predictive, validated models that support safer, and longer-lasting battery technologies.

Accurate estimation of the state of charge (SoC) is a foundational requirement for automotive applications, as it determines available energy, power limits, and safe operation boundaries. Model-based estimation is typically preferred due to its superior robustness and ability to incorporate physics-consistent constraints. Traditional nonlinear observers, such as the extended Kalman filter (EKF), however, require local linearization and may suffer performance degradation when nonlinearities become dominant. To overcome these limitations, Liu *et al.* proposed replacing the EKF with an unscented Kalman particle filter, combining unscented transform-based uncertainty propagation with particle filtering to capture stronger nonlinear behaviors [216]. A Thevenin-type equivalent circuit model (ECM) was parameterized as a function of SoC and temperature using a discrete fitting method. Importantly, the authors employed a CCD-based DoE to structure the parameter identification stage, ensuring coverage of the nonlinear response surface and enabling a statistically validated polarization-voltage model. Verification through dynamic stress tests and federal urban driving cycles showed that the DoE-guided model-identification step improved both accuracy and generalization at -10°C and 25°C, demonstrating the practical value of coupling observer design with a statistically optimized identification campaign.

Since the SoC is not measurable online, its estimation can be made in the battery management system (BMS), where a SoC estimator based on a nonlinear battery model is implemented. Non-road hybrid electric vehicles (HEVs) and machinery need high power densities and loads dynamics, which makes the modeling of the batteries more complex. Three battery model approaches are commonly reported in the literature: i) ECMs; ii) electrochemical models (EMs); iii) data-based models. All these models require measurements, which are obtained by applying a current excitation to the battery cell and recording the voltage response. In this context, DoE becomes particularly valuable because it enables the systematic design of excitation signals that maximize model identifiability while minimizing the number of experiments. To reach this goal, starting from a reference model, the information obtained is maximized and parameters can be estimated with minimum variance. Unger *et al.* used a local model network which consists of a series of local

linear models (LLMs) interpolated each other to give a nonlinear output [217]. This model was constructed by an iterative algorithm, which began with a global linear model to reach a threshold after a number of iterations. Unger *et al.* used an LLM tree algorithm. It was fundamental that the system dynamics were sufficiently excited and that all SoC range was covered during the measurements, even more in non-road applications. A load current excitation signal U was defined and applied to a battery cell, and cell voltage was recorded. Optimized high dynamic excitation sequences were created by optimal model-based DoE. Fisher information matrix (FIM), a way to measure the information content of a signal, was applied for optimization purpose. This is a noteworthy example of good DoE practice, because the authors explicitly quantify information gain using FIM and demonstrate that the optimized excitation reduces parameter uncertainty compared to conventional heuristic signals—a point often overlooked in battery modeling studies. The optimal excitation signal U was then applied respecting the battery constraints in terms of current values, battery voltage limits, and SoC. The current constraints were defined by taking into account a real road cycle. Measurement procedure was also defined in order to avoid different initial battery conditions and so excluding unexpected and undefined effects during measurements. The procedure is reported as follows: i) initial capacity check at 25°C; ii) set temperature of climate chamber; iii) fully charge the battery cell; iv) discharge until initial SoC was reached; v) apply excitation signal; vi) repeat iii to v until all excitation signals were recorded; vii) repeat ii to vi until all temperatures were recorded. However, the authors did not report whether center points or replicate excitations were included to quantify experimental noise, which would strengthen model validation and help assess robustness – an aspect highlighted as a gap in many DoE-based identification studies. The results showed that DoE approach resulted in an increase in accuracy of the model starting from a linear reference model used for the optimization of the excitation signal. Overall, this work demonstrates that DoE-driven excitation planning can significantly enhance the fidelity of dynamic battery models, especially in applications with wide operating ranges and complex load profiles.

Referring to the spread of plug-in hybrid electric vehicles (PHEVs), great interest was dedicated to the development of reliable models to describe capacity and power fade of LIBs in order to predict the long-term evolution of capacity and resistance. Battery aging models are developed to make this possible, and can be classified as physics-based or semi-empirical. The latter are often preferred for PHEV applications, since they balance accuracy and computational cost. Cordoba-Arenas *et al.* approached the investigation of battery aging under PHEV operation by developing a semi-empirical model applied to LIBs constituted by blended cathodes [218]. This kind of cathode is composed of layered-oxide positive electrodes as $LiNi_{1/3}Mn_{1/3}Co_{1/3}O_2$ (NMC) and spinel oxide positive electrodes as $LiMn_2O_4$; they were considered the most promising for PHEV applications. The factors that were studied to investigate their influence on capacity and power fade of LIBs were: i) charge sustaining (CS)/charge depleting (CD) operation; ii) minimum SoC; iii) charging rate (CR); iv) temperature. The distinction between CS and CD operation was compactly described through a dimensionless ratio R, which quantifies the fraction of time spent in CD *versus* CS mode:

$$R = \frac{t_{CD}}{t_{CD} + t_{CS}} \quad \text{(Eq. 2)}$$

assuming the value of 1 if all the operating time is spent in CD, 0 if all the operating time is spent in CS, and a value between 0 and 1 for mixed operation. Four factors were chosen for DoE as follows: i) CR; ii) battery skin temperature; iii) R; iv) SoC_{min}. Although the authors did not explicitly label the design type, the structured variation of these four factors follows a clear DoE logic and allows for the estimation of main and interaction effects with a limited number of tests. Three sets of experiments were carried out: i) CD operation, $R = 1$; ii) CS operation, $R = 0$; iii) Mixed operation, $0 < R < 1$. This experimental structure ensured that pure CS, pure CD, and mixed regimes were all represented, which is essential to decouple the effects of R, SoC window, and temperature on aging. At the end of each experiment, the charge throughput (Ah) was measured. Each cell was characterized before and after aging campaign by a capacity test and a hybrid power pulse characterization to assess discharge and regen power capability. Taking into account that the number of cycles was expressed as the total ampere-hour throughput [Ah] in both charge and discharge, the capacity fade was then expressed as:

$$S_{loss}(Ah) = 100 * \frac{S_0 - S\ (Ah)}{S_0} \quad \text{(Eq. 3)}$$

with S_0 the cell nominal capacity and S (Ah) the cell capacity after Ah > 0 charge throughput. Therefore, the functional form adopted was:

$$S_{loss}\ (Ah) = f_C(SoC_{min}, R, CR, T) * \ Ah^z \quad \text{(Eq. 4)}$$

with f_C nonlinear function of the aging factors investigated and $z > 0$. Using the nonlinear optimization toolbox in MATLAB, fitting parameters for each i_{th} experiment were defined. The expression following the characterization points obtained from tests resulted as:

$$S_{loss,i}\ (Ah) = f_{C,i} * \ Ah^{Z_i} \quad \text{(Eq. 5)}$$

Results showed there was no significant dependence of capacity fade on CR. For this reason, CR was excluded from the model. This factor screening step is an important strength of the study, as it avoids over-parameterization and focuses the model on statistically significant variables. Regarding temperature, at high values the capacity fade followed an Arrhenius relation, so the following expression was adopted:

$$f_C(\bullet) = a_C(SoC_{min}, R) * exp\left(\frac{-E_{a_c}}{R_g T}\right) \quad \text{(Eq. 6)}$$

with cell activation energy for the capacity fade process $E_{a_c} = 22{,}406$ J mol^{-1}, R_g universal gas constant, and T cell absolute temperature. An increase of temperature led to an increase of the capacity fade. Referring to R, the experimental severity factor values were fitted to the following equation:

$$a_C(SoC_{min} = 35\%,\ T = 30\ ^\circ C, R) * \alpha_1 + \beta * R^b \quad \text{(Eq. 7)}$$

with identified constants α_1, β, and b equal to 145, 420, and 0.34, respectively. The higher was R, the higher was the capacity fade. For SoC_{min}, the experimental severity factor values were fitted to the following equation:

$$a_C(R = 0, T = 30\ ^\circ C, SoC_{min}) * \alpha_2 + \gamma * (SoC_{min} - SoC_0)^c \quad \text{(Eq. 8)}$$

with identified constants α_2 and γ equal to 137 and 9610, respectively, for $SoC_0 = 0.25$ and $c = 3$. Results showed an increase in capacity fade with an increase of SoC_{min}. Capacity fade was finally described by:

$$S_{loss}\ (Ah) = a_C(SoC_{min}, R, T) * \ exp\left(\frac{-E_{a_c}}{R_g T}\right) * Ah^z \quad \text{(Eq. 9)}$$

with $a_C(\bullet)$ given by:

$$a_C(\bullet) = \alpha_C + \beta_C * R^b + \gamma_C * (SoC_{min} - SoC_0)^c \quad \text{(Eq. 10)}$$

Results from the experiments validated the model. Moreover, the goodness of the model was evaluated through the root mean square error (RMSE) with a result of 0.0047 %. Despite the very low RMSE, the study did not report independent validation data or explicit LOF tests, so potential overfitting and the robustness of the model outside the tested design space remain open questions.

Prochazka *et al.* analyzed pouch cells of two different chemistries, LFP and nickel cobalt aluminum (NCA), using a large-scale DoE approach [219]. The targets were capacity decrease and impedance

increase, defined as EoL criteria. A full-factorial test plan was initially generated using temperature, current, SoC windows, and cycling profiles as factors. Given the high dimensionality of the factor space, the authors reduced the test plan using a modular D-optimality algorithm, preserving statistical identifiability with a smaller set of 46 experiments (Fig. 3**C**). Results showed that for both chemistries there was a strong dependency of the capacity decrease on temperature. SoC showed opposite effects for NCA (low SoC favorable) and LFP (high SoC favorable). Current and SoC interactions were also significant. Although the DoE structure was well designed, the study did not report replicate points, center points, or independent validation tests. This limits the ability to quantify experimental noise and assess model robustness.

Battery aging models play a really important role in applications where management strategies are critical to limit degradation. LIBs suffer of solid electrolyte interphase (SEI) layer formation and lithium plating at the negative electrode, but also the intercalation of lithium ions can cause volume changes in both electrodes generating particle cracking and loss of electrical contact. Battery aging models can be divided into two groups: i) physical-chemical approach; ii) semi-empirical approach. The first one uses chemical reaction kinetics and physical equations, while the second is based on aging tests and mathematical fitting. Mathieu *et al.* applied a D-optimal DoE in order to further optimize the initial design of a battery capacity aging model [220]. Calendar and cycling tests were used to calibrate the model, and the dependence of the degradation rate on temperature, SoC, and current was thoroughly modeled. The pre-specified model adopted included linear effects of the three factors and two interaction effects: i) temperature and SoC to consider SEI layer growth; ii) temperature and charging current for lithium plating effect. The final model consisted of 9 parameters; the capacity fade computed with MATLAB showed an absolute relative error of 0.85 % with respect to experimental data. The fit was evaluated as satisfactory for both calendar and cycling data. The use of a D-optimal design was a clear strength of this work, as it minimizes the experimental burden while preserving parameter identifiability; however, no explicit LOF analysis or independent validation set is reported, so the risk of overfitting and the robustness of the model outside the explored design space remain partially unquantified.

An interesting DoE application in real scenario was represented by the SIMSTOCK program adopted in France among cars manufacturers, suppliers, and research labs to share costs and efforts to go forward in the studying of the ESS aging [221]. The first step was to create a battery model. Open circuit voltage (OCV), which represents the voltage of the battery at its thermodynamical equilibrium, the voltage drop η_{CT} (named also overpotential or overvoltage) caused by the charge transfer, diffusion η_{diff}, and ohmic losses η_{Ω} were the parameters used to determine the model, as follows:

$$U = OCV - \eta_{tot} = OCV - \eta_{CT} - \eta_{diff} - \eta_{\Omega} \quad \text{(Eq. 11)}$$

An equivalent electrical circuit was defined to describe the mentioned phenomena. At this point, DoE became necessary to determine the aging laws for each parameter. Aging was expressed as the useful capacity representative of the SoC range where performances are met. Current, temperature, Ah throughput, and SoC variations were the selected parameters for each of them. At least 11 tests were necessary to derive the coefficient of the simplified polynomial expression of aging. Results showed a greater fade for the testing condition with the highest current and Ah throughput. A differential approach was adopted since the aging conditions were subjected to change in a usage vehicles scenario. The analysis of the coefficients stabilized that temperature had the strongest effect, followed by the Ah throughput, and then current. The final step was to implement the results of the measurements into a model to forecast the capacity fade and resistance increase during vehicle life. In this case, DoE was mainly used to regress empirical "aging laws" from a reduced test matrix, which is highly relevant for industrial deployment; nonetheless, the choice of a low-order polynomial form and the limited number of test points per condition may restrict extrapolation capability, and confidence intervals on the fitted coefficients were not extensively discussed.

In the automotive context, it is important to understand the effect of different operating conditions on degradation of batteries. More in detail, cyclic aging is more complex in comparison with calendar aging. Moreover, experiments for lifetime modeling of batteries are very expensive and have a duration of years. In this regard, DoE has become fundamental. Stadler *et al.* carried out a test matrix based on 62 automotive grade Li-ion cells with a planned real-world operating cycling [222]. 63 Ah nominal capacity cells were used, all with a starting SoC of 75 %. 5 main aging factors were defined according to the literature: i) temperature; ii) SoC_{min}; iii) SoC_{max}; iv) charging power P_{CH}; v) the ratio of energy throughput between micro and macro-cycles (EV_{ratio}). A CCD was used with 5 factors and 2 levels. The cells were tested among 27 different variations according to the CCD for a time longer than 2 years. A regression model with second-order terms was defined because of its accuracy in approximating measurement data. Using a stepwise backwards selection, the terms with a p-value higher than 0.1 were automatically removed because statistically insignificant. Firstly, a single regression model was created to describe capacity loss at 175 kAh. About the influence of temperature, the lowest aging was observed at 31°C and both an increase (up to 50°C) and a decrease (down to 11°C) in temperature led to an acceleration in aging. Referring to the charging power, a slight increase in aging was observed moving from a charging power value of 136 to 264 W, but it was a small effect. The upper SoC limit had a strong effect on aging. It was observed a strong acceleration in aging with SoC values over 90 %. Even a greater value of lower SoC exacerbated the capacity degradation of the batteries. Lastly, the EV_{ratio} had the greatest impact on cycling aging. The explanation was that, with higher ratio of EV-cycles, the cell was charged more frequently and so more charge throughput was accumulated. The AMs were solicited more and particle cracking, SEI layer cracking, and contact loss of particles occurred more frequently. About the interactions, six of them were defined as relevant; in particular, the term related to SoC_{max}: SoC_{min} had the strongest effect on capacity loss, as it is shown in Fig. 3**D**. This study nicely illustrated how CCD-based regression can rank the relative importance of factors (in particular the SoC window and EV_{ratio}), but the use of stepwise term selection without cross-validation may bias the model toward the specific dataset, and prediction errors or confidence bounds were not quantified in detail.

The experimental design and analysis can also be used to study factors that impact battery aging. A quantitative analysis was provided to determine the aging effect of the root mean square (RMS) current factor, which can be useful for designing battery pack filters using direct current (DC) bus capacitors. The growth of a SEI layer can increase resistance and lead to capacity loss and power fade. Many studies have been conducted to determine the aging performance of LIBs under various conditions [223,224], including calendar life models and cycling conditions. Factors that may influence battery aging are temperature, end-of-discharge voltage, charging voltage, and the superimposed alternating current (AC) component of the battery. The AC component of the battery has been proposed as a factor in battery aging, but more research is needed to determine its significance. To reduce the AC component of the discharge current, passive filtering or other methods may be necessary. The design of the DC bus filter in EV power electronics, which filters the AC component from the battery pack, could be impacted by the role of the AC component in battery aging. A first experiment was conducted by Juang *et al.* using 16 ICR14500NM cells, which were operated at 760 mAh, 4.2 V constant voltage charging limit, 2.8 V fully discharged cut-off voltage, and 300 charge/discharge cycles [225]. The goal of the first experiment was to determine the impact of a superimposed AC component on the cell aging characteristics. Among a total of 16 cells, the AC component for 8 of them was added to the DC discharge current, so the RMS value of the total discharge current waveform was 905 mA (AC-905), while for treatments DC-800 and

DC-905 4 cells were used. The focus of the study was on the battery aging as determined by changes in its series resistance value, which was interpolated from the EIS results. The battery was cycled 300 times, with the reference performance tests performed at the beginning and every 30 cycles. The statistical method consists in the definition of a normalized cycle number:

$$Z = \frac{C - \overline{C}}{\Delta C} \quad \text{(Eq. 12)}$$

where C is the cycle number, $\overline{C}$ the average value of all the cycle numbers, and $\Delta C = 30$ cycles. The equation of the model is the following:

$$R_{ij} = \widehat{\beta}_0 + \widehat{\beta}_1 R_{i0} + \widehat{\beta}_2 X_{1j} + \ldots + \widehat{\beta}_{17} X_{16j} + \varepsilon_{ij} \quad \text{(Eq. 13)}$$

with

$$X_{kj} = Z_j \delta(i-k) \quad \text{(Eq. 14)}$$

$$Z_j = \frac{C_j - \overline{C}}{\Delta C} \quad \text{(Eq. 15)}$$

R_{ij} is the resistance of the i^{th} battery cell for the j^{th} EIS measurement, R_{i0} is the initial resistance measurement of the i^{th} battery cell, X_{kj} the resistance predictor value for the k^{th} and j^{th} measurements, δ the Kronecker delta function, and ε_{ij} the error unaccounted. For each battery cell, an estimated slope was determined. Moreover, for each group an average estimated slope and its variance were defined as follows:

$$\widehat{\beta}_{avg} = \sum \frac{\widehat{\beta}_i}{\mathrm{n}} \quad \text{(Eq. 16)}$$

$$Var(\widehat{\beta}_{avg}) = \frac{Var(\widehat{\beta}_i)}{n} \quad \text{(Eq. 17)}$$

The null hypothesis, or the statement being tested, was that the groups cell ages at the same rate. The t-statistic, with its degrees of freedom, was used to calculate the p-value, which is a measure of the strength of evidence against the null hypothesis. t-statistic formula (following Student's distribution) was defined as follows:

$$t = \frac{\widehat{\beta}_{avg1}\ 1 - \widehat{\beta}_{avg2}}{\sqrt{Var(\widehat{\beta}_{avg1}) + Var(\widehat{\beta}_{avg2})}} \quad \text{(Eq. 18)}$$

If the p-value is small, typically 5 % or less, the null hypothesis is rejected. This means that the mean estimated resistance slope (a measure of aging rate) for the two test treatments being compared is statistically different. If the p-value is larger, it means there is not enough evidence to reject the null hypothesis and the two test treatments are assumed to have statistically similar mean estimated resistance slopes and therefore similar rates of aging. The t-statistic and p-values for the group comparisons showed that the AC-905 and DC-905 groups (same RMS current) had approximately the same aging rate, while the DC-800 group (different RMS current) had a noticeably different aging rate. It was also found that the difference in depth of discharge (DoD) between treatments was not significant, supporting the conclusion that RMS current affects aging, but DC offset current alone does not. A second experiment was performed to confirm the influence of RMS value on battery aging, to investigate the possible influence of AC current waveform shape and frequency on aging. The experiment was conducted using the same schedule of the first one, but using 4 treatments. The model was defined as follows:

$$R_{ij} = \widehat{\beta}_0 + \widehat{\beta}_1 R_{i0} + \widehat{\beta}_2 X_{1j} + \ldots + \widehat{\beta}_{32} X_{31j} + \varepsilon_{ij} \quad \text{(Eq. 19)}$$

because of the use of the data collected in the first experiment. Results showed that there is no correlation influence of frequency or the shape of the current waveform on battery aging and that RMS current influenced aging, while DC current alone did not. It is also shown that the resistance of the batteries increased faster for higher RMS cases. Overall, the results of these experiments suggested that the RMS value of the discharge current waveform was the most important factor contributing to battery aging. This work was a good example of how DoE combined with statistical hypothesis testing can isolate the physically relevant factor (RMS current) from confounding variables such as DC offset and waveform shape; at the same time, the relatively small number of cells per treatment means that confidence intervals on the estimated slopes should be interpreted with caution.

On-board energy and power capability of LIBs decrease over time due to various mechanisms such as cracking or dissolution of the AM and growth of the SEI. The rate of these mechanisms is dependent on operating conditions like temperature, SoC, voltage, DoD, and current magnitude. Developing a global battery aging model that considers all these factors and unifies calendar and power cycling operation is difficult and time-consuming. Baghdadi *et al.* investigated the sensitivity of battery capacity to aging rate at different temperatures, currents, and SoCs [226]. A reduced DoE was proposed to determine the 27 degradation rates resulting from 27 different conditions, which were: i) 3 ambient temperatures of 0, 25, and 60°C; ii) 3 SoCs of 30, 60, and 90 %; iii) 3 current levels of 0, 1, and 3C. Thanks to DoE, only 9 different battery cells were used in less than 100 days of test. The simplifying hypotheses were based on the cumulative damage theory developed by Palmgren-Miner, which defines that damages occurring under several aging events are additive and the degradation associated to one event is not influenced by other previous events. The validity of this hypothesis was assumed in this study. The Dakin's degradation equation was used to determine battery aging rates for each condition:

$$\frac{d\xi}{dt^{\alpha\xi}} = \pm\ k_\xi\ \xi^{n\xi} \quad \text{(Eq. 20)}$$

with $\alpha\xi$ the time dependent factor, k_ξ the degradation rate of ξ, and $n\xi$ the reaction order of the aging reaction. $\alpha\xi$ and $n\xi$ were assumed equal to 1 according to previous studies [229]. By the integration and then the derivative over aging, it was possible to determine the degradation rate k_ξ as follows:

$$k_\xi = \pm \frac{d\left(\ln\left(\frac{\xi(t)}{\xi_0}\right)\right)}{dt} \quad \text{(Eq. 21)}$$

with t the aging time and ξ_0 the parameter at BoL. The battery model that was used for the experiments was a commercial lithium polymer battery (LiPB) with a capacity of 12 Ah and cutoff voltages of 4.2 and 2.7 V. 9 aging tests were performed and each battery was aged under one temperature and one current level among the defined values around 3 different average SoCs. The evolution of battery capacity (Q) over time was defined as follows:

$$Q(t) = Q(t_0)\ x\exp(-k_Q t) \quad \text{(Eq. 22)}$$

with $Q(t_0)$ the battery capacity at BoL and k_Q the battery capacity degradation rate as a function of T_{amb}, SoC, and current, and identified by linear fitting. The highest degradation occurred at 0°C and max current magnitude (36 A). A polynomial function of $\ln(k_Q)$ depending on the aging factors was defined considering linear effects, first order interactions, and quadratic effects as follows:

$$\ln(k_Q) = a_0 + \sum_{i=1}^{3} a_i X_i + \sum_{i,j=1\ i\neq j}^{3} a_{ij} X_i X_j + \sum_{i=1}^{3} a_{ii} X_i^2 \quad \text{(Eq. 23)}$$

The results of the study show that the battery capacity degradation rate is a function of the operating test conditions and that the degradation rates are linear in the logarithmic scale. The results also show that the average of the available regression factors R^2 for degradation rate identification is 0.937, indicating a fair approximation of the linearity of

the aging rates. The results show that the proposed model is a valid tool for predicting battery aging rates and for optimizing the battery usage strategies to extend the system lifetime. Here DoE was explicitly used to drastically compress the experimental matrix (9 cells instead of 27), showing how degradation rates can be mapped in a multidimensional space; nevertheless, the cumulative damage hypothesis and the assumed exponential decay law introduced a strong model structure that may not capture irreversible or path-dependent degradation phenomena.

There are several factors causing faults in LIBs that can be linked to structural or thermal failures, but also to a combination of manufacturing defects, over charge/discharge, and short circuits. A way to study the behavior of LIBs is to create a model of them. The ECM is very appreciated because it allows for a good representation of cell dynamics with low computational resource usage. The *f(SOC)* was defined as the nonlinear function that relates the OCV with the SoC of the battery. The experimental OCV-SoC curve was modeled with a ninth-degree polynomial function. Considering the complexity of the process, the cost and the range of operation, Singh *et al.* applied a model-based fault diagnosis with Kalman filter (KF) as observer filter that worked in parallel with the battery and by measuring the load/charge current and the terminal voltage estimated the states of the battery model [227]. For nonlinear process models, the KF was substituted with the EKF. Furthermore, the single observer was extended to a series of observers. In this way, each observer represented a particular fault/operational condition allowing for a robust LIB monitoring. A multiple model adaptive estimation, which is one of the observer-based fault diagnosis techniques, was applied employing a KF bank of n filters. One observer represents the healthy condition of the process, while the $n-1$ observers represent the fault conditions. The parameter values were extracted with the use of recursive least square technique, which consisted in fitting battery mathematical model to a sequence of observed battery current and voltage data by maximizing the sum of the squares of the difference between observed and computed data recursively. To test the performance of the condition monitoring setup, a scenario was created with consecutive changes in the battery condition in a total simulation time of 213 s. The scenario was divided into four equal parts representatives of the healthy and deteriorated performance of the battery due to over-discharge. The four parts were as follows: i) 0 - 53.25 s: healthy battery operation; ii) 53.26 - 106.5 s: battery operation after two 24 h over-discharge cycles; iii) 106.51 - 159.75 s: battery operation after 25 Navy overdischarge cycles; iv) 159.76 - 213 s: healthy battery operation. The analysis gave values for y_m, that represents the healthy battery operation in terms of terminal voltage measurement; it was then compared to the estimated terminal voltage y_{mew} (for the 1st and 4th phase), $y_{24\ h\ OD}$ (for the 2nd phase), and $y_{Navy\ OD}$ (referred to the 3rd phase). Each of them showed good match with the measured voltage within the associated range and marked deviation in the other time intervals. Finally, the residuals were evaluated with a probability density function that confirmed the accurate behavior of the process by detecting the correct battery condition associated to the correct time. In this study, DoE was not used to design the excitation profile, but the underlying parametric model and observer structure implicitly rely on the richness of the operating conditions. From a methodological viewpoint, the work demonstrated how model-based approaches can discriminate different aging and fault scenarios; however, the absence of a formal DoE or sensitivity analysis on model parameters makes it difficult to quantify how robust the fault classification remains under measurement noise or modeling errors.

Within the broader framework of battery life prediction, Guo *et al.* investigated how the battery performance metric of capacity fade is affected by different operating factors, usage profiles, and battery design factors [228]. Four samples for two types of batteries (CS2 with a rating capacity of 1100 mAh and CX2 with a rating capacity of 1350 mAh) were investigated with different discharge rates. Each battery was cycled at a constant discharge rate (1C or 0.5C) until the cutoff values of 4.2 V (for charging) and 2.7 V (for discharging). A full factorial design (FFD) was used considering the following design factors: i) number of cycles (0 - 300; 300 - 600; 600 - 900; > 900); ii) discharge rate (0.5C; 1C); iii) battery type (CS; CX) to investigate the capacity fade of the batteries. Two battery samples were used at each of the 16 treatment combinations and battery capacity was recorded at the end of each charge/discharge cycle. The results pointed out that the capacity of batteries decreased as the number of cycles increased, but the rate of this decrease was not so marked within the first 200 cycles. Moreover, the decline in capacity was more severe when the discharge rate was 1C than when it was 0.5C, regardless of the number of cycles or type of battery. The CX battery showed a relatively higher capacity due to its higher rating and unique design. Finally, the number of cycles can be a strong indicator for monitoring the battery health status. In this study, the 3-factor FFD provided a clear ranking of the main effects of usage profile (cycle window, C-rate) and cell design on capacity fade with a limited number of tests. However, the statistical treatment remained relatively simple: the use of only two replicates per treatment, together with the absence of explicit ANOVA tables, confidence intervals, or explicit model validation, limited the quantitative assessment of prediction error and may under-represent possible interactions beyond the explored factor ranges.

Constant current constant voltage (CCCV) is the most used method for charging LIBs. However, its intrinsic trade-off between charging time, temperature rise, and energy efficiency motivates the search for optimized multi-stage charging profiles. Vo *et al.* investigated a DoE-based strategy for LiPBs using the TM combined with SoC estimation [229]. The goal was to reduce charging time and temperature variation while maximizing energy efficiency. DoE was applied to search for the optimal charging current pattern. CCCV was first used to evaluate how different current levels influenced temperature rise, charging efficiency, and duration. Four constant-current stages (each spanning 25 % SoC) were selected as controllable factors, and TM was used to reduce the full 81-experiment matrix to only nine tests. An observer-based SoC estimator enabled real-time switching among current stages, allowing for the assessment of energy efficiency, charging time and thermal stress under each TM combination. The optimized strategy reduced charging time by 22.5 % (~15 min) and halved the temperature variation compared to CCCV. Although the TM-based exploration efficiently identified the dominant factors, the statistical treatment remained limited; in particular, the final protocol was not fully validated over independent repetitions or different ambient temperatures. As a result, robustness, generalizability, and potential overfitting to the tested operating window could not be fully assessed. A comparison against a response-surface model or a multi-objective optimization would have further clarified trade-offs between thermal constraints and charging speed.

The internal resistance of a battery cell is the characteristic most affected by degradation. Monitoring it is very important, but at the same time complex. For EVs, having an on-board system to monitor the state of health (SoH) of the battery is desirable. Therefore, Remmlinger *et al.* developed a model deduced from an equivalent circuit that used specific signal intervals with a defined timespan occurring regularly during the normal operation of the battery in EVs [230]. Recorded data from inner-city driving of an EV were selected and analyzed in a laboratory. Engine-start pulses were identified as suitable excitation events for resistance estimation. Two batteries were used: a new one and a degraded 6.5 Ah one. The identification of the internal resistance was done through the special identification signals of terminal voltage and current at the start of the combustion engine with an adapted model. This model was the result of a simplification from the continuous-time frequency domain to the discrete-time frequency domain (z-domain):

$$G(z) = \frac{U(z) - U_{OCV}}{I(z)} = \frac{b_1 z^{-1}}{1 + a_1 z^{-1}} \quad \text{(Eq. 24)}$$

with a_1 and b_1 linear parameters. The internal resistance was then

calculated as:

$$R_i(\theta) = \frac{b_1(\theta)}{1 + a_1(\theta)} \quad \text{(Eq. 25)}$$

The next step was to express a degradation index k_d with respect to the internal resistance independent of the actual cell temperature of the measurement:

$$R_{i,new}(\theta) = a\, e^{-b\theta} + c \quad \text{(Eq. 26)}$$

and k_d was calculated by solving the equation:

$$R_{i,act} = k_d R_{i,new}(\theta_{act}) \quad \text{(Eq. 27)}$$

The approach provided consistent k_d values for both cells, showing that operational current pulses can support in-vehicle resistance tracking. However, the analysis was not based on a structured DoE and the influence of different pulse amplitudes, temperatures, or SoC levels was not systematically evaluated.

Use of LIBs is very popular due to their high energy density, but they also exhibit the rare, but severe failure mode of fire/explosion for EVs. Therefore, for the further growth of the LIB business, the safety problem should be addressed [231–240]. The current method of thermal monitoring for EVs uses multiple thermostats. However, as the size of the battery system increases, the number of thermostats also increases, which can lead to sensor malfunction and increased maintenance costs. To address these issues, Kim *et al.* investigated an alternative method of monitoring to reduce the number of required sensors through temperature prediction [241]. Three phases were defined to reach the objective: i) devising battery thermal characterization tests under various operating conditions; ii) developing an online-applicable temperature prediction model using artificial neural networks (ANNs); iii) validating the temperature prediction model. The proposed temperature prediction model was demonstrated using an EV battery pack that consisted of 12 battery modules. For the first phase, LIB cells with 50 Ah capacity and 3.7 V nominal voltage were employed. Thermal parameters (C the heat capacity, h the heat transfer coefficient) were experimentally extracted to enable accurate estimation of heat generation. A dynamic current profile derived from EV driving was then condensed into three representative current levels. Similarly, coolant temperature was discretized into three representative conditions. A computer model, based on computational fluid dynamics (CFD) simulation, was used to generate training data for the ANN, which used three inputs – coolant fan velocity, heat generation rate, and one sensed module temperature – to estimate the remaining module temperatures. The ANN showed high accuracy in semi-transient validation, with a maximum error of 0.27°C and an average error of 0.20°C. This study effectively demonstrated that data-driven prediction can reduce sensor count, although no DoE framework was employed to systematically explore interactions between thermal parameters.

Even if the current scenario is mostly populated by LIBs, lead-acid batteries are still appreciated for their capability to work at high voltages, acceptable specific energy, and for working at a wide range of temperatures, but also for their predisposition to be recycled. Within this typology, flooded lead acid batteries (FLABs) are the most widely used. During the process of charge and discharge, the electrochemical reactions cause a sharp increase of the TR rate and, consequently, of the C-rate. This is always followed by a decrease in their capacity, which may cause damages to the battery. For this reason, a DoE was adopted by Nahidi *et al.* to investigate the effect of 3 parameters on the capacity and the TR rate [242]. These parameters are: i) electrode gaps; ii) roughness quality of electrode surfaces; iii) C-rate. Two methods were applied: the CCD and the RSM. Twenty charge/discharge tests were designed. FLAB cells were prepared with gaps from 2 to 10 mm and different surface roughness values. Capacity and TR rate were measured during testing. Model adequacy metrics (adjusted/predicted R^2, predicted residual error sum of squares) confirmed a reliable fit. Optimization indicated that maximum capacity (15.72 Ah) and minimal TR rate (0.003) occurred for an 8 mm electrode gap and 2.5 mm surface roughness. The study provides a clear example of DoE-driven optimization, though it did not fully address the reproducibility of optimal conditions or potential nonlinear interactions beyond the quadratic model.

The studies reviewed in this section clearly demonstrate the pivotal role of DoE in advancing our understanding of battery performance and aging. From SoC/SoH estimation to the development of lifetime models, DoE enables the systematic exploration of factors such as temperature, current rate, and SoC windows. Applications range from estimator optimization to degradation modeling across different chemistries, highlighting how DoE supports reproducible and statistically meaningful insights. Looking forward, unified frameworks integrating calendar and cycling aging, multi-objective optimization, and hybrid DoE-ML approaches appear particularly promising. Furthermore, accelerated aging protocols based on statistically efficient designs may considerably reduce development time. Beyond LIBs, DoE is expected to play an expanding role in post-lithium chemistries [243–252] and related energy systems [253–262], reinforcing its value as a strategic methodology for designing smarter experiments and enabling safer and more durable battery technologies.

5. Materials synthesis and optimization

The synthesis of advanced materials is at the core of progress in electrochemical energy storage. The structural, morphological, and chemical properties of AMs, CAs, binders, and electrolytes directly dictate the performance, cost, and safety of rechargeable batteries. Achieving precise control over these properties, however, is far from trivial: synthesis processes are often governed by a complex interplay of parameters such as precursor composition, solvent environment, temperature, pressure, and processing time [263–265]. Small variations in these factors can lead to significant differences in materials performance, making it essential to adopt systematic and efficient approaches to experimental design. In this context, DoE offers a structured methodology to explore synthesis conditions and materials optimization in a way that goes beyond traditional trial-and-error practices. By investigating multiple factors and their interactions simultaneously, DoE provides a statistical framework that helps identifying the most influential parameters, reducing experimental redundancy, and guiding researchers toward reproducible and scalable processes. This is particularly relevant for the battery field, where the translation of laboratory-scale discoveries into practical technologies requires both high-performing materials and robust, scalable synthesis routes. This section introduces the role of DoE in the synthesis and optimization of battery materials, highlighting its potential to streamline the development of next-generation components. In addition to summarizing representative studies, the strengths and limitations of each DoE implementation will be also briefly commented from a practical perspective.

A positive example of the use of DoE in the search for high energy cathode materials for LIBs was reported by Martinet *et al.*, who determined the optimal mixture to produce lithium-rich lamellar oxides as iron-substituted lithiated phosphate materials [266]. More in detail, starting from the general formula $LiFe_xM_{1-x}PO_4$ (with $0 \leq x < 1$ and M = Mn, Co, Ni, or a mixture of them), the challenge was to investigate which was the best composition among several possibilities. The objective was to maximize the capacity of the compound (expressed in mAh g^{-1}). A surface response design including six input parameters was used to quantify their influence on capacity and to perform a multiparameter optimization, which increased the discharge capacity from 200 to 250 mAh g^{-1} while significantly reducing the number of experiments. This study illustrates how response surface DoE can efficiently map a high-dimensional compositional space, although the transferability of the optimal composition to different synthesis routes or cell configurations was not systematically addressed.

Phospho-olivines, and in particular LFP, are increasingly used as cathode materials for LIBs due to their thermal stability, which is fundamental from a safety point of view. They also suffer from a lower average voltage in discharge in comparison with other lithiated metal oxides used for Li-ion cells. Martinet *et al.* investigated the method of substituting iron by other transition metals as manganese or cobalt [267]. DoE was applied for multi-transition metal phosphate optimization. The focus was on manganese "rich" compounds in a specific solid solution domain: 0–33 % for both iron and cobalt; 28.4–90 % for manganese. Moreover, boron doping was evaluated up to a maximum of 5 %. Studied materials followed the formula $LiFe_{(1-x-y-z)}Mn_xCo_yB_zPO_4$. The fact that the sum of iron, manganese, cobalt, and boron had to be always equal to 1 led to a "mixture designs" DoE. MINITAB software was used resulting in a set of 21 trials. The trials were performed in random order. Obtained results of specific capacities varied in a range between 14 and 115 mAh g^{-1}. The data were analyzed based on a linear model consisting of 4 linear effects and 6 interactions. It was noticed that results were very sensitive to boron content, so an optimal value was identified (2.5 %). It was notable that high values of discharge capacity were reached at minimum level of manganese. So, an additional test was performed with a further synthesized compound (*i.e.*, $Mn_{0.309}Co_{0.333}B_{0.025}PO_4$) with a result of 123 mAh g^{-1}. Overall, the mixture-design approach was effective in revealing non-intuitive trends, such as the detrimental effect of excess Mn and the narrow optimum in B content, but the relatively simple linear model may underestimate higher-order interactions in the multi-cation space.

SSBs are defined as the next generation of LIBs. They are composed of a composite cathode, a solid electrolyte separator layer, and an anode composite (or Li metal [268]). There are two groups of solid electrolytes: i) sulfides/oxides; ii) polymers. Within this framework, Teo *et al.* investigated a cathode composite preparation process for improved electrochemical performance with a DoE approach [269]. Constituent elements (three types of binders and two types of carbon additives) were selected, and a set of various combinations were tested within SSB full cells with a carbon-coated $Li_4Ti_5O_{12}$ anode. RSM was used to investigate the interactions among variables. Capacity retention was monitored to establish the cell degradation; the specific discharge capacity was investigated to obtain an indication of the practical energy storage capability of the cell. The specific discharge capacity was chosen to represent the electrochemical performance: a slurry-cast cathode with 1.0 wt % polyisobutene and 0.5 wt % vapor-grown carbon fibers was found as the optimum. Binding and punching tests were realized to investigate the processability of the slurry-cast cathodes. The optimum was found with a larger fraction of polymer binder (2.7 wt %). This work highlighted how DoE can simultaneously target electrochemical performance and processability in SSB composites, although the study was restricted to a single cathode chemistry and did not explore scale-up effects.

Among the different types of DoE, optimal combined design uses categoric factors such as the material of a binder, and numerical factors such as the temperature. The response is expressed as a function of different factors based on the empirical model. This approach was applied by Rynne *et al.* to study the effect of electrode formulation on the capacity of LIBs at high currents [270]. The scope of the study was to identify a new binder material and to understand the importance of CAs for high-power applications. After that, electrode capacity under high currents was defined as a response. An optimal combined design, including categoric choices for binder and additives and numerical levels for their loading, was used to balance AM content, electronic conductivity, and high-rate performance. The study showed that the type and amount of CA strongly influence high-current capacity, but it only partially addressed long-term stability under repeated high-power cycling.

LIB is a complex system in which a series of different phenomena occur. These are ions transportation, charges movements, and electrochemical surface reactions that occur within different media inside the electrode. Optimizing the electrode and the microstructures is one of the strategies to overcome performance limitations. To do this, the parametrization of physics-based models is fundamental, but requires expensive investments in terms of economy and time. DoE can be really useful for this aim. Kerdja *et al.* developed a multi-physics model to simulate electrochemical cycling at the electrode microstructure level [271]. Starting from a 2D scanning electron microscopy image of a NMC 111 ($LiNi_{1/3}Mn_{1/3}Co_{1/3}O_2$) electrode, they obtained the microstructure used for their model. More specifically, the electrode was made of commercial NMC 111 (92 %) AM, black carbon (4 %), and PVDF as mechanical binder. The focus was on 5 parameters of interest: i) diffusion coefficient in solid phase (D_s); ii) diffusion coefficient in liquid phase (D_l); iii) effective conductivity of carbon-binder domain (σ_{CBD}); iv) ionic conductivity of electrolyte (σ_{ion}); and v) exchange current density (i_{00ref}). Each parameter was varied around its reference medium value to investigate the influence over discharge capacity and AM lithiation heterogeneities. Then, a combined optimization was performed. Butler-Volmer theory described that the intercalation and deintercalation reactions occurred at the AM. Three levels for each parameter were chosen in accordance with the literature (reference, minimal, and maximal value). Based on the statistical theory, 3^5 combinations were obtained for a total of 243 potential experiments. DoE methodology enabled to reduce them to 46 sets. Pareto diagram was used to classify the different terms according to their normalized effect and to study their positive or negative effect on the measured values. The analysis was conducted with an imposed 2C current of 1.76 mA cm^{-2}. Capacity values for the 46 experiments were classified into three groups: i) inferior to 80 mAh g^{-1}, ii) between 96 and 131 mAh g^{-1}, and iii) superior to 135 mAh g^{-1}. DoE analysis allowed to suppress the non-significant terms. So, the regression equation Y for the discharge capacity was obtained. The exchange current density (i_{00ref}) dominated in terms of influence followed by the liquid diffusion (D_l) and solid diffusion (D_s), all contributing with their linear and quadratic effects. Only a single interaction between D_l and i_{00ref} was included in the model according to its value. Moreover, the effects of D_l and D_s were compared focusing on the three groups of capacity values as follows: 1) 129 ± 2 mAh g^{-1} (D_l and D_s minimal or medium); 2) 117 ± 4 mAh g^{-1} (D_s minimal and D_l medium or maximal); 3) 98 ± 2 mAh g^{-1} (D_l minimal and D_s medium or maximal). In the last two groups, discharge capacity was limited. A further analysis was conducted to compare the influence of solid and liquid diffusion limitations mechanisms focusing on the final lithium concentrations maps of the electrolyte and the AM according to the cases ii) and iii). It was found that many limitations mechanisms co-exist and that lithiation can be limited by liquid diffusion influenced by particles position and by solid diffusion influenced by particles developed surface. Finally, with the help of DoE, the statistical influence of the five parameters was investigated taking into account two types of heterogeneities: local (within a single particle) and global (the whole AM phase). The study consisted in the quantification through a normalized absolute average deviation to quantify the deviation of lithium concentration from its average value. At the end, with the use of Minitab18 software, the optimization of the discharge capacity with the lowest local lithiation heterogeneities (first case) and global (second case) was obtained. In both cases, the predicted ranges of values were really close to the obtained values. The relative error was never larger than 6 %, thus reflecting the effectiveness of the model. This work underscored how DoE can be coupled to microstructural multiphysics models to rank transport and kinetic parameters and to target both capacity and lithiation homogeneity, although it remained limited to a single electrode architecture and charge rate.

The design of LIBs through experiments is almost difficult because the relationship between design variables and performance is not linear. The use of numerical models is a way to overcome this kind of difficulty. Kim *et al.* conducted a study with the use of DoE to analyze the sensitivity of eight cell design factors: anode, cathode, and separator

thickness; anode, cathode, and separator porosity; anode and cathode particle size [272]. The progressive quadratic response surface method (PQRSM) was applied as optimization algorithm to maximize the specific energy density of LIB and then the initial and optimized cells were compared. Factors with a p-value lower than 0.05 were selected: cathode, anode, and separator thicknesses and porosities of cathode and anode. PQRSM optimization process was applied and generated a full quadratic response surface model. The battery cell was subjected to a constant current discharge at a rate of 1C with a cutoff voltage of 3.0 V. The DoE analysis proved to be relevant in studying how to optimize the LIB cells in terms of specific energy density. Also, the polarization phenomenon was reduced by 11.5 %. Overall, this combined DoE–PQRSM framework effectively identified the most influential geometrical parameters and delivered a design with higher specific energy and reduced polarization. However, the optimized configuration was only assessed in terms of initial performance, and additional work would be needed to evaluate its impact on long-term cycling and safety.

Recycling EoL LIBs is necessary because of a series of factors, that are: i) the increasing demand of LIBs for EVs; ii) the serious environmental risks of the electrolyte salt (*e.g.* lithium hexafluorophosphate); iii) the efficiency of the recycling process compared to the extraction one. In the framework of the recycling methods, and specifically of direct recycling one that involves physical and chemical separation phases, Li *et al.* developed a novel presorting process [273]. It focused on the organic solvent extraction method with the aim of evaluating the cathode material retrieval yield by properly changing the processing parameters. The analysis was done using Taguchi DoE method and regression analysis. During the organic solvent extraction process, the binder (commonly PVDF) was dissolved in organic solvents (dimethylacetamide and dimethylformamide were found as the most efficient) through soaking and sonication processes conducted at high temperature. The yield of the cathode retrieved material was estimated as the difference in weight of cathodes before ($W_{initial}$) and after (W_{post}) soaking and sonication as follows:

$$Yield = \frac{W_{initial} - W_{post}}{W_{initial}\ x\ 0.72} \quad \text{(Eq. 28)}$$

considering that weight of cathode electrodes ($W_{initial}$) consisted of 28 % Al current collector and 72 % cathode coating. In order to define the control factors, a 5-factor 2-level PB screening experiment was performed. The records were tested with ANOVA to determine the significance of each factor. The insignificant factors were taken out of the Taguchi experimental design. The most significant resulted to be: i) sonication time; ii) sheet size; iii) solid-liquid weight ratio. TM was then applied to select subsets of 3 control factors at 4 levels. To verify the performance characteristics of the TM, a continuous quality loss function was used. The loss function calculated the deviation of a design parameter from the desired value, which is called the S /N ratio. In the case of yield, which was expected to be the highest possible, the equation was:

$$S/N = -10\ x\ \log\left(\sum\left(1/y_i^2\right)/n\right) \quad \text{(Eq. 29)}$$

with y_i the response of the i_{th} run and n the total number of runs. ANOVA was applied to S/N and the individual contribution (P_i%) of each factor was calculated as follows:

$$P_i\% = \frac{S_{eq}\ SS_i}{S_{eq}\ SS_{total}} \quad \text{(Eq. 30)}$$

with $S_{eq}\ SS_i$ the sequential sum of squares of i_{th} factor and $S_{eq}\ SS_{total}$ the sequential sum of squares of all factors. Results showed that the sonication had the highest contribution of 86.55 %, followed by solid-liquid weight ratio at 7.44 % and sheet size at 4.90 %. This two-step strategy, combining PB screening and Taguchi optimization, provided a clear ranking of the governing parameters for cathode retrieval yield and allowed the authors to maximize recovery using a limited number of experiments. A potential limitation is that the optimal conditions were demonstrated for a specific cathode chemistry and binder system, and their robustness across realistic mixed EoL waste streams remains to be validated.

LFP has been recently investigated as positive AM in substitution of the expensive conventional $LiCoO_2$ due to its high theoretical capacity and stability, low cost, and toxicity. On the other hand, LFP suffers from low Li ionic diffusivity and electric conductivity that imply high overpotential and limited high-rate vehicle performances. Awarke *et al.* applied DoE methodology to generate a model to capture the effects of AM particle size, CB wt %, and carbon nano-coat (CNC) wt % on LFP conductivity [274]. The use of nanosized particles resulted in shorter diffusion distances; moreover, the addition of conductive particles as CB and of a carbon coating on LFP particles surface favored the improvement of overall conductivity. The model was first validated by a series of measurements performed on a PVDF-CB composite at different volume ratios. Then, a full factorial DoE was adopted to capture the variation of conductivity with three factors: i) nano-AM particle size; ii) CB particle wt %; iii) CNC wt %. Three equidistant levels for the AM particle size (50, 100, and 200 nm) and for the carbon coating wt % (0, 1, 3) were defined. Four levels for CB wt % (0, 5, 10, 15) were identified resulting in 36 runs. The FFD, combined with the tunneling-percolation model, enabled the construction of a predictive map of electrode electronic conductivity as a function of particle size and carbon content and highlighted the existence of a percolation threshold for conductive pathways. However, the study exclusively focused on electronic transport and did not directly correlate the optimized formulations with full-cell electrochemical performance or rate capability.

Secondary batteries are very suitable for the implementation of renewable energy into the grid. An alternative to the most common LIBs is represented by SIBs. While lithium offers the highest energy density among present battery technology, but at a high price, sodium is very abundant and so cheaper. The challenge for this type of battery is related to the choice of the anode materials: graphite cannot be used because of its low performance if combined with sodium ions. One of the solutions under study was titanium dioxide (TiO_2), which has a comparable behavior to graphite as anode in LIBs. This is not sufficient because of its intrinsic low electronic conductivity. The use of one-dimensional TiO_2 nanostructures like nanowires, nanorods, or nanotubes (NTs) provides a suitable solution leading to shorter electron diffusion paths. Nanotubular arrays (TiO_2 NTs) made by anodic oxidation represent a very effective strategy. Within this framework, researchers are investigating what is the best polymorph (*e.g.* amorphous or crystalline anatase/rutile) referring to the overall capacity output and long-term performance considering the potential modification to the nanostructure during the cell operation. Bella *et al.* proposed a DoE approach to identify the best TiO_2 polymorph for SIBs [275]. The identified parameters of interest were: i) TiO_2 NTs array length; ii) effect of crystallization. The tests on the sodium cells were performed at ambient temperature through constant current at various regimes between 0.1 and 5 mA cm^{-2}. Using a DoE approach, the growth time of TiO_2 NTs (in a range of 1 to 10 min) and the annealing temperature (in a range between 25 to 600°C) were concurrently varied to study their correlation and weight with the results. 14 sodium cells were assembled and tested using a chemometric approach. The chemometric matrix was filled with data related to the capacity values of the sodium cells at the 85th cycle. This approach consisted in choosing a set of "potential good experiments" included in the experimental domain. After that, a statistical criterion was chosen, *i.e.* the G-efficiency (G_{eff}):

$$G_{eff} = \frac{100 * p}{n * d} \quad \text{(Eq. 31)}$$

where p is the number of terms in the model, n the number of experiments in the design, and d the maximum relative prediction variance

over the candidate set. Higher values of G_{eff} mean higher probability of obtaining the maximum amount of information from the experimental setup. The parameters of the multiple linear regression were $Q^2 = 0.79$ and $R^2 = 0.95$, which are very close to 1 indicating a high quality of the model fitting. It was shown that the anatase phase had a better long-term cycling performance over the amorphous phase (Fig. 4**A**); also, the bad influence of the rutile phase (obtained upon calcination at 600°C) affected the specific capacity output. It was clear that there was a distinction in performance among anatase, rutile, and amorphous TiO_2. In particular, the single-phase anatase polymorph obtained by calcination at 450°C reached the highest specific capacity value after 300 discharge/charge cycles. Also, the presence of rutile formed by calcination at 600°C determined a decrease in the overall specific capacity output. The chemometric DoE allowed the authors to decouple the short-term capacity maximum from long-term stability, demonstrating that although amorphous TiO_2 can deliver high initial capacities, anatase obtained at intermediate annealing temperatures is superior in terms of sustained performance. This work clearly showcased the strength of DoE-based response surface methods for identifying robust operating windows rather than single-point optima.

Copper powders are widely used in batteries and fuel cells due to their high electrical and thermal conductivities. A way to produce fine and ultra-fine copper of high purity is electrolysis, which is one of the most valuable methods because of its low energy consumption, ease of control, and implementation. It is based on two steps: i) nucleation; ii) growth. The best way to produce fine copper particles is to control the relative rates of nucleation and crystal growth. Nekouei *et al.* applied DoE with electrolysis to produce fine copper powders from acid sulfate solutions [276]. Four parameters were studied to optimize the process in terms of purity, current efficiency, and morphology of copper powders: i) current density; ii) copper ion concentration [Cu^{2+}]; iii) sulfuric acid concentration [H_2SO_4]; iv) chloride ion concentration [Cl^-]. Nonregular fractional factorial design was applied instead of a full factorial experiment to reduce the number of runs to 15. Three levels for each parameter were properly selected. The experiments were realized using two copper plates with a purity greater than 99.5 % as anode and cathode immersed in the electrolyte bath at a constant distance of 5 cm in between after being washed with acetone and grinded with sandpaper. A first-order linear polynomial model was defined as follows:

$$Y = b_0 + \sum b_i X_i + \sum b_{ij} X_i X_j + \varepsilon \quad \text{(Eq. 32)}$$

with b_0 the mean of responses of all the experiments, b_i the coefficient representing the effect of the variable X_i, b_{ij} the coefficient representing the effect of the interaction of variables X_i and X_j, ε the experimental error. The most influential parameter was the current density: as it increased, the grain size of the deposit decreased. A higher value of [Cu^{2+}] led to adherent deposit and, consequently, to a coarser particle size. Moreover, the presence of chloride [Cl^-] was ineffective on the particle size. Also, the increase of [H_2SO_4] had a negative effect on the particle size. According to the chemical process and the experiments, overvoltage varied between 1 and 2.2 V. With the increase of the overvoltage, also the powder became finer, but the hydrogen evolution occurred diminishing the current efficiency. Finally, a confirmation test was performed in the optimized conditions according to the model. The predicted particle size was 0.71 μm and the actual experimental result was 0.68 μm. The model was acceptable. This fractional factorial DoE efficiently isolated the dominant electrochemical parameters controlling copper particle size and validated a simple predictive model with good agreement between predicted and measured grain size. The study, however, was conducted in batch conditions and did not fully address how the optimized parameters would translate to continuous or industrial-scale electrolysis lines.

The examples discussed in this section collectively highlight how DoE has become a strategic enabler for the rational development of battery materials. DoE has proven effective across a broad spectrum of chemistries, ranging from phospho-olivine cathodes and layered oxides to advanced formulations for solid-state systems and next-generation sodium-ion anodes; the same applies for supercapacitors [277–286] and other energy-related technologies [287–296]. Across these disparate material families, DoE reliably identifies dominant parameters,

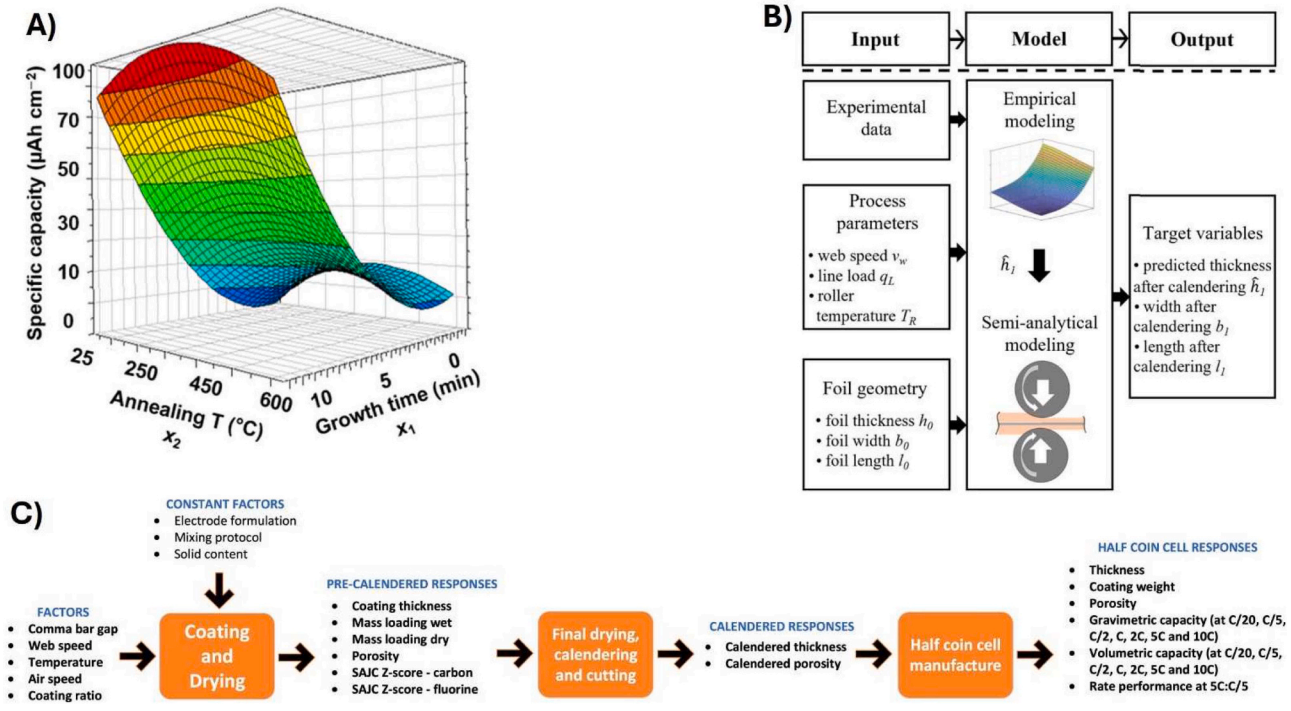

Fig. 4. A) Response surface showing the effect of annealing temperature and growth time on the specific capacity at the 250th cycle of lab-scale TiO_2-based sodium cells. **B)** Schematic structure of the process model for the calendering of lithium foil. **C)** Parameters diagram for the coating-drying process. Adapted and reprinted with permission from [229,278,337,340].

quantifies interactions, and helps determine whether improvements arise from true mechanistic effects or from simple experimental bias. Another key strength of DoE in synthesis optimization lies in its adaptability to both conventional solid-state approaches and emerging methods such as sol-gel, hydrothermal, and electrochemical syntheses [297–306]. This comparative advantage is quantitatively illustrated in Fig. 5, which synthesizes representative studies and shows how substantial reductions in experimental effort are consistently achieved alongside measurable gains in performance and model quality. A key added value emerging from the reviewed literature is the ability of DoE to discriminate between statistically significant and negligible factors, preventing overinterpretation of trends that lack experimental robustness. This methodological discipline is particularly valuable when synthesis involves intertwined variables, such as temperature-time interactions in crystallization or multi-component formulations in composite electrodes. This efficiency directly supports the broader goals of sustainable and circular battery technologies. Looking forward, the synergy between DoE, physics-based modeling, and machine learning (ML) represents a promising evolution, enabling predictive synthesis routes and reducing experimental uncertainty. To fully exploit this potential, future studies should report validation statistics, model adequacy metrics, and cross-checks across multiple synthesis batches, ensuring that optimized recipes are both reproducible and scalable. Overall, DoE emerges not only as a practical optimization tool but as an analytical framework that strengthens experimental rigor, clarifies structure-property relationships, and accelerates the development of robust, high-performance, and sustainable battery materials.

6. Battery safety and management

Battery safety and management are decisive factors in the deployment of electrochemical energy storage across all domains, from consumer electronics to grid-scale systems, and especially in EVs. As energy density rises and pack designs grow more compact, even small deviations in temperature or operating conditions can cause accelerated aging, performance loss, or – in extreme cases – thermal runaway. Guaranteeing safe operation is therefore not only a regulatory requirement, but also essential for user trust and market adoption; the same applies for the whole plethora of current energy technologies [307–318]. In this context, DoE provides a structured way to investigate safety-critical parameters in a systematic and efficient manner. Unlike traditional trial-and-error approach, DoE enables the analysis of multiple interacting factors – such as coolant flow rates, cell spacing, or SoC thresholds – revealing nonlinear effects that strongly influence battery safety. This approach is particularly valuable for thermal management studies, where balancing safety, efficiency, and cost requires careful optimization [319–328]. Overall, DoE-based frameworks help quantify safe operating windows and identify conditions that may trigger hazardous behavior, thereby supporting the design of more robust BMS strategies.

EoL batteries need to be disassembled to recycle and reclaim the materials for both environmental and economical sustainability. Automatic disassembly is important to make the process more precise and faster, but also to avoid health effects on workers who would be exposed to toxic substances. First step of the process is to identify the battery in terms of brand and dimensions to set the cutting machine. Another necessity is to monitor the temperature to prevent spikes. After cutting, quality verification is ensured by computer vision. The deep learning technique adopted by Lu *et al.* was the convolutional neural network for classification and cutting quality control and long short-term memory for temperature spike prediction [329]. In this context, the role of DoE was to tune process parameters under explicitly safety-oriented criteria. To derive the control rules of deep learning tools, DoE was used. Focusing on cutting process, different parameters influenced the maximum cutting temperature: i) cutting speed; ii) feed rate; iii) blade tooth density. Each factor was considered at low and high values. Main and interaction effects were calculated and then ANOVA was applied. As a result, it was demonstrated that it was necessary to reduce cutting speed and blade tooth density, but at the same time feed rate had to be controlled through an optimized strategy to compensate for the loss in efficiency and safety caused by the minimalization of the other two factors. This study illustrates how DoE can be combined with ML to explicitly trade off throughput and thermal safety during automated battery disassembly.

Analytical DoE was applied by Sun and Dixon to study the effects of cooling strategies on a battery pack [330]. The objective was to identify the optimal configuration and geometry of cooling ducts, plates, and control modules to maximize battery pack capacity and durability. The design space for each design factor was uniformly divided and combined to generate the first design matrix using Latin-hypercube technique. Then, an optimization process was applied to design an optimal design matrix that uniformly contained the design points. The model was then validated by running a series of physical tests on a “U-type cooled” battery pack. Results were in agreement with the model with a maximum deviation of the predicted transient temperature between the simulation and physical test of less than 0.5°C. Next step was the investigation of cooling duct geometry. “Z-type” cooling duct was investigated, in which cool air flowed through the upper channel and

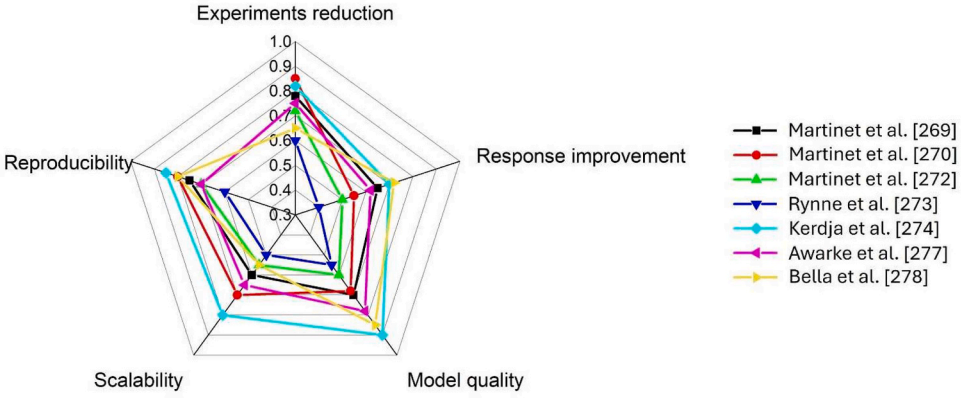

Fig. 5. Radar plot comparing representative DoE studies in the field of battery materials synthesis and optimization. The five axes represent key performance indicators: reduction in experimental effort relative to full-factorial or OFAT approaches (Experiments reduction), improvement of the targeted response after optimization (Response improvement), quality of the statistical model (Model quality), relevance for scale-up and manufacturing (Scalability), and reproducibility/robustness of the experimental strategy (Reproducibility). Each polygon corresponds to a representative literature study. Values are reported on a normalized, semi-quantitative scale to enable cross-study comparison. While absolute metrics differ among systems, the plot highlights consistent trends showing how DoE enables substantial experimental savings while achieving significant performance gains and robust predictive capability.

exited from the opposite side of the bottom channel. This configuration resulted in a great disparity of flow rate between inlet side and outlet side. To improve this, cross-section of the channels was varied along the battery pack to uniform the pressure drop of inlet and outlet sides. The height of the inlet and outlet and the heights of closed ends of upper and lower ducts were defined as design factors for DoE. By reducing the closed ends of upper and lower ducts and increasing the inlet and outlet ends, the lumped temperature variation across the pack was reduced as desirable. In this way, the lumped cell temperature variation across the modified battery pack was reduced from 10.8°C (conventional "Z-type" flow battery pack) to 3.6°C. This quantitative reduction in temperature spread directly supports safer and more homogeneous pack operation.

Charge/discharge process generates heat due to mainly ohmic losses leading to self-heating phenomenon generated by the movement of the ions into the cell. SoC, terminal voltage, and temperature must be predicted and monitored for safety and lifetime requirements on electrical energy storage technology. Initially, single-particle approach was used. A new and easy-to-handle lumped parameter model was investigated by Schmidt *et al.* to better reproduce input/output behavior of a commercially available lithium-ion cell [331]. A small set of experiments was chosen, and it was sufficient to the whole operating range of the device. This was obtained thanks to the application of DoE. By effectively analyzing and identifying the parameters in the model and by combining different methods such as the FIM technique along with sensitivity analysis, they estimated how each parameter could be identified based on the available measurement data. With this approach, they selected a few key experiments that were enough to fully define the model parameters. Such parsimonious experimental plans are particularly relevant when safety-critical models must be calibrated over wide operating windows without excessive testing.

A coupled electro-thermal model for an air-cooled pack was established by Xie *et al.* to better predict the temperature dynamics of an air-cooled battery back [332]. This is critical for the battery thermal management system (BTMS), which has the function of ensuring safety and efficiency of the battery pack. A current distribution model was defined to calculate the distribution of the branch current due to inhomogeneous cooling, then the model was coupled with the thermal one to improve the prediction of the heat production inside the cell. Battery consistency was integrated into both the structural design and determination of operating parameters of the BTMS. Two DoEs were applied to optimize the air channel. Firstly, an FFD was used to make the structural parameters cover the full optimization range and obtain the approximate location of the optimal solution. Secondly, the first DoE results were analyzed to determine the correct direction, and the orthogonal DoE was employed to search for the exact position of the optimal air channel structure. The pack thermal model was solved through CFD method: the velocity inlet was used for the air entrance and the pressure outlet for the air exit. The simulated terminal voltage showed similar evolution compared to the tested one. Also for the temperature, the simulated one was similar to the tested one. DoE was then used to optimize the distance (horizontal S_x and vertical S_y) between two cells to reduce the cell temperature and the temperature difference among cells. The process was divided into two phases. The first phase consisted of the application of an FFD to determine which distance (among S_x and S_y) had the most influence: S_x and S_y were defined as the two factors. Three levels were chosen within 21–26 mm due to installation space limitations. The range and variance analyses were performed. S_y revealed to show the most significant impact on cooling performance. The second DoE was applied to S_x, while S_y was fixed to 21 mm according to the lowest registered values of the average SoC difference and maximum cell temperature. The three values S_{x1}, S_{x2}, and S_{x3} were chosen as the factors of the second DoE. The orthogonal experiment design was applied to obtain representative cases and reduce the computational effort. The best case was found with $S_{x1} = 21$ mm, $S_{x2} = 26$ mm, and $S_{x3} = 26$ mm. Overall, the study shows how sequential DoE (screening followed by refinement) can be used to shape pack geometry and improve cooling uniformity under realistic constraints.

The series hybrid electric bus is an EV in which all the propulsion energy is produced by the electric machine and is characterized by high power and energy demands. Commonly, the ESS of EVs is a battery due to its portability and low cost. The peak-to-average ratios for a common battery are between 0.5 and 2. An alternative to batteries is the ultra-capacitor (UC), which has good life cycle and peak-to-average ratios of 10 to 12. Use of both batteries and UC is defined as hybrid ESS (HESS); it was adopted to reduce the current stress in the batteries decreasing size and costs and improving their lifetime. Tehrani *et al.* compared a traditional ESS (based on only batteries) with 2 HESSs: a UC-based power distribution control strategy (PDCS) to use UC as prior ESS and a battery-based PDCS to use battery as prior ESS [333]. Two different bus driving cycle profiles were defined according to the collected data of two different cities, Tehran and Manhattan. 4 criteria were chosen to compare the performance of PDCS of ESS and HESSs: i) cycle count; ii) the sum of over-continuous current (Ah); iii) the sum of brake resistor power (kWh); iv) the sum of shortage power (kWh). Cycle count method was utilized to make an estimation of the number of charge/discharge cycles of batteries in real driving cycles. The sum of over-continuous current was an indicator of high current stress of battery, which reduced its lifetime. The sum of brake resistor power indicated the energy saving loss. The sum of shortage power was the difference between the ESS power demand and the ESS power provided. A DoE was applied to optimize the parameters of the battery-based PDCS. Results indicated that UC-based HESS was the best configuration for Tehran driving cycle, while battery-based HESS performed better for Manhattan driving cycle. This highlights how DoE-assisted control tuning can adapt hybrid storage architectures to specific duty cycles, reducing current stress and indirectly improving safety margins.

BMS is the supervising control unit that processes the actual status of the battery cells sharing the data with the other controllers of the vehicle. To do this, a mathematical model describes the nonlinear dynamic behavior of the cell terminal voltage in dependance of charge/discharge current with the objective to predict the dynamics of the battery in the specific environmental and loads conditions. SoC is not directly measurable, so a series of modeling approaches exists: i) EMs; ii) ECMs; iii) black/grey box techniques-based modeling. Hametner *et al.* used the third approach to define a nonlinear model structure and automated nonlinear observer design [334]. DoE played a critical role in defining SoC excitation signal of the cell current. The signal was adjusted to the specific prior process model: in this way, the model parameters could be estimated from measured data. The optimization was based on a linear dynamic cell model. Then, the FIM was used, *i.e.* a tool to measure the information content of the excitation signal. The definition of the FIM was based on the partial derivative of the model output with respect to the model parameters. The following conditions were adopted to optimize the cell current excitation signal: i) SoC operating range was defined and included in experimental design; ii) cell current excitation predefined levels were adopted; iii) hysteresis and relaxation phases were applied which consisted in zero current phases between charge/discharge pulses. The resulting optimized excitation profiles improved observability of internal states, which is crucial for robust SoC estimation in safety-relevant BMS functions.

Battery charging is an imperative research topic. Improving battery charging means increased battery charge, energy efficiencies, life cycle, and – at the same time – reduced charge time, but also the possibility to avoid thermal runway. LiPBs, which are constituted of gel-like polymer electrolytes (instead of LIBs that use liquid electrolyte), have stringent charging algorithms. The most known and used is the CCCV. Pulse charging algorithm can improve the battery charging phase involving the use of charge current pulses. As shown by Amanor-Boadu and Guiseppi-Elie, the use of pulse charging algorithm ensures that the Li ions electrochemically produced during each pulse migrate from the cathode to the anode and successfully intercalate without accumulation

on the electrode surface of the ions produced by the successive pulse [335]. The investigation of the best combination of these parameters can be performed with OAs, which allow at the same time to reduce the number of experiments and to get comparable results to FFD. The chosen parameters were duty cycle of the pulses, frequency, and the ambient temperature at which the battery was charged. Frequency and duty cycle had the greatest impact on the battery performance. Moreover, a confirmation experiment was performed and compared with the benchmark CCCV charging algorithm. Pulse charge led to an improvement of 12 % in battery energy efficiency, 2 % in battery charge efficiency, and to a 48 % reduction in charging time. The impact of the peak amplitude of pulse charging current was also investigated and, even if the higher the peak, the faster the charging time, the peak charge current amplitude had to be within the specification of the battery to avoid damages caused by the increase of its surface temperature. Referring to the life cycle, DoE was applied, more specifically a 36-row OA was constructed. At 23°C, both CCCV charged battery and pulse charged battery revealed similar impedance values. Frequency and duty cycle had the greatest impact on life cycle. 12 kHz and 50 % duty cycle were the best values leading to the lowest level of impedance, which meant the highest conversion of input to stored energy and equal time allocated to anode and cathode reversal. This set associated with pulse charging allowed for 100 more cycles with respect to the same set associated with CCCV charging method. Overall, the study showed that DoE-designed pulse protocols can simultaneously target fast charging, higher efficiency, and extended life, while keeping surface temperatures within safe limits. In this context, the concept of smart charging becomes prevalent in order to improve the efficiency of the batteries and reduce their progressive decay.

LIBs suffer from initial capacity losses caused by the formation of the SEI layer. This effect consumes Li-ions with the result of reducing the energy density and the life cycle. An approach to compensate this is the prelithiation, which consists in adding lithium to the cell before the first charge and discharge cycle of the formation process. To do this, Stumper *et al.* investigated a roll-to-roll process for direct prelithiation focusing on the compaction properties of the electrodes [336]. The process was realized by calendering a lithium foil until reaching target thickness. DoE was applied to analyze the process. As shown in Fig. 4**B**, an empirical model first and a semi-analytical model then were used. Input variables were geometry and material characteristics, while the output was the thickness and the new geometry of the foil after calendering. For the empirical model, an FFD was carried out to define the range of values for each input parameter represented in the form of vectors. Various assumptions were made as follows: i) lithium is isotropic, so its deformation does not depend on direction; ii) density of lithium does not change before and after calendering, so the volume constancy is valid; iii) there is no relative sliding between lithium foil and the carrier foil and between the calenderer roller and the rolled material; iv) the temperature distribution is uniform; v) no deformation of the carrier foil (made of copper) occurs due to the line loads applied. Moreover, the web speed, the input thickness of the Li foil, and the temperature of the roller were kept constant and equal to 0.1 m min^{-1}, 50 μm, and 20°C, respectively. In addition to the empirical model, a semi-analytical modeling was carried out to verify the length and the width of the foil after calendering. The data calculated with such a model offered a very good approximation of the data measured during the tests. A validation of the empirical model was done by considering the residuals *r* in the 3D space. For the largest residuum, the deviation was about 6.3 % referred to the measured value. Regression coefficient was calculated to estimate the quality of the regression. A result of 0.99 was achieved, which confirmed the high quality of the proposed model. Such a statistically optimized prelithiation step is crucial to control initial lithium losses in a reproducible way and to avoid uncontrolled metallic lithium deposition.

The rise in global energy demand (expected to increase by 11–27 % until 2050) due to socioeconomic development and climate warming emphasizes the urgency of addressing battery calendar and cycle life in a safety-oriented perspective. Corrosion, particularly affecting the aluminum current collector in the positive electrode, is a significant factor influencing the calendar life of batteries. The hydrolysis of lithium hexafluorophosphate ($LiPF_6$) produces compounds that deteriorate battery performance. The TM was employed to design experiments targeting the corrosion process in LIBs, aiming to extend their lifespan [337]. The factors investigated were the type of lithium salt, concentration of ethylene carbonate in the electrolyte, and operating temperature. TM involves calculating averages and standard deviations to determine the S/N and sensitivity to noise ratio. Objective functions were created based on optimization criteria, such as 'the smaller, the better' or 'the bigger, the better'. ANOVA assessed the influence of control and noise parameters on the corrosion process. The study utilized three lithium salts, *i.e.* $LiPF_6$, $LiB(C_2O_4)_2$ (LiBOB), and $LiN(CF_3SO_3)_2$ (LiTFSI), and cyclic voltammetry and EIS were performed at various temperatures. Results indicated that corrosion was more pronounced in electrolytes containing $LiPF_6$, suggesting that the composition of the electrolyte had a more significant impact than temperature on aluminum current collector behavior. An ECM helped to analyze impedance data, showing variations in resistance with the progress of the experiment. The corrosion current densities were the lowest with LiBOB and the highest with LiTFSI, exhibiting temperature dependence. TM predictions aligned with experimental findings, suggesting TM reliability in guiding electrochemical measurements. Overall, TM-based DoE quantified that lithium salt type had the most significant influence, followed by temperature and solvent composition, providing a statistically robust guideline for electrolyte formulation under corrosion constraints.

Large format LIBs suffer from large temperature differences due to their large dimensions. This causes rapid reduction in cell capacity. Newman's model, which was the most used in last years, had the limitation of predicting the temperature distribution only in the thickness direction of the LIB cell. 3D electrochemical/thermal models were introduced to dimensionally extend the temperature distribution prediction. Lee *et al.* proposed a new approach based on DoE procedure and starting from the Rao and Newman's electrochemical/thermal model to analyze the temperature distribution of a 45 Ah LFP/graphite pouch cell [338]. The negative and positive tab attachment positions and cell aspect ratio were defined as design factors, while maximum and minimum temperatures in LIB cell and the difference between maximum and minimum temperature were identified as responses. The EM allowed for the calculation of the SoC, the potential distribution, the current density distribution, and the heat generation, while the thermal model was able to calculate the temperature distribution. The cell aspect ratio was defined as the ratio of the width to the length, while the tab attachment positions were defined as the ratio of the attached position to the attachable range. The sampling points were defined performing an FFD on three factors with five levels. ANOVA analysis was carried out to determine if the design factors were statistically significant. The cell aspect ratio was assumed as the most effective followed by the positive tab attachment position. Moreover, the fact that the positive tab was made of aluminum led to an increase of its effect on the difference between the maximum and the minimum temperature. The study clearly showed that geometric design factors, often treated as fixed constraints, strongly affected in-plane temperature gradients and therefore had to be included as explicit decision variables in safety-oriented pack design.

Electrode manufacturing plays an important role in final LIBs performance. There are many steps involved in this process, each stage being critical to the final result. Romàm-Ramìrez *et al.* applied DoE methodology to a pilot scale manufacturing of NMC622 cathodes to study the main influencing process variables of the coating-drying step [339]. Process variables were identified as: i) comma bar gap; ii) web speed; iii) coating ratio; iv) drying temperature; v) air speed. Physical and chemical electrode properties were thickness, mass loading, porosity, gravimetric capacity, volumetric capacity, and rate performance. Multiple linear regression analysis was performed using a PB

experimental design. Dependent variables were measured at three different steps: before calendering, after final drying, and on the coin cells produced from the strips (Fig. 4**C**). From ANOVA, coefficient of determination (R^2) and predicted R^2 (R^2_{pred}) were obtained to establish the predictive capabilities of the model. The analysis comprised 12 experimental runs and it was divided into two parts. Bar gap and coating ratio were classified as the most influencing factors for the thickness, mass loadings, and cell coating weight showing a closely link to battery performance. A regression analysis was also performed to determine possible relationship between electrochemical properties on half of coin cells and physical characteristics by taking into account coating weight and porosity as input variables. Coating weight was identified as the most important property. With thinner electrodes, superior performances were obtained. Porosity was critical only at the lower C-rates. In terms of safety and management, this DoE-based screening provided quantitative process windows for coating uniformity, indirectly constraining local current densities, and hotspot formation in large-format cells.

The broad working temperature range for LIBs is -20 to 60°C, while the optimum range is limited from 15 to 35°C. Above the high limit, the cells are subjected to capacity degradation, while at lower temperatures they are affected by an increase of internal resistance. Active and passive cooling techniques were studied in this regard. In the case of EVs, the use of a passive cooling system is considered to reduce power consumption. Phase change materials (PCMs) were used in this system since they can absorb the excess heat generated during charge/discharge cycles. From another point of view, PCMs are limited by their low thermal conductivity. So, additional dissipation media as fins and heat pipes are coupled as secondary heat sinks. Verma *et al.* developed a model where PCM layers were inserted in between the cells of a battery module coupled with an array of longitudinal fins [340]. The thermal performance was defined by evaluating five parameters: i) volume average temperature of the four cells constituting the battery pack after 1200 s; ii) active time as the time after which the PCM had to be solidified for the next discharge cycle; iii) temperature uniformity as variation between the maximum and minimum temperature; iv) heat duty as the ratio of heat flux to a body surface and the body mass that absorbs the incoming heat; v) non-dimensional temperature drop as the ratio of actual and maximum temperature difference in the battery pack. This study exemplified how DoE on non-dimensional retrofit parameters can guide lightweight passive cooling solutions that keep cells within the optimal operating window while minimizing additional mass.

Redox flow batteries (RFBs) are recently emerging as a valid alternative to Li-based counterparts. They are subjected to a characterization process that is composed of a large number of charge/discharge cycles to measure battery capacity and round-trip efficiency (RTE). This procedure requires too much time. The implementation of a method to model the RFB performances with a limited set of factors and through the use of DoE methodology was investigated by Delbeke *et al.* [341]. The study was based on two basic principles: the Pareto principle, which declares that any real process is mostly driven by a limited number of important factors, and the Taylor's theorem, which states that any function can be approximated by a polynomial (of first, second, or higher order) in a sufficiently small area. Various parameters influenced the battery performance, but some of them could not be controlled by RFB operators so they were discarded from the DoE. The chosen RFB output parameters were the DC discharge capacity and the DC RTE as follows:

$$\eta_{DC,i} = \frac{Scaled\ DC\ discharge\ capacity_i}{Scaled\ DC\ charge\ capacity_i} \quad \text{(Eq. 33)}$$

DoE was applied as follows: first of all, 4 experiments were conducted on the single RFB module using D-optimal design scheme to identify the most influential controllable parameters in the system. This set of experiments included 4 of 6 controllable parameters: i) charge rate; ii) discharge rate; iii) minimum SoC; iv) maximum SoC. Among them, the most dominant turned out to be charge and discharge rate. Electrolyte temperature, which was uncontrollable but easy to measure, had a high influence on the process. A second set of experiments was run with the same controllable parameters of the first set, but adding an I-optimal extension to study the potential improvement of the models. The third set of experiments was focused on finding a way to properly quantify the influence of the temperature on the battery performance. Resting time was varied to let the electrolyte cool off. The adopted range was 15 to 720 min. The resting time at maximum SoC was detected as statistically consistent parameter for predicting DC efficiency and DC discharge capacity. Based on the insights of the previous designs, the most influential controllable parameters were identified, and a corresponding orthogonal characterization experiment could be conducted with a reduced time of 6.5 days with respect to nearly 13 days of classical characterization experiments. This DoE-based protocol halved the characterization time while preserving predictive power, which is crucial to safely qualify new RFB chemistries and operating windows without excessively long test campaigns.

The studies presented in this section clearly demonstrate how the application of DoE has brought a new level of rigor and efficiency to the investigation of battery safety and management. From the optimization of automatic disassembly processes to the fine-tuning of cooling architectures and the design of predictive electro-thermal models, DoE has proven to be a versatile tool capable of handling the complexity of safety-critical variables. By combining screening, response-surface modeling, robust design, and OAs, DoE enables the identification of safe operating windows and the quantification of trade-offs between performance, lifetime, and safety with a reduced experimental burden. Looking ahead, the integration of DoE with digital technologies such as ML, cyber-physical systems, and advanced multiphysics simulations will further expand its potential. In disassembly and recycling, for instance, DoE could be combined with real-time sensor data to dynamically adapt cutting or sorting processes, ensuring both worker safety and material recovery efficiency. The activities related to DoE for sensors design are truly numerous in the literature [342–351]. In thermal management, coupling DoE with high-fidelity digital twins may allow for the design of adaptive cooling systems that respond in real time to changing load conditions. Moreover, the rising importance of hybrid energy storage architectures, as well as the diversification toward sodium-ion and redox flow batteries, opens new frontiers where DoE can serve as a methodological backbone to ensure safety across chemistries and formats. Ultimately, the future of battery safety will depend not only on better materials and smarter algorithms, but also on the capacity to frame safety as an optimization challenge to be solved systematically. In this sense, DoE can act as a bridge between experimental evidence and predictive analytics, providing statistically robust datasets for the calibration and validation of safety-relevant models. As battery technologies scale up to meet global energy demands, its role will become even more critical in guiding the design of safer, more reliable, and more sustainable ESSs.

7. Perspective

The rapid expansion of battery technologies across synthesis, manufacturing, deployment, and EoL management calls for a more systematic and harmonized use of DoE. While the studies reviewed in this work clearly demonstrate the value of statistically structured experimentation, the field still lacks shared protocols, interoperable datasets, and a unifying roadmap. Moving beyond isolated applications requires coordinated methodological advancement. In this section, three pillars that could anchor the next phase of DoE-enabled battery research are outlined.

First, a field-specific roadmap for DoE along the battery value chain. Across each segment of the battery ecosystem, DoE can support different classes of decisions, and different design families are appropriate:

- Materials synthesis: typical factors include precursor ratios, annealing profiles, solvent composition, and dopant levels; responses span phase purity, particle morphology, conductivity, and interface stability. Early-stage exploration benefits from screening designs (PB, fractional factorial), followed by RSM or mixture designs for compositional optimization. Sequential designs can reduce experimental load and allow for the rapid elimination of unpromising regions.
- Electrodes and cells manufacturing: process parameters such as coating speed, drying temperature, porosity, calendering pressure, and binder/carbon composition require combined designs (categorical + continuous factors) and multi-stage DoE to account for process-structure-performance coupling. Here, linking DoE with physics-based manufacturing models can substantially reduce experimental burden.
- Performance and aging testing: temperature, SoC windows, CR, duty cycling, RMS current, and stress factors are high-dimensional variables that influence capacity fade and impedance rise. Efficient identification of dominant effects requires optimal designs, while robust designs can quantify sensitivity to uncontrolled variability (*e.g.*, ambient fluctuations). Integrating DoE with aging models and digital twins can support accelerated testing protocols.
- Batteries management, estimation, and safety: parameter identification for BMS algorithms, excitation signal optimization, and thermal management architecture design are ideally suited to model-based DoE, where Fisher information and optimal input design are used to define minimally redundant test sequences. In fault diagnostics, DoE can aid in creating well-conditioned datasets for algorithm training and validation.
- Recycling, direct regeneration, and disassembly: process variables include solvent systems, reaction times, temperatures, mechanical separation strategies, and pre-treatments. Because sustainability metrics must be considered alongside efficiency, multi-objective DoE is essential. Coupling DoE with ML surrogate models can drastically shorten the optimization of eco-efficient recycling routes.

Beyond its traditional role in experimental planning, DoE can play a concrete enabling role in the development of adaptive algorithms for BMSs. In this context, DoE is not intended as an online optimization tool, but rather as an upstream methodology to generate compact, validated, and interpretable surrogate models from structured experimental datasets. DoE-derived models trained on systematic aging and performance campaigns can be embedded within BMS architectures to define safe operating envelopes in terms of temperature, current, and SoC windows. These models can inform rule-based or model-predictive control strategies by explicitly quantifying parameter sensitivities and interaction effects, thereby enabling adaptive adjustment of operating limits as a function of usage history or environmental conditions. In this way, DoE provides a statistically grounded bridge between extensive offline experimentation and real-time, safety-critical decision making without increasing onboard computational complexity.

The integration of DoE with ML represents another key direction for future battery research. Rather than replacing DoE, ML can be most effectively deployed when built upon DoE-generated datasets, which are information-dense, balanced, and explicitly designed to capture interactions. In practical workflows, DoE can be used in an initial exploration phase to identify dominant factors, relevant interactions, and suitable parameter ranges; the resulting datasets can then serve as high-quality training and validation inputs for ML models aimed at prediction, classification, or optimization. Sequential or adaptive DoE strategies may further refine the design space as ML models highlight regions of high uncertainty or sensitivity. This hybrid DoE-ML approach offers a clear roadmap toward scalable, interpretable, and physically consistent data-driven models across materials development, manufacturing optimization, and battery management.

The second pillar is given by a proposal for an open, curated database of DoE-based battery studies. Indeed, a major limitation in today landscape is the absence of a shared, structured repository of DoE applications in batteries. A community-driven, open-access database is here proposed, where each entry includes: i) Design metadata: type (*e.g.*, PB, CCD, D-optimal), size, factor definitions, levels and ranges, constraints, randomization strategy; ii) Response definitions and measurement protocols: including units, instrumentation, calibration, and uncertainty reporting; iii) Model structure and validation: regression form, interaction terms, goodness-of-fit metrics (R^2, Q^2, RMSE), residual analysis, and cross-validation methods; iv) Reported optima and practical significance: including operating windows, confidence intervals, and scalability considerations; v) Application domain: synthesis, manufacturing, aging, safety, BMS, or recycling; vi) Industrial relevance: process throughput, cost implications, environmental constraints, and robustness to variability. Such a database would enable meta-analysis across chemistries and processes, reveal recurring influential factors, identify underexplored parameter spaces, support ML-assisted design of new DoE campaigns, and serve as a foundation for reproducible science.

The last pillar aims at standardized DoE reporting protocols in battery research. To ensure reproducibility, comparability, and industrial uptake, a reporting checklist for all future battery-related DoE studies is here proposed: i) Clear definition of factors (continuous/categorical), factor ranges, and justification of boundaries; ii) Explicit design description, including the full design matrix or a complete level-coding table; iii) Model equations with identification of linear, quadratic, and interaction terms; iv) Statistical validation, including residuals, LOF tests, prediction intervals, and sensitivity analysis; v) Practical significance, not only statistical significance: interpretation of optima, operating windows, and scaling considerations; vi) Discussion of reproducibility and robustness, including how noise factors were controlled, randomization applied, and uncertainties quantified; vii) Recommendations for follow-up designs, highlighting where sequential or adaptive DoE could refine current findings. Standardizing these elements would accelerate knowledge transfer across laboratories and industries, facilitate automated data extraction for databases, and support the future integration of DoE into autonomous experimentation platforms.

DoE has the potential to evolve from a specialized statistical tool into a unifying methodological framework for the battery field. By adopting a shared roadmap, contributing to an open community database, and converging toward standardized reporting protocols, the community can transition from isolated case studies to a coordinated, data-rich research ecosystem. In this vision, DoE becomes the backbone linking experiments, models, and ML, ultimately enabling faster, safer, and more sustainable battery innovation.

8. Conclusion

This review has illustrated the multifaceted role of DoE in the development and optimization of electrochemical batteries. Across materials synthesis, performance and aging studies, safety management, and recycling processes, DoE has consistently proven its ability to extract meaningful insights from complex experimental spaces, identify critical variables, and accelerate optimization. By reducing redundancy and improving reproducibility, DoE bridges laboratory-scale research with industrial scalability, contributing to both scientific discovery and technological deployment.

The evidence collected highlights that DoE is not merely a statistical tool, but a strategic enabler for innovation in the field of energy storage. Its applications extend from optimizing electrode formulations and cathode chemistries to designing safer pack architectures and improving recycling efficiencies. The systematic frameworks provided by DoE enhance the robustness of conclusions, foster comparability across studies, and lay the groundwork for reproducible research in an increasingly interdisciplinary field.

In conclusion, DoE emerges as a cornerstone methodology for

advancing the reliability, sustainability, and performance of current and future battery technologies. As the energy transition accelerates, the approaches and insights summarized in this review will remain fundamental to guiding research and development, supporting the creation of safer, more efficient, and environmentally responsible electrochemical ESSs.

CRediT authorship contribution statement

Diego Pugliese: Writing – original draft, Supervision, Conceptualization. **Roberto Staffieri:** Writing – review & editing, Conceptualization. **Federico Bella:** Writing – original draft, Supervision, Project administration, Funding acquisition, Conceptualization.

Declaration of competing interest

The authors declare that they have no known competing financial interests or personal relationships that could have appeared to influence the work reported in this paper.

Acknowledgments

This study was carried out within the «GREEN2MOVE» project [FISA-2022-00983] funded by Ministero dell'Università e della Ricerca (Bando FISA 2022). The support from the European Union—NextGenerationEU under the National Recovery and Resilience Plan (NRRP), Mission 04 Component 2 Investment 3.1 | Project Code: IR0000027—CUP: B33C22000710006—iENTRANCE@ENL: Infrastructure for Energy TRAnsition aNd Circular Economy @EuroNanoLab is gratefully acknowledged.

Data availability

No data was used for the research described in the article.

References

[1] F. Li, Y. Wang, R.-S. Bai, X.-X. Wang, M.-L. Li, J.-J. Xu, Resolving the cathode passivation of lithium–oxygen batteries with an amination SiO_2/TiO_2 functional separator, J. Power. Sources 483 (2021) 229180, https://doi.org/10.1016/j.jpowsour.2020.229180.

[2] K.S.R. Mawonou, A. Eddahech, D. Dumur, D. Beauvois, E. Godoy, State-of-health estimators coupled to a random forest approach for lithium-ion battery aging factor ranking, J. Power. Sources. 484 (2021) 229154, https://doi.org/10.1016/j.jpowsour.2020.229154.

[3] L. Li, Y. Shan, X. Yang, New insights for constructing solid polymer electrolytes with ideal lithium-ion transfer channels by using inorganic filler, Mater. Today Commun. 26 (2021) 101910, https://doi.org/10.1016/j.mtcomm.2020.101910.

[4] F. Fu, W. Lu, Y. Zheng, K. Chen, C. Sun, L. Cong, Y. Liu, H. Xie, L. Sun, Regulating lithium deposition via bifunctional regular-random cross-linking network solid polymer electrolyte for Li metal batteries, J. Power. Sources. 484 (2021) 229186, https://doi.org/10.1016/j.jpowsour.2020.229186.

[5] E. Zhao, Y. Guo, Y. Xin, G. Xu, X. Guo, Enhanced electrochemical properties and interfacial stability of poly(ethylene oxide) solid electrolyte incorporating nanostructured $Li_{1.3}Al_{0.3}Ti_{1.7}(PO_4)_3$ fillers for all solid state lithium ion batteries, Int. J. Energy Res. 45 (2021) 6876–6887, https://doi.org/10.1002/er.6278.

[6] A.L. Mong, Q.X. Shi, H. Jeon, Y.S. Ye, X.L. Xie, D. Kim, Tough and flexible, super ion-conductive electrolyte membranes for lithium-based secondary battery applications, Adv. Funct. Mater. 31 (2021) 2008586, https://doi.org/10.1002/adfm.202008586.

[7] J. Chen, Y. Fu, F. Sun, Z. Hu, X. Wang, T. Zhang, F. Zhang, X. Wu, H. Chen, G. Cheng, R. Zheng, Oxygen vacancies and phase tuning of self-supported black TiO_{2-X} nanotube arrays for enhanced sodium storage, Chem. Eng. J. 400 (2020) 125784, https://doi.org/10.1016/j.cej.2020.125784.

[8] X. Casas, M. Niederberger, E. Lizundia, A sodium-ion battery separator with reversible voltage response based on water-soluble cellulose derivatives, ACS. Appl. Mater. Interfaces. 12 (2020) 29264–29274, https://doi.org/10.1021/acsami.0c05262.

[9] H. Wang, J. Xiong, X. Cheng, G. Chen, T. Kups, D. Wang, P. Schaaf, Hydrogen–nitrogen plasma assisted synthesis of titanium dioxide with enhanced performance as anode for sodium ion batteries, Sci. Rep. 10 (2020) 11817, https://doi.org/10.1038/s41598-020-68838-x.

[10] R.R. Maça, D. Cíntora Juárez, M. Castillo Rodríguez, V. Etacheri, Nanointerface-driven pseudocapacitance tuning of TiO_2 nanosheet anodes for high-rate, ultralong-life and enhanced capacity sodium-ion batteries, Chem. Eng. J. 391 (2020) 123598, https://doi.org/10.1016/j.cej.2019.123598.

[11] C. Bao, B. Wang, P. Liu, H. Wu, Y. Zhou, D. Wang, H. Liu, S. Dou, Solid electrolyte interphases on sodium metal anodes, Adv. Funct. Mater. 30 (2020) 2004891, https://doi.org/10.1002/adfm.202004891.

[12] J.I. Kim, Y.G. Choi, Y. Ahn, D. Kim, J.H. Park, Optimized ion-conductive pathway in UV-cured solid polymer electrolytes for all-solid lithium/sodium-ion batteries, J. Membr. Sci. 619 (2021) 118771, https://doi.org/10.1016/j.memsci.2020.118771.

[13] P. Kuray, W. Mei, S.E. Sheffield, J. Sengeh, C.R.F. Pulido, C. Capparelli, R. J. Hickey, M.A. Hickner, Ion transport in solvated sodium-ion conducting gel polymer electrolytes, Front. Energy Res. 8 (2020) 569387, https://doi.org/10.3389/fenrg.2020.569387.

[14] J. Chen, S. Ebrahimi-Koodehi, B. Iliev, Y. Steinberg, M. Leskes, T.J.S. Schubert, E. Castillo-Martínez, D. Bresser, M. Zarrabeitia, Polymer electrolytes for potassium batteries: incorporating ionic liquids to enhance the room temperature ionic conductivity, J. Mater. Chem. A 13 (2025) 25476–25488, https://doi.org/10.1039/D5TA02762D.

[15] I. Dueramae, M. Okhawilai, P. Kasemsiri, H. Uyama, R. Kita, Properties enhancement of carboxymethyl cellulose with thermo-responsive polymer as solid polymer electrolyte for zinc ion battery, Sci. Rep. 10 (2020) 12587, https://doi.org/10.1038/s41598-020-69521-x.

[16] L.K. Nivedha, M. Raja, K. Ramanujam, Interplay of the functional units of a binder in the oxygen reduction process of zinc-air battery, Catal. Today 370 (2021) 66–74, https://doi.org/10.1016/j.cattod.2020.09.022.

[17] G. Wang, Y. Wang, B. Guan, J. Liu, Y. Zhang, X. Shi, C. Tang, G. Li, Y. Li, X. Wang, L. Li, Hierarchical K-birnessite MnO_2 carbon framework for high-energy-density and durable aqueous zinc-ion battery, Small 17 (2021) 2104557, https://doi.org/10.1002/smll.202104557.

[18] Y. Zhang, J. Qin, M. Batmunkh, W. Li, H. Fu, L. Wang, M. Al-Mamun, D. Qi, P. Liu, S. Zhang, Y.L. Zhong, Scalable spray drying production of amorphous V_2O_5–EGO 2D heterostructured xerogels for high-rate and high-capacity aqueous zinc ion batteries, Small. 18 (2022) 2105761, https://doi.org/10.1002/smll.202105761.

[19] L. Wang, X. Wang, B. Song, Z. Wang, L. Zhang, Q. Lu, Facile *in situ* synthesis of PEDOT conductor interface at the surface of MnO_2 cathodes for enhanced aqueous zinc-ion batteries, Surf. Interfaces. 33 (2022) 102222, https://doi.org/10.1016/j.surfin.2022.102222.

[20] P. Shivakumar, K.S.M. Kumara, S.K. Bose, D.H. Nagaraju, Advances in zinc and magnesium battery polymer cathode materials, ACS. Appl. Energy Mater. 5 (2022) 10331–10358, https://doi.org/10.1021/acsaem.2c01555.

[21] X. Zhang, S. Yang, Z. Huang, Z. Zeng, Y. Zhang, Z. Wang, Recyclable nanopaper separators with uniform sub-20 nm nanopores for high-power and high-capacity zinc metal anodes, Electrochim. Acta 430 (2022) 141081, https://doi.org/10.1016/j.electacta.2022.141081.

[22] D. Frattini, E. García Gaitán, A. Bustinza Murguialday, M. Armand, N. Ortiz-Vitoriano, Essential data for industrially relevant development of bifunctional cathodes and biopolymer electrolytes in solid-state zinc–air secondary batteries, Energy Environ. Sci. 15 (2022) 5039–5058, https://doi.org/10.1039/D2EE02421G.

[23] N. Mittal, A. Ojanguren, D. Kundu, E. Lizundia, M. Niederberger, Bottom-up design of a green and transient zinc-ion battery with ultralong lifespan, Small 19 (2023) 2206249, https://doi.org/10.1002/smll.202206249.

[24] M.F. Bósquez-Cáceres, L. De Lima, V. Morera Córdova, A.D. Delgado, J. Béjar, N. Arjona, L. Álvarez-Contreras, J.P. Tafur, Chitosan-carboxymethylcellulose hydrogels as electrolytes for zinc–air batteries: an approach to the transition towards renewable energy storage devices, Batteries (Basel) 8 (2022) 265, https://doi.org/10.3390/batteries8120265.

[25] T.-B. Song, Z.-H. Huang, X.-Q. Niu, J. Liu, J.-S. Wei, X.-B. Chen, H.-M. Xiong, Applications of carbon dots in next-generation lithium-ion batteries, ChemNanoMat. 6 (2020) 1421–1436, https://doi.org/10.1002/cnma.202000355.

[26] S. Zhao, Y. Zhang, H. Pham, J.-M.Y. Carrillo, B.G. Sumpter, J. Nanda, N. J. Dudney, T. Saito, A.P. Sokolov, P.-F. Cao, Improved single-ion conductivity of polymer electrolyte via accelerated segmental dynamics, ACS. Appl. Energy Mater. 3 (2020) 12540–12548, https://doi.org/10.1021/acsaem.0c02079.

[27] Y. Wang, J. Feng, H. Wang, M. Zhang, X. Yang, R. Yuan, Y. Chai, Fabricating porous ZnO/Co_3O_4 microspheres coated with N-doped carbon by a simple method as high capacity anode, J. Electroanal. Chem. 873 (2020) 114479, https://doi.org/10.1016/j.jelechem.2020.114479.

[28] Z. Chen, D. Steinle, H.-D. Nguyen, J.-K. Kim, A. Mayer, J. Shi, E. Paillard, C. Iojoiu, S. Passerini, D. Bresser, High-energy lithium batteries based on single-ion conducting polymer electrolytes and $Li[Ni_{0.8}Co_{0.1}Mn_{0.1}]O_2$ cathodes, Nano Energy 77 (2020) 105129, https://doi.org/10.1016/j.nanoen.2020.105129.

[29] D. Zhou, M. Zhang, F. Sun, T. Arlt, J.E. Frerichs, K. Dong, J. Wang, A. Hilger, F. Wilde, M. Kolek, M.R. Hansen, P. Bieker, I. Manke, M.C. Stan, M. Winter, Performance and behavior of LLZO-based composite polymer electrolyte for lithium metal electrode with high capacity utilization, Nano Energy 77 (2020) 105196, https://doi.org/10.1016/j.nanoen.2020.105196.

[30] L. Zhang, J. Miao, J. Li, Q. Li, Halide perovskite materials for energy storage applications, Adv. Funct. Mater. 30 (2020) 2003653, https://doi.org/10.1002/adfm.202003653.

[31] P. Bunyanidhi, M. Sawangphruk, Improving interfacial contact within solid-state lithium batteries using the composite materials at the cathode produced by a scalable mechanofusion process, ECS Trans. 97 (2020) 267–277, https://doi.org/10.1149/09707.0267ecst.

[32] J. Qian, B. Jin, Y. Li, X. Zhan, Y. Hou, Q. Zhang, Research progress on gel polymer electrolytes for lithium-sulfur batteries, J. Energy Chem. 56 (2021) 420–437, https://doi.org/10.1016/j.jechem.2020.08.026.

[33] R. Rahamathullah, W.M. Khairul, M.I.N. Isa, Contribution of stilbene–imine additives on the structural, ionic conductivity performance and theoretical evaluation of CMC-based biopolymer electrolytes, Carbohydr. Polym. 250 (2020) 116935, https://doi.org/10.1016/j.carbpol.2020.116935.

[34] A.G. Olabi, M.A. Abdelkareem, T. Wilberforce, E.T. Sayed, Application of graphene in energy storage devices – a review, Renewable Sustainable Energy Rev. 135 (2020) 110026, https://doi.org/10.1016/j.rser.2020.110026.

[35] V.S. Avvaru, I.J. Fernandez, W. Feng, S.J. Hinder, M.C. Rodríguez, V. Etacheri, Extremely pseudocapacitive interface-engineered CoO@3D-NRGO hybrid anodes for high energy/power density and ultralong life lithium-ion batteries, Carbon. N. Y. 171 (2021) 869–881, https://doi.org/10.1016/j.carbon.2020.09.058.

[36] F. Wang, D. Ouyang, Z. Zhou, S.J. Page, D. Liu, X. Zhao, Lignocellulosic biomass as sustainable feedstock and materials for power generation and energy storage, J. Energy Chem. 57 (2021) 247–280, https://doi.org/10.1016/j.jechem.2020.08.060.

[37] C.M. McAnulty, D.J. Edwards, A comparison of experimental designs for calibration, Chemom. Intell. Lab. Syst. 202 (2020) 104025, https://doi.org/10.1016/j.chemolab.2020.104025.

[38] N. Pirrone, S. Garcia-Ballesteros, J. Amici, M. Castellino, S. Hernández, F. Bella, Chemometrics-boosted protocols for effortless evaluation of factors affecting the electrochemical nitrate reduction to ammonia, J. Energy Chem. 107 (2025) 599–611, https://doi.org/10.1016/j.jechem.2025.03.072.

[39] A. Mangini, J.B.V. Mygind, S. Garcia Ballesteros, A. Pedico, M. Armandi, I. Chorkendorff, F. Bella, Multivariate approaches boosting lithium-mediated ammonia electrosynthesis in different electrolytes, Angew. Chem. Int. Ed. 64 (2025) e202416027, https://doi.org/10.1002/anie.202416027.

[40] V. Tolardo, S. García-Ballesteros, L. Santos-Juanes, R. Vercher, A.M. Amat, A. Arques, E. Laurenti, Pentachlorophenol removal from water by soybean peroxidase and iron(II) salts concerted action, Water. Air. Soil. Pollut. 230 (2019) 140, https://doi.org/10.1007/s11270-019-4189-7.

[41] P. Micó, S. García-Ballesteros, M. Mora, R. Vicente, A.M. Amat, A. Arques, EEMlab: a graphical user-friendly interface for fluorimetry experiments based on the drEEM toolbox, Chemom. Intell. Lab. Syst. 188 (2019) 6–13, https://doi.org/10.1016/j.chemolab.2019.03.001.

[42] E. Aleksanyan, A. Aprahamian, A.S. Mukasyan, V. Harutyunyan, K.V. Manukyan, Mechanisms of mechanochemical synthesis of cesium lead halides: pathways toward stabilization of α-$CsPbI_3$, J. Mater. Sci. 55 (2020) 8665–8678, https://doi.org/10.1007/s10853-020-04617-3.

[43] Y. Zhang, Z. Jiang, W. Zhang, L. Yan, C. Lu, C. Ni, Pre-crystallisation applied in sequential deposition approaches to improve the photovoltaic performance of perovskite solar cells, J. Alloys. Compd. 832 (2020) 153616, https://doi.org/10.1016/j.jallcom.2019.153616.

[44] K. Suwa, T. Suga, K. Oyaizu, H. Segawa, H. Nishide, Phenolic antioxidant-incorporated durable perovskite layers and their application for a solar cell, MRS. Commun. 10 (2020) 312–316, https://doi.org/10.1557/mrc.2020.25.

[45] M. Elnaggar, M. Elshobaki, A. Mumyatov, S.Y. Luchkin, N.N. Dremova, K. J. Stevenson, P.A. Troshin, Molecular engineering of the fullerene-based electron transport layer materials for improving ambient stability of perovskite solar cells, Sol. RRL. 3 (2019) 1900223, https://doi.org/10.1002/solr.201900223.

[46] Z. Liu, L. Wu, X. Wang, Q. Xu, Y. Hu, K. Meng, G. Chen, Improving efficiency and stability of colorful perovskite solar cells with two-dimensional photonic crystals, Nanoscale 12 (2020) 8425–8431, https://doi.org/10.1039/D0NR00459F.

[47] D. Yang, H. Liang, Y. Liu, M. Hou, L. Kan, Y. Yang, Z. Zang, A large-area luminescent downshifting layer containing an Eu^{3+} complex for crystalline silicon solar cells, Dalton. Trans. 49 (2020) 4725–4731, https://doi.org/10.1039/C9DT04858H.

[48] F. Gu, Z. Zhao, C. Wang, H. Rao, B. Zhao, Z. Liu, Z. Bian, C. Huang, Lead-free tin-based perovskite solar cells: strategies toward high performance, Sol. RRL. 3 (2019) 1900213, https://doi.org/10.1002/solr.201900213.

[49] R.D. Chavan, D. Prochowicz, P. Yadav, M.M. Tavakoli, A. Nimbalkar, S.P. Bhoite, C.K. Hong, Effect of CsCl additive on the morphological and optoelectronic properties of formamidinium lead iodide perovskite, Sol. RRL. 3 (2019) 1900294, https://doi.org/10.1002/solr.201900294.

[50] A.A. Zaky, N. Balis, K. Gkini, C. Athanasekou, A. Kaltzoglou, T. Stergiopoulos, P. Falaras, Dye engineered perovskite solar cells under accelerated thermal stress and prolonged light exposure, ChemistrySelect. 5 (2020) 4454–4462, https://doi.org/10.1002/slct.202000771.

[51] N. Tessler, Y. Vaynzof, Insights from device modeling of perovskite solar cells, ACS. Energy Lett. 5 (2020) 1260–1270, https://doi.org/10.1021/acsenergylett.0c00172.

[52] C. Balcik-Canbolat, B. Van der Bruggen, Efficient removal of dyes from aqueous solution: the potential of cellulose nanocrystals to enhance PES nanocomposite membranes, Cellulose 27 (2020) 5255–5266, https://doi.org/10.1007/s10570-020-03157-y.

[53] D. Tekin, D. Birhan, H. Kiziltas, Thermal, photocatalytic, and antibacterial properties of calcinated nano-TiO_2/polymer composites, Mater. Chem. Phys. 251 (2020) 123067, https://doi.org/10.1016/j.matchemphys.2020.123067.

[54] S. Sun, L. Ling, Y. Xiong, Y. Zhang, Z. Li, Trifluoromethanesulfonimide-based hygroscopic semi-interpenetrating polymer network for enhanced proton conductivity of nafion-based proton exchange membranes at low humidity, J. Membr. Sci. 612 (2020) 118339, https://doi.org/10.1016/j.memsci.2020.118339.

[55] M. Yan, Y. Wu, Fabrication and evaluation of bioinspired pDA@TiO_2-based ibuprofen-imprinted nanocomposite membranes for highly selective adsorption and separation applications, New. J. Chem. 44 (2020) 10703–10712, https://doi.org/10.1039/D0NJ01836H.

[56] K.J. Heo, S.B. Jeong, J. Shin, G.B. Hwang, H.S. Ko, Y. Kim, D.Y. Choi, J.H. Jung, Water-repellent TiO_2-organic dye-based air filters for efficient visible-light-activated photochemical inactivation against bioaerosols, Nano Lett. 21 (2021) 1576–1583, https://doi.org/10.1021/acs.nanolett.0c03173.

[57] B. Caram, S. García-Ballesteros, L. Santos-Juanes, A. Arques, F.S. García-Einschlag, Humic like substances for the treatment of scarcely soluble pollutants by mild photo-Fenton process, Chemosphere 198 (2018) 139–146, https://doi.org/10.1016/j.chemosphere.2018.01.074.

[58] H. Pujiarti, Z.A. Pangestu, N. Sholeha, N. Nasikhudin, M. Diantoro, J. Utomo, M. S.A. Aziz, The effect of acetylene carbon black (ACB) loaded on polyacrylonitrile (PAN) nanofiber membrane electrolyte for DSSC applications, Micromachines. (Basel) 14 (2023) 394, https://doi.org/10.3390/mi14020394.

[59] T.D. Kusworo, A.C. Kumoro, N. Aryanti, F.F. Lingga, A. Widiastuti, A.A. Vetcher, F. Dalanta, Development of anti-foulant ultraviolet-assisted polyvinyl alcohol layer on the polysulfone-based nanohybrid membrane for industrial rubber wastewater decontamination, Front. Environ. Sci. 11 (2023) 1175957, https://doi.org/10.3389/fenvs.2023.1175957.

[60] S. Baachaoui, W. Mabrouk, A. Rabti, O. Ghodbane, N. Raouafi, Laser-induced graphene electrodes scribed onto novel carbon black-doped polyethersulfone membranes for flexible high-performance microsupercapacitors, J. Colloid. Interface Sci. 646 (2023) 1–10, https://doi.org/10.1016/j.jcis.2023.05.024.

[61] S. Osali, Y. Ghiyasi, H. Esfahani, R. Jose, S. Ramakrishna, Electrospun nanomembranes at the liquid–liquid and solid–liquid interface - a review, Mater. Today 67 (2023) 151–177, https://doi.org/10.1016/j.mattod.2023.05.005.

[62] A.L.-S. Eh, J. Chen, S.H. Yu, G. Thangavel, X. Zhou, G. Cai, S. Li, D.H.C. Chua, P. S. Lee, A quasi-solid-state tristate reversible electrochemical mirror device with enhanced stability, Adv. Sci. 7 (2020) 1903198, https://doi.org/10.1002/advs.201903198.

[63] Y. Xie, F. Guan, Z. Li, Y. Meng, J. Cheng, L. Li, Q. Pei, A phase-changing polymer film for broadband smart window applications, Macromol. Rapid. Commun. 41 (2020) 2000290, https://doi.org/10.1002/marc.202000290.

[64] D.-G. Kang, M. Rim, H. Ko, J. Koo, S.-I. Lim, M. Park, W.-J. Yoon, Y.-J. Choi, K.-U. Jeong, Uniaxially oriented and polymerized chromonic nanocolumns for redox-responsive smart glass, Chem. Mater. 32 (2020) 7630–7638, https://doi.org/10.1021/acs.chemmater.0c00669.

[65] A.R.M. Velarde, E.R. Bartlett, N.S. Makarov, C. Castañeda, A. Jackson, K. Ramasamy, M.R. Bergren, H. McDaniel, Optimizing the aesthetics of high-performance $CuInS_2$/ZnS quantum dot luminescent solar concentrator windows, ACS. Appl. Energy Mater. 3 (2020) 8159–8163, https://doi.org/10.1021/acsaem.0c01288.

[66] M. Pugliese, F. Bisconti, A. Rizzo, S. Colella, C.T. Prontera, G. Gigli, V. Maiorano, P. Cossari, Highly efficient all-solid-state WO_3-perovskite photovoltachromic cells for single-glass smart windows, ACS. Appl. Energy Mater. 3 (2020) 10453–10462, https://doi.org/10.1021/acsaem.0c01442.

[67] D.S. Kim, H. Lee, K. Keum, J.W. Kim, G. Jung, J. Kim, M. Park, J. Lee, H. Kang, S. J. Sim, J.S. Ha, A stretchable patch of multi-color electrochromic devices for driving integrated sensors and displaying bio-signals, Nano Energy 113 (2023) 108607, https://doi.org/10.1016/j.nanoen.2023.108607.

[68] I. Mondal, M.K. Ganesha, A.K. Singh, G.U. Kulkarni, Affordable smart windows with dual-functionality: electrochromic color switching and charge storage, Adv. Mater. Technol. 8 (2023) 2300651, https://doi.org/10.1002/admt.202300651.

[69] C. Preston, Y. Dobashi, N.T. Nguyen, M.S. Sarwar, D. Jun, C. Plesse, X. Sallenave, F. Vidal, P.-H. Aubert, J.D.W. Madden, Intrinsically stretchable integrated passive matrix electrochromic display using PEDOT:PSS ionic liquid composite, ACS. Appl. Mater. Interfaces. 15 (2023) 28288–28299, https://doi.org/10.1021/acsami.3c02902.

[70] P.V. Chavan, P.V. Rathod, H. Kim, Sodium alginate grafted phase-changing electrolyte for energy-efficient thermochromic and electrochromic synergy with uniquely tunable optical states and simultaneous Vis-NIR modulation, Chem. Eng. J. 497 (2024) 154835, https://doi.org/10.1016/j.cej.2024.154835.

[71] P.Y. Naidu, S. Naskar, M. Pal, M. Deepa, Ion conducting and hole transporting Ta_2O_5 coupled with MoO_3 and photoactive BiOI microflowers in a durable photoelectrochromic device, ACS. Appl. Energy Mater. 8 (2025) 778–789, https://doi.org/10.1021/acsaem.4c02210.

[72] V. Sharma, R. Kumar, N. Arora, S. Singh, N. Sharma, A. Anand, S.K. Jain, S. Sharma, Effect of heat treatment on thermal and mechanical stability of NaOH-doped xanthan gum-based hydrogels, J. Solid. State Electrochem. 24 (2020) 1337–1347, https://doi.org/10.1007/s10008-020-04641-y.

[73] M. Motola, L. Hromadko, J. Prikryl, H. Sopha, M. Krbal, J.M. Macak, Intrinsic properties of high-aspect ratio single- and double-wall anodic TiO_2 nanotube layers annealed at different temperatures, Electrochim. Acta 352 (2020) 136479, https://doi.org/10.1016/j.electacta.2020.136479.

[74] N. Ma, S. Wang, H. Li, X. Xu, L. Huang, Y. Wang, P.E. Strizhak, J. Tang, Direct fabrication of graphene oxide fiber by injection spinning for flexible and wearable electronics, J. Mater. Sci. 55 (2020) 12065–12081, https://doi.org/10.1007/s10853-020-04798-x.

[75] F. Danafar, Recent development and challenges in synthesis of cellulosic nanostructures and their application in developing paper-based energy devices, Cellulose Chem. Technol. 54 (2020) 327–346, https://doi.org/10.35812/CelluloseChemTechnol.2020.54.34.

[76] S. Borah, M. Deka, Effect of silica nanofiber dispersion on electrochemical properties of cellulose acetate composite gel electrolytes, Mater. Chem. Phys. 252 (2020) 123218, https://doi.org/10.1016/j.matchemphys.2020.123218.

[77] Z.-K. He, A.R. Kamali, Z.-R. Wang, Q. Sun, Z. Shi, D. Wang, Rapid preparation and characterization of oxygen-deficient SnO_2 nanobelts with enhanced Li diffusion kinetics, J. Electroanal. Chem. 871 (2020) 114276, https://doi.org/10.1016/j.jelechem.2020.114276.

[78] Z. Gonzalez, J. Yus, Y. Bravo, A.J. Sanchez-Herencia, A. Rodríguez, J. Dewalque, L. Manceriu, C. Henrist, B. Ferrari, Heteroacoagulation of lignocellulose fibers-based biotemplates and functionalized TiO_2 nanoparticles to tailor film microstructures, Cellulose 27 (2020) 7543–7559, https://doi.org/10.1007/s10570-020-03297-1.

[79] S. Mundinamani, Large area, multilayer graphene films as a flexible electronic material, ACS Omega 5 (2020) 17479–17485, https://doi.org/10.1021/acsomega.0c01982.

[80] H. Saraswat, S. Chaudhary, M. Varshney, D. Devi, F. Singh, S.O. Won, H.-J. Shin, A. Sharma, 150 keV Cu^- ion-implantation in $SrVO_3$ thin films: a study of Cu induced defect states, Vacuum. 181 (2020) 109655, https://doi.org/10.1016/j.vacuum.2020.109655.

[81] M. Sala de Medeiros, D. Chanci, R.V. Martinez, Moisture-insensitive, self-powered paper-based flexible electronics, Nano Energy 78 (2020) 105301, https://doi.org/10.1016/j.nanoen.2020.105301.

[82] L.A. Román-Ramírez, J. Marco, Design of experiments applied to lithium-ion batteries: a literature review, Appl. Energy 320 (2022) 119305, https://doi.org/10.1016/j.apenergy.2022.119305.

[83] E. Lizundia, D. Kundu, Advances in natural biopolymer-based electrolytes and separators for battery applications, Adv. Funct. Mater. 31 (2021) 2005646, https://doi.org/10.1002/adfm.202005646.

[84] Z. Wu, Z. Xie, J. Wang, T. Yu, X. Du, Z. Wang, X. Hao, A. Abudula, G. Guan, Simultaneously enhancing the thermal stability and electrochemical performance of solid polymer electrolytes by incorporating rod-like $Zn_2(OH)BO_3$ particles, Int. J. Hydrogen. Energy 45 (2020) 19601–19610, https://doi.org/10.1016/j.ijhydene.2020.05.086.

[85] K. Liu, S. Jiang, T.L. Dzwiniel, H.-K. Kim, Z. Yu, N.L. Dietz Rago, J.J. Kim, T. T. Fister, J. Yang, Q. Liu, J. Gilbert, L. Cheng, V. Srinivasan, Z. Zhang, C. Liao, Molecular design of a highly stable single-ion conducting polymer gel electrolyte, ACS. Appl. Mater. Interfaces. 12 (2020) 29162–29172, https://doi.org/10.1021/acsami.0c03363.

[86] M. Zhang, J. Becking, M.C. Stan, A. Lenoch, P. Bieker, M. Kolek, M. Winter, Wetting phenomena and their effect on the electrochemical performance of surface-tailored lithium metal electrodes in contact with cross-linked polymeric electrolytes, Angew. Chem. Int. Ed. 59 (2020) 17145–17153, https://doi.org/10.1002/anie.202001816.

[87] X. Guo, W. Peng, Y. Wu, H. Guo, Z. Wang, X. Li, Y. Ke, L. Wu, H. Fu, J. Wang, $Al_4B_2O_9$ nanorods-modified solid polymer electrolytes with decent integrated performance, Sci. China Mater. 64 (2021) 296–306, https://doi.org/10.1007/s40843-020-1393-2.

[88] F. Wu, K. Zhang, Y. Liu, H. Gao, Y. Bai, X. Wang, C. Wu, Polymer electrolytes and interfaces toward solid-state batteries: recent advances and prospects, Energy Storage Mater. 33 (2020) 26–54, https://doi.org/10.1016/j.ensm.2020.08.002.

[89] G. Homann, L. Stolz, K. Neuhaus, M. Winter, J. Kasnatscheew, Effective optimization of high voltage solid-state lithium batteries by using poly(ethylene oxide)-based polymer electrolyte with semi-interpenetrating network, Adv. Funct. Mater. 30 (2020) 2006289, https://doi.org/10.1002/adfm.202006289.

[90] S. Wang, S. Li, B. Wei, X. Lu, Interfacial engineering at cathode/LATP interface for high-performance solid-state batteries, J. Electrochem. Soc. 167 (2020) 100528, https://doi.org/10.1149/1945-7111/ab9a00.

[91] R. Zhao, Y. Wu, Z. Liang, L. Gao, W. Xia, Y. Zhao, R. Zou, Metal–organic frameworks for solid-state electrolytes, Energy Environ. Sci. 13 (2020) 2386–2403, https://doi.org/10.1039/D0EE00153H.

[92] M.V. Reddy, C.M. Julien, A. Mauger, K. Zaghib, Sulfide and oxide inorganic solid electrolytes for all-solid-state Li batteries: a review, Nanomaterials 10 (2020) 1606, https://doi.org/10.3390/nano10081606.

[93] H. Wang, L. Sheng, G. Yasin, L. Wang, H. Xu, X. He, Reviewing the current status and development of polymer electrolytes for solid-state lithium batteries, Energy Storage Mater. 33 (2020) 188–215, https://doi.org/10.1016/j.ensm.2020.08.014.

[94] M. Jiang, Z. Zhang, B. Tang, T. Dong, H. Xu, H. Zhang, X. Lu, G. Cui, Polymer electrolytes for Li-S batteries: Polymeric fundamentals and performance optimization, J. Energy Chem. 58 (2021) 300–317, https://doi.org/10.1016/j.jechem.2020.10.009.

[95] J. Kozakiewicz, J. Przybylski, B. Hamankiewicz, K. Sylwestrzak, J. Trzaskowska, M. Krajewski, M. Ratyński, W. Sarna, A. Czerwiński, UV-cured poly(siloxane-urethane)-based polymer composite materials for lithium ion batteries—the effect of modification with ionic liquids, Materials. (Basel) 13 (2020) 4978, https://doi.org/10.3390/ma13214978.

[96] Q. Wang, H. Wang, J. Wu, M. Zhou, W. Liu, H. Zhou, Advanced electrolyte design for stable lithium metal anode: from liquid to solid, Nano Energy 80 (2021) 105516, https://doi.org/10.1016/j.nanoen.2020.105516.

[97] L. Schwich, M. Küpers, M. Finsterbusch, A. Schreiber, D. Fattakhova-Rohlfing, O. Guillon, B. Friedrich, Recycling strategies for ceramic all-solid-state batteries—part I: study on possible treatments in contrast to Li-ion battery recycling, Metals. (Basel) 10 (2020) 1523, https://doi.org/10.3390/met10111523.

[98] J. Wang, S. Li, Q. Zhao, C. Song, Z. Xue, Structure code for advanced polymer electrolyte in lithium-ion batteries, Adv. Funct. Mater. 31 (2021) 2008208, https://doi.org/10.1002/adfm.202008208.

[99] H. Dai, Y. Chen, W. Xu, Z. Hu, J. Gu, X. Wei, F. Xie, W. Zhang, W. Wei, R. Guo, G. Zhang, A review of modification methods of solid electrolytes for all-solid-state sodium-ion batteries, Energy Technol. 9 (2021) 2000682, https://doi.org/10.1002/ente.202000682.

[100] X.-L. Xue, X.-X. Zhang, J.-H. Lin, S.-J. Chen, Y.-Q. Chen, Y.-C. Liu, Y.-N. Zhang, Effects of bulky LATP in PEO-based hybrid solid electrolytes, Jiegou Huaxue 39 (2020) 1941–1948, https://doi.org/10.14102/j.cnki.0254-5861.2011-2738.

[101] Y.L.N.K. Mallela, S.Y. Jeong, S. Kumar, J.-S. Lee, Hyperbranched poly(glycidol)-grafted silica nanoparticles for enhancing Li-ion conductivity of poly(ethylene oxide), Macromol. Mater. Eng. 306 (2021) 2000572, https://doi.org/10.1002/mame.202000572.

[102] H. Pan, Z. Cheng, P. He, H. Zhou, A review of solid-state lithium–sulfur battery: ion transport and polysulfide chemistry, Energy Fuels. 34 (2020) 11942–11961, https://doi.org/10.1021/acs.energyfuels.0c02647.

[103] Y. Chen, C. Li, D. Ye, Y. Zhang, H. Bao, H. Cheng, Lithiated polyanion supported $Li_{1.5}Al_{0.5}Ge_{1.5}(PO_4)_3$ composite membrane as single-ion conducting electrolyte for security and stability advancement in lithium metal batteries, J. Membr. Sci. 620 (2021) 118926, https://doi.org/10.1016/j.memsci.2020.118926.

[104] C.W. Anson, S.S. Stahl, Mediated fuel cells: soluble redox mediators and their applications to electrochemical reduction of O_2 and oxidation of H_2, alcohols, biomass, and complex fuels, Chem. Rev. 120 (2020) 3749–3786, https://doi.org/10.1021/acs.chemrev.9b00717.

[105] F. Zhang, H. Lu, J. Tong, J.J. Berry, M.C. Beard, K. Zhu, Advances in two-dimensional organic-inorganic hybrid perovskites, Energy Environ. Sci. 13 (2020) 1154–1186, https://doi.org/10.1039/C9EE03757H.

[106] S. Kahmann, E.K. Tekelenburg, H. Duim, M.E. Kamminga, M.A. Loi, Extrinsic nature of the broad photoluminescence in lead iodide-based Ruddlesden–Popper perovskites, Nat. Commun. 11 (2020) 2344, https://doi.org/10.1038/s41467-020-15970-x.

[107] H. Yi, L. Duan, F. Haque, J. Bing, J. Zheng, Y. Yang, A.C.-H. Mo, Y. Zhang, C. Xu, G. Conibeer, A. Uddin, Thiocyanate assisted nucleation for high performance mix-cation perovskite solar cells with improved stability, J. Power. Sources. 466 (2020) 228320, https://doi.org/10.1016/j.jpowsour.2020.228320.

[108] L.-H. Chou, Y.-T. Yu, X.-F. Wang, I. Osaka, C.-G. Wu, C.-L. Liu, Sequential ultrasonic spray-coating planar three layers for 1 cm^2 active area inverted perovskite solar cells, Energy Technol. 8 (2020) 2000216, https://doi.org/10.1002/ente.202000216.

[109] X. Jiang, J. Zhang, S. Ahmad, D. Tu, X. Liu, G. Jia, X. Guo, C. Li, Dion-Jacobson 2D-3D perovskite solar cells with improved efficiency and stability, Nano Energy 75 (2020) 104892, https://doi.org/10.1016/j.nanoen.2020.104892.

[110] Z. Xiong, J. Gong, Y. Xiong, Y. Lan, M. Yin, Z. Ding, Z. Zhang, X. Xiao, Constructing a spectral down converter to enhance $Cu(In,Ga)Se_2$ solar cell performance using yttrium aluminum garnet:Ce^{3+} ceramics, Sol. RRL. 4 (2020) 1900518, https://doi.org/10.1002/solr.201900518.

[111] A.H. Teodor, B.D. Bruce, Putting photosystem I to work: truly green energy, Trends Biotechnol. 38 (2020) 1329–1342, https://doi.org/10.1016/j.tibtech.2020.04.004.

[112] M. Jošt, B. Lipovšek, B. Glažar, A. Al-Ashouri, K. Brecl, G. Matič, A. Magomedov, V. Getautis, M. Topič, S. Albrecht, Perovskite solar cells go outdoors: field testing and temperature effects on energy yield, Adv. Energy Mater. 10 (2020) 2000454, https://doi.org/10.1002/aenm.202000454.

[113] A.D. Printz, O. Zhao, S. Hamann, N. Rolston, O. Solgaard, R.H. Dauskardt, Self-aligned concentrating immersion-lens arrays for patterning and efficiency recovery in scaffold-reinforced perovskite solar cells, Appl. Mater. Today 20 (2020) 100704, https://doi.org/10.1016/j.apmt.2020.100704.

[114] X. Deng, L. Xie, S. Wang, C. Li, A. Wang, Y. Yuan, Z. Cao, T. Li, L. Ding, F. Hao, Ionic liquids engineering for high-efficiency and stable perovskite solar cells, Chem. Eng. J. 398 (2020) 125594, https://doi.org/10.1016/j.cej.2020.125594.

[115] I. Benesperi, R. Singh, M. Freitag, Copper coordination complexes for energy-relevant applications, Energies (Basel) 13 (2020) 2198, https://doi.org/10.3390/en13092198.

[116] S.N. Katea, P. Broqvist, J. Kullgren, E. Hemmer, G. Westin, Fast, low-cost synthesis of ZnO:Eu nanosponges and the nature of Ln doping in ZnO, Inorg. Chem. 59 (2020) 7584–7602, https://doi.org/10.1021/acs.inorgchem.0c00472.

[117] T.C.D. Fernandes, H.M.R. Rodrigues, F.A.A. Paz, J.F.M. Sousa, A.J.M. Valente, M. M. Silva, V. de Zea Bermudez, R.F.P. Pereira, Highly conducting *Bombyx mori* silk fibroin-based electrolytes incorporating glycerol, dimethyl sulfoxide and [Bmim]PF_6, J. Electrochem. Soc. 167 (2020) 070551, https://doi.org/10.1149/1945-7111/ab8313.

[118] J. Zhou, S.-K. Dong, Z.-H. He, Y.-H. Zhang, Refractive index of ionic liquids under electric field: methyl propyl imidazole iodide and several derivatives, Chin. Phys. B 29 (2020) 047801, https://doi.org/10.1088/1674-1056/ab75cd.

[119] R.-H. Li, J. Ma, Y. Sun, H. Li, Tailoring two-dimensional surfaces with pillararenes based host–guest chemistry, Chin. Chem. Lett. 31 (2020) 3095–3101, https://doi.org/10.1016/j.cclet.2020.06.041.

[120] X. Hu, J. Yu, S. Jiang, Y. Gao, F. Sun, Naphthalimide derivatives containing benzyl-sulfur bond as cleavable photoinitiators for near-UV LED polymerization, J. Sulfur Chem. 41 (2020) 616–634, https://doi.org/10.1080/17415993.2020.1795175.

[121] J. Warnan, E. Reisner, Synthetic organic design for solar fuel systems, Angew. Chem. Int. Ed. 59 (2020) 17344–17354, https://doi.org/10.1002/anie.202006013.

[122] M.O. Alas, F.B. Alkas, A. Aktas Sukuroglu, R. Genc Alturk, D. Battal, Fluorescent carbon dots are the new quantum dots: an overview of their potential in emerging technologies and nanosafety, J. Mater. Sci. 55 (2020) 15074–15105, https://doi.org/10.1007/s10853-020-05054-y.
[123] H. Ye, X. Dong, M. Xu, X. Cheng, J. Dai, J. Zhang, Research progress of europium complexes luminescent materials, Mater. Sci. Forum 1001 (2020) 1–15, https://doi.org/10.4028/www.scientific.net/MSF.1001.1.
[124] R. Liu, Y. Xu, L. Wang, F. Zhang, P. Chen, Y. Li, Y. Chen, Visible light-induced cationic photopolymerization by diphenyliodonium hexafluorophosphate and benzothiadiazole dyes, Polym. Bull. 78 (2021) 4849–4862, https://doi.org/10.1007/s00289-020-03345-7.
[125] J.A. Hernández-Flores, A.B. Morales-Cepeda, C.F. Castro-Guerrero, F. Delgado-Arroyo, M.R. Díaz-Guillén, J. de la Cruz-Soto, L. Magallón-Cacho, U. León-Silva, Morphological and electrical properties of nanocellulose compounds and its application on capacitor assembly, Int. J. Polym. Sci. 2020 (2020) 1891064, https://doi.org/10.1155/2020/1891064.
[126] S.K. Chirauri, A.K. Dehury, Y.S. Chaudhary, Photosupercapacitors: a perspective of planar and flexible dual functioning devices, WIREs Energy Environ. 9 (2020) e377, https://doi.org/10.1002/wene.377.
[127] T. Li, J. Hu, B. Wei, Understanding of anion transport in polymer electrolytes for supercapacitors, Adv. Theor. Simul. 2 (2019) 1800140, https://doi.org/10.1002/adts.201800140.
[128] V. Ramasubbu, F.S. Omar, K. Ramesh, S. Ramesh, X.S. Shajan, Three-dimensional hierarchical nanostructured porous TiO_2 aerogel/cobalt based metal-organic framework (MOF) composite as an electrode material for supercapattery, J. Energy Storage 32 (2020) 101750, https://doi.org/10.1016/j.est.2020.101750.
[129] B.D. Boruah, Recent advances in off-grid electrochemical capacitors, Energy Storage Mater. 34 (2021) 53–75, https://doi.org/10.1016/j.ensm.2020.08.031.
[130] W. Ye, H. Wang, J. Ning, Y. Zhong, Y. Hu, New types of hybrid electrolytes for supercapacitors, J. Energy Chem. 57 (2021) 219–232, https://doi.org/10.1016/j.jechem.2020.09.016.
[131] C.X. Xing, H.T. Zhang, S.S. Pan, M. Yao, B.S. Li, Y.Q. Zhang, S.J. Zhang, Boosting the safety and energy density of molybdenum disulfide/carbon nanotubes based solid-state sodium-ion supercapacitors with an ionogel electrolyte, Mater. Today Energy 18 (2020) 100527, https://doi.org/10.1016/j.mtener.2020.100527.
[132] S.K. Tiwari, A.K. Thakur, A. De Adhikari, Y. Zhu, N. Wang, Current research of graphene-based nanocomposites and their application for supercapacitors, Nanomaterials 10 (2020) 2046, https://doi.org/10.3390/nano10102046.
[133] L. Li, N. Lu, D. Jiang, Z. Chen, W. Zhang, W. Zheng, X. Zhu, G. Wang, A universal strategy to improve interfacial kinetics of solid supercapacitors used in high temperature, J. Colloid. Interface Sci. 586 (2021) 110–119, https://doi.org/10.1016/j.jcis.2020.10.075.
[134] D. Majumdar, Recent progress in copper sulfide based nanomaterials for high energy supercapacitor applications, J. Electroanal. Chem. 880 (2021) 114825, https://doi.org/10.1016/j.jelechem.2020.114825.
[135] M.Ijadi Bajestani, S.M. Mousavi, S.A. Shojaosadati, Bioleaching of heavy metals from spent household batteries using *Acidithiobacillus ferrooxidans*: statistical evaluation and optimization, Sep. Purif. Technol. 132 (2014) 309–316, https://doi.org/10.1016/j.seppur.2014.05.023.
[136] G. Bona, L. Viganò, M. Cantoni, R. Mantovan, B. Di Credico, S. Mostoni, R. Scotti, R. Nisticò, An experimental demonstration on the recyclability of hybrid magnetite-humic acid nanoparticles, Sustainable Mater. Technol. 43 (2025) e01275, https://doi.org/10.1016/j.susmat.2025.e01275.
[137] X. Zhao, C. Kuang, R. Zhou, N. Yang, C. An, J. Xu, M. Wang, Deep eutectic solvent-assisted recycling of spent lithium-ion batteries into electrocatalysts for polyethylene terephthalate upcycling, Chem. Commun. 61 (2025) 2989–2992, https://doi.org/10.1039/D4CC06411A.
[138] M.S. Simas, K. Bly, M.A. Arega, F.R. Aponte, T.L. Silva, K.S. Wiebe, Sustainability effects of material demand by next-generation lithium-ion battery technologies: a global value chain perspective, Resour. Conserv. Recycl. 219 (2025) 108294, https://doi.org/10.1016/j.resconrec.2025.108294.
[139] H. Yu, S. Wang, Blockchain-enabled closed-loop supply chain optimization for power battery recycling and cascading utilization, Sustainability. 17 (2025) 4192, https://doi.org/10.3390/su17094192.
[140] F. Schoden, M. Dotter, D. Knefelkamp, T. Blachowicz, E. Schwenzfeier Hellkamp, Review of state of the art recycling methods in the context of dye sensitized solar cells, Energies. (Basel) 14 (2021) 3741, https://doi.org/10.3390/en14133741.
[141] H. Duan, Q. Zhao, J. Song, Z. Duan, Identifying opportunities for initiating waste recycling: experiences of typical developed countries, J. Cleaner Prod. 324 (2021) 129190, https://doi.org/10.1016/j.jclepro.2021.129190.
[142] F. Schoden, A.K. Schnatmann, E. Davies, D. Diederich, J.L. Storck, D. Knefelkamp, T. Blachowicz, E. Schwenzfeier-Hellkamp, Investigating the recycling potential of glass based dye-sensitized solar cells—melting experiment, Materials. (Basel) 14 (2021) 6622, https://doi.org/10.3390/ma14216622.
[143] S. Ullah, H. Wang, G. Hang, T. Zhang, L. Li, S. Zheng, Poly(thiourethane-*co*-ethylene oxide) networks crosslinked with disulfide bonds: reinforcement with POSS and use for recyclable solid polymer electrolytes, Polymer. (Guildf) 284 (2021) 126318, https://doi.org/10.1016/j.polymer.2023.126318.
[144] H. Akram Cheema, S. Ilyas, H. Kang, H. Kim, Comprehensive review of the global trends and future perspectives for recycling of decommissioned photovoltaic panels, Waste Manage. 174 (2024) 187–202, https://doi.org/10.1016/j.wasman.2023.11.025.
[145] J. Han, S. Li, W. Zhang, M. Wei, J. Liu, W. Wei, X. Liu, X. Li, Fabrication of recyclable polyurethane elastomers with excellent mechanical and creep-resistant properties based on a bio-sourced azine chain extender, ACS. Appl. Polym. Mater. 6 (2024) 712–721, https://doi.org/10.1021/acsapm.3c02336.
[146] W. Shan, H. Zhang, C. Hu, Y. Zhou, K.-H. Lam, S. Wang, X. Hou, The cycle performance of high nickel cathode materials significantly enhanced by the $LiAlO_2$@Al_2O_3 dual-modified coating, Electrochim. Acta 367 (2021) 137216, https://doi.org/10.1016/j.electacta.2020.137216.
[147] A. Wolf, A. Flegler, J. Prieschl, T. Stuebinger, W. Witt, F. Seiser, T. Vinnay, T. Sinn, M. Gleiß, H. Nirschl, K. Mandel, Centrifugation based separation of lithium iron phosphate (LFP) and carbon black for lithium-ion battery recycling, Chem. Eng. Process. Process Intensif. 160 (2021) 108310, https://doi.org/10.1016/j.cep.2021.108310.
[148] Y.J. Jung, B.Y. Yoo, S.C. Park, S.H. Son, Design optimization of selective lithium leaching of cathodic active materials from spent lithium-ion batteries based on the Taguchi method, Metals (Basel) 11 (2021) 108, https://doi.org/10.3390/met11010108.
[149] M. Kahl, S. Pavón, M. Bertau, Recycling of primary lithium batteries production residues, Chemphyschem. 22 (2021) 577–584, https://doi.org/10.1002/cphc.202000867.
[150] S. Pavón, D. Kaiser, R. Mende, M. Bertau, The COOL-process—a selective approach for recycling lithium batteries, Metals. (Basel) 11 (2021) 259, https://doi.org/10.3390/met11020259.
[151] K. Chabhadiya, R.R. Srivastava, P. Pathak, Two-step leaching process and kinetics for an eco-friendly recycling of critical metals from spent Li-ion batteries, J. Environ. Chem. Eng. 9 (2021) 105232, https://doi.org/10.1016/j.jece.2021.105232.
[152] K. Deng, L. Li, Optical design in perovskite solar cells, Small. Methods 4 (2020) 1900150, https://doi.org/10.1002/smtd.201900150.
[153] G. Saianand, P. Sonar, G.J. Wilson, A.-I. Gopalan, V.A.L. Roy, G.E. Unni, K. Mamun Reza, B. Bahrami, K. Venkatramanan, Q. Qiao, Current advancements on charge selective contact interfacial layers and electrodes in flexible hybrid perovskite photovoltaics, J. Energy Chem. 54 (2021) 151–173, https://doi.org/10.1016/j.jechem.2020.05.050.
[154] J. Yang, Q. Bao, L. Shen, L. Ding, Potential applications for perovskite solar cells in space, Nano Energy 76 (2020) 105019, https://doi.org/10.1016/j.nanoen.2020.105019.
[155] M. Hadadian, J.-H. Smått, J.-P. Correa-Baena, The role of carbon-based materials in enhancing the stability of perovskite solar cells, Energy Environ. Sci. 13 (2020) 1377–1407, https://doi.org/10.1039/C9EE04030G.
[156] T.J. Jacobsson, A. Hultqvist, S. Svanström, L. Riekehr, U.B. Cappel, E. Unger, H. Rensmo, E.M.J. Johansson, M. Edoff, G. Boschloo, 2-terminal CIGS–perovskite tandem cells: a layer by layer exploration, Sol. Energy 207 (2020) 270–288, https://doi.org/10.1016/j.solener.2020.06.034.
[157] W. Zhang, Z. Zhang, Q. Jiang, Z. Wei, Y. Zhang, H. You, D. Chen, W. Zhu, F. He, C. Zhang, Charge-transporting-layer-free, vacuum-free, all-inorganic $CsPbIBr_2$ perovskite solar cells via dipoles-adjusted interface, Nanomaterials 10 (2020) 1324, https://doi.org/10.3390/nano10071324.
[158] Y. Wu, W. Zhang, F. Qian, H. Zhao, K. Guo, M. Wang, X. Li, Z. Liu, H. Wang, B. Xu, An efficient phenylaminecarbazole-based three-dimensional hole-transporting material for high-stability perovskite solar cells, Dyes. Pigm. 182 (2020) 108663, https://doi.org/10.1016/j.dyepig.2020.108663.
[159] L. Gao, T.H. Schloemer, F. Zhang, X. Chen, C. Xiao, K. Zhu, A. Sellinger, Carbazole-based hole-transport materials for high-efficiency and stable perovskite solar cells, ACS. Appl. Energy Mater. 3 (2020) 4492–4498, https://doi.org/10.1021/acsaem.0c00179.
[160] H. Liu, Y. Xie, P. Wei, W. Wang, H. Chen, C. Geng, Y. Qiang, Interface optimization of hole-conductor free perovskite solar cells using porous carbon materials derived from biomass soybean dregs as a cathode, J. Alloys. Compd. 842 (2020) 155851, https://doi.org/10.1016/j.jallcom.2020.155851.
[161] K. Wu, B. Li, X. Dong, P. Wu, K. Sun, S. Yang, J. Wu, J. Hou, Z. Liu, X. Guo, Flexible and recyclable PPy-TiO_2@WO_3 photocatalyst supported by cellulose aerogel beads, ChemistrySelect. 5 (2020) 6527–6536, https://doi.org/10.1002/slct.202001045.
[162] M. Singh, I. Sinha, Halide perovskite-based photocatalysis systems for solar-driven fuel generation, Sol. Energy 208 (2020) 296–311, https://doi.org/10.1016/j.solener.2020.08.007.
[163] S. Riese, J.S. Brand, D. Mims, M. Holzapfel, N.N. Lukzen, U.E. Steiner, C. Lambert, Giant magnetic field effects in donor–acceptor triads: on the charge separation and recombination dynamics in triarylamine–naphthalenediimide triads with bis-diyprrinato-palladium(II), porphodimethenato-palladium(II), and palladium(II)–porphyrin photosensitizers, J. Chem. Phys. 153 (2020) 054306, https://doi.org/10.1063/5.0013941.
[164] Z. Wang, H.-C. Chiu, A. Paolella, R. Gauvin, K. Zaghib, G.P. Demopoulos, A sustainable light-chargeable two-electrode energy storage system based on aqueous sodium-ion photo-intercalation, Sustainable Energy Fuels 4 (2020) 4789–4799, https://doi.org/10.1039/D0SE00628A.
[165] S.B. Aziz, M.A. Brza, M.M. Nofal, R.T. Abdulwahid, S.A. Hussen, A.M. Hussein, W. O. Karim, A comprehensive review on optical properties of polymer electrolytes and composites, Materials (Basel) 13 (2020) 3675, https://doi.org/10.3390/ma13173675.
[166] M. Subburu, R. Gade, V. Guguloth, P. Chetti, K.R. Ravulapelly, S. Pola, Effective photodegradation of organic pollutants in the presence of mono and bi-metallic complexes under visible-light irradiation, J. Photochem. Photobiol., A 406 (2021) 112996, https://doi.org/10.1016/j.jphotochem.2020.112996.
[167] F. Wang, K. Pan, S. Wei, Y. Ren, H. Zhu, H.-H. Wu, Q. Zhang, Solvothermal preparation and characterization of ordered-mesoporous ZrO_2/TiO_2 composites for photocatalytic degradation of organic dyes, Ceram. Int. 47 (2021) 7632–7641, https://doi.org/10.1016/j.ceramint.2020.11.104.

[168] Z. Jiang, L. Feng, J. Zhu, B. Liu, X. Li, Y. Chen, S. Khan, Construction of a hierarchical $NiFe_2O_4$/$CuInSe_2$ (p-n) heterojunction: highly efficient visible-light-driven photocatalyst in the degradation of endocrine disruptors in an aqueous medium, Ceram. Int. 47 (2021) 8996–9007, https://doi.org/10.1016/j.ceramint.2020.12.022.
[169] H. An, Y. Wang, X. Xiao, J. Liu, Z. Ma, T. Gao, W. Hong, L. Zhao, H. Wang, Q. Zhu, S. Chen, Z. Yin, Photocatalytic seawater splitting by 2D heterostructure of $ZnIn_2S_4$/WO_3 decorated with plasmonic Au for hydrogen evolution under visible light, J. Energy Chem. 93 (2024) 55–63, https://doi.org/10.1016/j.jechem.2024.01.041.
[170] M. Zhong, Y. Sun, Recent advancements in the molecular design of deep-red to near-infrared light-absorbing photocatalysts, Chem. Catal. 4 (2024) 100973, https://doi.org/10.1016/j.checat.2024.100973.
[171] J. He, C. Janáky, Recent advances in solar-driven carbon dioxide conversion: expectations *versus* reality, ACS. Energy Lett. 5 (2020) 1996–2014, https://doi.org/10.1021/acsenergylett.0c00645.
[172] Y. Bentounsi, K. Seintis, D. Ameline, S. Diring, D. Provost, E. Blart, Y. Pellegrin, D. Cossement, E. Vauthey, F. Odobel, Chemistry on the electrodes: post-functionalization and stability enhancement of anchored dyes on mesoporous metal oxide photoelectrochemical cells with copper-free Huisgen cycloaddition reaction, J. Mater. Chem. A 8 (2020) 12633–12640, https://doi.org/10.1039/D0TA04982D.
[173] X. Zhang, H. Li, H. Yang, F. Xie, Z. Yuan, L. Zajickova, W. Li, Phase-engineering of 1T/2H molybdenum disulfide by using ionic liquid for enhanced electrocatalytic hydrogen evolution, ChemElectroChem. 7 (2020) 3347–3352, https://doi.org/10.1002/celc.202000745.
[174] A. Mota-Lima, Ratio oxalate to formate tuned by pH during CO_2 reduction driven by solvated electron at the electrified plasma/liquid interface, Electrocatalysis 11 (2020) 618–627, https://doi.org/10.1007/s12678-020-00620-z.
[175] P. Agbo, Rate-potential decoupling: a biophysical perspective of electrocatalysis, J. Phys. D: Appl. Phys. 57 (2024) 462001, https://doi.org/10.1088/1361-6463/ad6008.
[176] Y.-H. Lo, Y.-H. Chen, C.-F. Huang, C. Pitchai, W.-S. Liu, C.-C. Chang, C.-M. Chen, A composite electrocatalytic poly(3,4-ethylenedioxythiophene) film incorporated with silver nanowires for bifacial dye-sensitized solar cells, Electrochim. Acta 507 (2024) 145132, https://doi.org/10.1016/j.electacta.2024.145132.
[177] C. Xu, H. Su, S. Zhao, A. Nilghaz, K. Tang, L. Ma, Z. Zou, Electrocatalytic and photocatalytic N_2 fixation using carbon catalysts, Nanomaterials 15 (2025) 65, https://doi.org/10.3390/nano15010065.
[178] J. Shi, Y. Zhao, J. Ma, D. Yu, Y. Fu, X. Yu, Z. Zhao, W. Kang, S.B. Aidarova, Facile preparation of nickel foam supported transition metal catalysts and their electrocatalytic activity for oxygen evolution reaction, Mater. Res. Bull. 188 (2025) 113416, https://doi.org/10.1016/j.materresbull.2025.113416.
[179] Y. Li, G. Shao, X. Zheng, Y. Jia, Y. Xia, Y. Dou, M. Huang, C. Gu, J. Shi, J. Zheng, S. Dou, Cutting-edge advances in pressurized electrocatalytic reactors, eScience 5 (2025) 100369, https://doi.org/10.1016/j.esci.2024.100369.
[180] P. Agbo, *J–V* decoupling: independent control over current and potential in electrocatalysis, J. Phys. Chem. C 124 (2020) 28387–28394, https://doi.org/10.1021/acs.jpcc.0c08142.
[181] R. Vidal, J.-A. Alberola-Borràs, I. Mora-Seró, Abiotic depletion and the potential risk to the supply of cesium, Resour. Policy. 68 (2020) 101792, https://doi.org/10.1016/j.resourpol.2020.101792.
[182] S. Ponce, M. Chavarria, F. Norabuena, D. Chumpitaz, A. Gutarra, Cellulose microfibres obtained from agro-industrial tara waste for dye adsorption in water, Water. Air. Soil. Pollut. 231 (2020) 518, https://doi.org/10.1007/s11270-020-04889-0.
[183] Q. Dang, L. Wang, J. Liu, D. Wang, J. Chai, M. Wu, L. Tang, Recent progress of photoelectrocatalysis systems for wastewater treatment, J. Water. Process. Eng. 53 (2023) 103609, https://doi.org/10.1016/j.jwpe.2023.103609.
[184] N. Albayati, M. Mohammed, H. Ahmed, M. Kadhom, The potential of Gundelia seeds waste as an emerging sustainable adsorbent for methylene blue-polluted water treatment, Prog. Color Colorants Coat. 18 (2024) 53–71, https://doi.org/10.30509/pccc.2024.167290.1285.
[185] Y. Tian, Z. Zeng, Y. Hu, Z. Liu, Enhanced photocatalytic degradation of rhodamine B in aqueous solution by activation of H_2O_2 with glucose modified $CuFeO_2$, Desalin. Water Treat. 321 (2025) 100960, https://doi.org/10.1016/j.dwt.2024.100960.
[186] X. Zhang, S. Sun, X. Han, S. Shu, Optimizing struvite recovery from wastewater treatment: insights from machine learning models, J. Water. Process. Eng. 77 (2025) 108520, https://doi.org/10.1016/j.jwpe.2025.108520.
[187] I. Zaborniak, A. Macior, P. Chmielarz, Stimuli-responsive rifampicin-based macromolecules, Materials (Basel) 13 (2020) 3843, https://doi.org/10.3390/ma13173843.
[188] H.H. Sønsteby, V.A.-L.K. Killi, T.A. Storaas, D. Choudhury, J.W. Elam, H. Fjellvåg, O. Nilsen, Understanding KO^{t}Bu in atomic layer deposition – *in situ* mechanistic studies of the $KNbO_3$ growth process, Dalton. Trans. 49 (2020) 13233–13242, https://doi.org/10.1039/D0DT02324H.
[189] H. Nederstedt, P. Jannasch, Synthesis, phase structure, and ion conductivity of poly(*p*-phenylene) functionalized with lithium trifluoromethanesulfonimide and tetra(ethylene oxide) side chains, ACS. Appl. Energy Mater. 3 (2020) 9066–9075, https://doi.org/10.1021/acsaem.0c01455.
[190] L. Jasmani, R. Rusli, T. Khadiran, R. Jalil, S. Adnan, Application of nanotechnology in wood-based products industry: a review, Nanoscale Res. Lett. 15 (2020) 207, https://doi.org/10.1186/s11671-020-03438-2.
[191] A. Martínez-Camarena, M. Savastano, J.M. Llinares, B. Verdejo, A. Bianchi, E. García-España, C. Bazzicalupi, Stabilization of polyiodide networks with Cu(II) complexes of small methylated polyazacyclophanes: shifting directional control from H-bonds to I···I interactions, Inorg. Chem. Front. 7 (2020) 4239–4255, https://doi.org/10.1039/D0QI00912A.
[192] B. Mahanty, K. Maity, S. Sarkar, D. Mandal, Polymer nanofiber based triboelectric nanogenerator for energy harvesting and self-powered electronics, AIP. Conf. Proc. 2265 (2020) 030655, https://doi.org/10.1063/5.0016777.
[193] W. Azouzi, I. Benabdallah, A. Sibari, H. Labrim, M. Benaissa, Structural and optical properties of $LaFe_{1-x}V_xO_3$ as predicted by a DFT study, Mater. Today Commun. 26 (2021) 101876, https://doi.org/10.1016/j.mtcomm.2020.101876.
[194] B. Pang, G. Jiang, J. Zhou, Y. Zhu, W. Cheng, D. Zhao, K. Wang, G. Xu, H. Yu, Molecular-scale design of cellulose-based functional materials for flexible electronic devices, Adv. Electron. Mater. 7 (2021) 2000944, https://doi.org/10.1002/aelm.202000944.
[195] C. Zhang, J. Mo, Q. Fu, Y. Liu, S. Wang, S. Nie, Wood-cellulose-fiber-based functional materials for triboelectric nanogenerators, Nano Energy 81 (2021) 105637, https://doi.org/10.1016/j.nanoen.2020.105637.
[196] H. Fazlı, Z. Biyiklioglu, E.T. Saka, Ö. Kesmez, F. Demir, Preparation and characterization of water-soluble phthalocyanine-modified nano-TiO_2 functional thin films and their photocatalytic activity in the degradation of methylene blue, Appl. Organomet. Chem. 39 (2025) e70352, https://doi.org/10.1002/aoc.70352.
[197] D. Sud, G. Kaur, A comprehensive review on synthetic approaches for metal-organic frameworks: from traditional solvothermal to greener protocols, Polyhedron. 193 (2021) 114897, https://doi.org/10.1016/j.poly.2020.114897.
[198] A. Sattar, N. Shahzad, M.A. Tariq, T. Yousaf, S. Garcia-Ballesteros, M.I. Shahzad, R. Liaquat, M. Ali, F. Bella, Role of bifunctional additives towards highly efficient and stable tin perovskite solar cells, Mater. Today Energy 53 (2025) 101986, https://doi.org/10.1016/j.mtener.2025.101986.
[199] S. Sathya, R.S. Kumar, S. Garcia-Ballesteros, F. Bella, D.J. Yoo, A.M. Stephan, Interplay between composition and cycling performance of pre-lithiated SiO_x-Si-C composite anodes for lithium–sulfur full cells, Materials. (Basel) 18 (2025) 1053, https://doi.org/10.3390/ma18051053.
[200] M. Kathiresan, A.K. Lakshmi, N. Angulakshmi, S. Garcia-Ballesteros, F. Bella, A. M. Stephan, Viologen as an electrolyte additive for extreme fast charging of lithium-ion batteries, Battery Energy 4 (2025) e20240039, https://doi.org/10.1002/bte2.20240039.
[201] Z. Ghamati, M. Pordel, A. Davoodnia, S.A. Beyramabadi, Synthesis, electrochemical, photophysical, and photovoltaic properties of new fluorescent compounds: 3*H*-benzofuro[2,3-*b*]pyrazolo[4,3-*f*]quinoline, Int. J. Energy Res. 45 (2021) 7797–7805, https://doi.org/10.1002/er.6363.
[202] W. Luo, A. Taleb, Large-scale synthesis route of TiO_2 nanomaterials with controlled morphologies using hydrothermal method and TiO_2 aggregates as precursor, Nanomaterials 11 (2021) 365, https://doi.org/10.3390/nano11020365.
[203] S. Wang, Y. Zhu, X. Sun, S. An, J. Cui, Y. Zhang, W. He, Microwave synthesis of N-doped modified graphene/mixed crystal phases TiO_2 composites for Na-ion batteries, Colloids Surf., A 615 (2021) 126276, https://doi.org/10.1016/j.colsurfa.2021.126276.
[204] M.S. Samuel, K.V. Savunthari, S. Ethiraj, Synthesis of a copper (II) metal–organic framework for photocatalytic degradation of rhodamine B dye in water, Environ. Sci. Pollut. Res. 28 (2021) 40835–40843, https://doi.org/10.1007/s11356-021-13571-9.
[205] R.W. Baker, L. Forfar, X. Liang, P.J. Cameron, Using design of experiment to obtain a systematic understanding of the effect of synthesis parameters on the properties of perovskite nanocrystals, React. Chem. Eng. 6 (2021) 709–719, https://doi.org/10.1039/D0RE00149J.
[206] V. Babu, R.Fuentes Pineda, T. Ahmad, A.O. Alvarez, L.A. Castriotta, A. Di Carlo, F. Fabregat-Santiago, K. Wojciechowski, Improved stability of inverted and flexible perovskite solar cells with carbon electrode, ACS. Appl. Energy Mater. 3 (2020) 5126–5134, https://doi.org/10.1021/acsaem.0c00702.
[207] E. Hwang, H. Kim, S.-H. Lee, J.H. Seo, H.-T. Kim, C. Lee, S.-Y. Jang, K. Seo, T.-H. Kwon, Fabrication of water-repellent platinum(II) complex-based photon downshifting layers for perovskite solar cells by ultrasonic spray deposition, Adv. Energy Mater. 10 (2020) 2001238, https://doi.org/10.1002/aenm.202001238.
[208] S. Zhang, Z. Liu, W. Zhang, Z. Jiang, W. Chen, R. Chen, Y. Huang, Z. Yang, Y. Zhang, L. Han, W. Chen, Barrier designs in perovskite solar cells for long-term stability, Adv. Energy Mater. 10 (2020) 2001610, https://doi.org/10.1002/aenm.202001610.
[209] N. Zhang, T. Jiang, C. Guo, L. Qiao, Q. Ji, L. Yin, L. Yu, P. Murto, X. Xu, High-performance semitransparent polymer solar cells floating on water: rational analysis of power generation, water evaporation and algal growth, Nano Energy 77 (2020) 105111, https://doi.org/10.1016/j.nanoen.2020.105111.
[210] M.T. Klug, R.L. Milot, J.B. Patel, T. Green, H.C. Sansom, M.D. Farrar, A. J. Ramadan, S. Martani, Z. Wang, B. Wenger, J.M. Ball, L. Langshaw, A. Petrozza, M.B. Johnston, L.M. Herz, H.J. Snaith, Metal composition influences optoelectronic quality in mixed-metal lead–tin triiodide perovskite solar absorbers, Energy Environ. Sci. 13 (2020) 1776–1787, https://doi.org/10.1039/D0EE00132E.
[211] Y. Hu, S. Ding, P. Chen, T. Seaby, J. Hou, L. Wang, Flexible solar-rechargeable energy system, Energy Storage Mater. 32 (2020) 356–376, https://doi.org/10.1016/j.ensm.2020.06.028.
[212] H. Parsimehr, A. Ehsani, Corn-based electrochemical energy storage devices, Chem. Rec. 20 (2020) 1163–1180, https://doi.org/10.1002/tcr.202000058.
[213] A. Kumar, S. Singh, Advancement in inorganic hole transport materials for inverted perovskite solar cells, J. Electron. Mater. 49 (2020) 5840–5881, https://doi.org/10.1007/s11664-020-08264-x.

[214] C. Cheng, N. Li, Z. Wang, H. Zhang, J. Chen, Thermodynamically driven surface dedoping of Nb-doped TiO_2 for stable perovskite solar cells, J. Phys. Chem. C 124 (2020) 14419–14423, https://doi.org/10.1021/acs.jpcc.0c01608.
[215] N.A.N. Ouedraogo, M. Yang, C. He, Y. Chen, X. Zhang, H. Yan, C.B. Han, Y. Zhang, Influence of polytetrafluoroethylene (PTFE) on photovoltaic performance and perovskite solar cell stability, Sustainable Energy Fuels 4 (2020) 4257–4263, https://doi.org/10.1039/D0SE00555J.
[216] X. Liu, X. Deng, Y. He, X. Zheng, G. Zeng, A dynamic state-of-charge estimation method for electric vehicle lithium-ion batteries, Energies. (Basel) 13 (2020) 121, https://doi.org/10.3390/en13010121.
[217] J. Unger, C. Hametner, S. Jakubek, M. Quasthoff, A novel methodology for non-linear system identification of battery cells used in non-road hybrid electric vehicles, J. Power. Sources 269 (2014) 883–897, https://doi.org/10.1016/j.jpowsour.2014.07.025.
[218] A. Cordoba-Arenas, S. Onori, Y. Guezennec, G. Rizzoni, Capacity and power fade cycle-life model for plug-in hybrid electric vehicle lithium-ion battery cells containing blended spinel and layered-oxide positive electrodes, J. Power. Sources. 278 (2015) 473–483, https://doi.org/10.1016/j.jpowsour.2014.12.047.
[219] W. Prochazka, G. Pregartner, M. Cifrain, Design-of-experiment and statistical modeling of a large scale aging experiment for two popular lithium ion cell chemistries, J. Electrochem. Soc. 160 (2013) A1039–A1051, https://doi.org/10.1149/2.003308jes.
[220] R. Mathieu, I. Baghdadi, O. Briat, P. Gyan, J.-M. Vinassa, D-optimal design of experiments applied to lithium battery for ageing model calibration, Energy 141 (2017) 2108–2119, https://doi.org/10.1016/j.energy.2017.11.130.
[221] P. Gyan, P. Aubret, J. Hafsaoui, F. Sellier, S. Bourlot, S. Zinola, F. Badin, Experimental assessment of battery cycle life within the SIMSTOCK research program, Oil Gas Sci. Technol. 68 (2013) 137–147, https://doi.org/10.2516/ogst/2013106.
[222] J. Stadler, C. Krupp, M. Ecker, J. Bandlow, B. Spier, A. Latz, Investigation and modeling of cyclic aging using a design of experiment with automotive grade lithium-ion cells, J. Power. Sources. 521 (2022) 230952, https://doi.org/10.1016/j.jpowsour.2021.230952.
[223] M. Arrese-Igor, M. Martinez-Ibañez, A. Orue, E. Pavlenko, E. Dumont, M. Armand, F. Aguesse, P.L. Aranguren, Influence of the operating temperature on the ageing and interfaces of double layer polymer electrolyte solid state Li metal batteries, Nano Res. 16 (2023) 8377–8384, https://doi.org/10.1007/s12274-022-5278-2.
[224] X. Fang, Y. He, X. Fan, D. Zhang, H. Hu, Modeling and simulation in capacity degradation and control of all-solid-state lithium battery based on time-aging polymer electrolyte, Polymers (Basel) 13 (2021) 1206, https://doi.org/10.3390/polym13081206.
[225] L.W. Juang, P.J. Kollmeyer, A.E. Anders, T.M. Jahns, R.D. Lorenz, D. Gao, Investigation of the influence of superimposed AC current on lithium-ion battery aging using statistical design of experiments, J. Energy Storage 11 (2017) 93–103, https://doi.org/10.1016/j.est.2017.02.005.
[226] I. Baghdadi, R. Mathieu, O. Briat, P. Gyan, J.-M. Vinassa, Lithium-ion battery ageing assessment based on a reduced design of experiments, in: Proc. IEEE Veh. Power Propuls. Conf. (VPPC), Belfort, France, 2017, pp. 1–6, https://doi.org/10.1109/VPPC.2017.8330871.
[227] A. Singh, A. Izadian, S. Anwar, Model based condition monitoring in lithium-ion batteries, J. Power. Sources. 268 (2014) 459–468, https://doi.org/10.1016/j.jpowsour.2014.06.052.
[228] J. Guo, Z. Li, T. Keyser, Y. Deng, Modeling Li-ion battery capacity fade using designed experiments, in: Proc. IIE Annu. Conf. Expo, Montréal, Canada, 2014, pp. 913–919.
[229] T.T. Vo, X. Chen, W. Shen, A. Kapoor, New charging strategy for lithium-ion batteries based on the integration of Taguchi method and state of charge estimation, J. Power. Sources. 273 (2015) 413–422, https://doi.org/10.1016/j.jpowsour.2014.09.108.
[230] J. Remmlinger, M. Buchholz, M. Meiler, P. Bernreuter, K. Dietmayer, State-of-health monitoring of lithium-ion batteries in electric vehicles by on-board internal resistance estimation, J. Power. Sources. 196 (2011) 5357–5363, https://doi.org/10.1016/j.jpowsour.2010.08.035.
[231] X. Lin, G. Zhou, J. Liu, J. Yu, M.B. Effat, J. Wu, F. Ciucci, Rechargeable battery electrolytes capable of operating over wide temperature windows and delivering high safety, Adv. Energy Mater. 10 (2020) 2001235, https://doi.org/10.1002/aenm.202001235.
[232] K. Acurio-Cerda, R. Keloth, O.A. Obewhere, S.K. Dishari, Lignin-based membranes for health, food safety, environmental, and energy applications: current trends and future directions, Curr. Opin. Chem. Eng. 47 (2025) 101098, https://doi.org/10.1016/j.coche.2025.101098.
[233] L. Zeng, L. Jia, X. Liu, C. Zhang, A novel silicon/phosphorus *co*-flame retardant polymer electrolyte for high-safety all-solid-state lithium-ion batteries, Polymers. (Basel) 12 (2020) 2937, https://doi.org/10.3390/polym12122937.
[234] K. Deng, T. Guan, F. Liang, X. Zheng, Q. Zeng, Z. Liu, G. Wang, Z. Qiu, Y. Zhang, M. Xiao, Y. Meng, L. Wei, Flame-retardant single-ion conducting polymer electrolytes based on anion acceptors for high-safety lithium metal batteries, J. Mater. Chem. A 9 (2021) 7692–7702, https://doi.org/10.1039/D0TA12437K.
[235] T.-H. Park, M.-S. Park, A.-H. Ban, Y.-S. Lee, D.-W. Kim, Nonflammable gel polymer electrolyte with ion-conductive polyester networks for sodium metal cells with excellent cycling stability and enhanced safety, ACS. Appl. Energy Mater. 4 (2021) 10153–10162, https://doi.org/10.1021/acsaem.1c02053.
[236] S.S. Park, S.A. Han, R. Chaudhary, J.H. Suh, J. Moon, M.-S. Park, J.H. Kim, Solid electrolyte: strategies to address the safety of all solid-state batteries, Adv. Energy Sustainability Res. 4 (2023) 2300074, https://doi.org/10.1002/aesr.202300074.
[237] S. Zhou, X. Wang, Z. Xu, T. Guan, D. Mo, K. Deng, Rapid self-healing, highly conductive and near-single-ion-conducting gel polymer electrolytes based on dynamic boronic ester bonds for high-safety lithium metal batteries, J. Energy Storage 75 (2024) 109712, https://doi.org/10.1016/j.est.2023.109712.
[238] S. Hu, D. Wang, Z. Yuan, H. Zhang, S. Tian, Y. Zhang, B. Zhang, Y. Han, J. Zhang, G. Cui, In-situ polymerized solid-state polymer electrolytes for high-safety sodium metal batteries: progress and perspectives, Batteries. (Basel) 9 (2023) 532, https://doi.org/10.3390/batteries9110532.
[239] H. Shi, Z. Fu, W. Xu, N. Xu, X. He, Q. Li, J. Sun, R. Jiang, Z. Lei, Z.-H. Liu, Dual-modified electrospun fiber membrane as separator with excellent safety performance and high operating temperature for lithium-ion batteries, Small. 20 (2024) 2309896, https://doi.org/10.1002/smll.202309896.
[240] H. Xiao, C. Lin, G. Kou, R. Peng, Reliability modeling and configuration optimization of a photovoltaic based electric power generation system, Reliab. Eng. Syst. Saf. 220 (2022) 108285, https://doi.org/10.1016/j.ress.2021.108285.
[241] T.J. Kim, B.D. Youn, H.J. Kim, Battery pack temperature estimation model for EVs and its semi-transient case study, Chem. Eng. Trans. 33 (2013) 955–960, https://doi.org/10.3303/CET1333160.
[242] S. Nahidi, M. Salari, I.J. Gavzan, S. Saedodin, Experimental investigation of the effect of C-rate, electrode gaps, and electrode surface roughness on the performance characterization of lead-acid batteries, Int. J. Energy Res. 45 (2021) 8231–8242, https://doi.org/10.1002/er.5836.
[243] L. Han, M.L. Lehmann, J. Zhu, T. Liu, Z. Zhou, X. Tang, C.-T. Heish, A.P. Sokolov, P. Cao, X.C. Chen, T. Saito, Recent developments and challenges in hybrid solid electrolytes for lithium-ion batteries, Front. Energy Res. 8 (2020) 202, https://doi.org/10.3389/fenrg.2020.00202.
[244] F. Ye, K. Liao, R. Ran, Z. Shao, Recent advances in filler engineering of polymer electrolytes for solid-state Li-ion batteries: a review, Energy Fuels. 34 (2020) 9189–9207, https://doi.org/10.1021/acs.energyfuels.0c02111.
[245] Y.L.N.K. Mallela, S. Kim, G. Seo, J.W. Kim, S. Kumar, J. Lee, J.-S. Lee, Crosslinked poly(allyl glycidyl ether) with pendant nitrile groups as solid polymer electrolytes for Li–S batteries, Electrochim. Acta 362 (2020) 137141, https://doi.org/10.1016/j.electacta.2020.137141.
[246] H.-K. Kim, V. Srinivasan, Status and targets for polymer-based solid-state batteries for electric vehicle applications, J. Electrochem. Soc. 167 (2020) 130520, https://doi.org/10.1149/1945-7111/abb70b.
[247] L.C. Merrill, X.C. Chen, Y. Zhang, H.O. Ford, K. Lou, Y. Zhang, G. Yang, Y. Wang, Y. Wang, J.L. Schaefer, N.J. Dudney, Polymer–ceramic composite electrolytes for lithium batteries: a comparison between the single-ion-conducting polymer matrix and its counterpart, ACS. Appl. Energy Mater. 3 (2020) 8871–8881, https://doi.org/10.1021/acsaem.0c01358.
[248] X. Yu, A. Manthiram, A review of composite polymer-ceramic electrolytes for lithium batteries, Energy Storage Mater. 34 (2021) 282–300, https://doi.org/10.1016/j.ensm.2020.10.006.
[249] L. Liu, X. Wang, C. Yang, P. Han, L. Zhang, L. Gao, Z. Wu, B. Liu, R. Liu, PVdF-HFP-based gel polymer electrolyte with semi-interpenetrating networks for dendrite-free lithium metal battery, Acta Metall. Sin. Engl. Lett. 34 (2021) 417–424, https://doi.org/10.1007/s40195-020-01142-9.
[250] X. Ao, X. Wang, J. Tan, S. Zhang, C. Su, L. Dong, M. Tang, Z. Wang, B. Tian, H. Wang, Nanocomposite with fast Li^+ conducting percolation network: solid polymer electrolyte with Li^+ non-conducting filler, Nano Energy 79 (2021) 105475, https://doi.org/10.1016/j.nanoen.2020.105475.
[251] H. Li, Z. Xu, J. Yang, J. Wang, S.-I. Hirano, Polymer electrolytes for rechargeable lithium metal batteries, Sustainable Energy Fuels 4 (2020) 5469–5487, https://doi.org/10.1039/D0SE01065K.
[252] M.I.H.A. Sohaimy, M.J.A. Fauzi, M.I.N. Mohamad Isa, Electrical behavior of ethylene carbonate-plasticized cellulose biopolymer electrolyte films, Malays. J. Chem. 22 (2020) 22–28.
[253] S. Molleti, M. Armstrong, Smart energy harvesting performance of photovoltaic roof assemblies in Canadian climate, Intell. Build. Int. 13 (2021) 70–88, https://doi.org/10.1080/17508975.2020.1802694.
[254] S.M. Abdulrahim, Z. Ahmad, J. Bahadra, N.J. Al-Thani, Electrochemical impedance spectroscopy analysis of hole transporting material free mesoporous and planar perovskite solar cells, Nanomaterials 10 (2020) 1635, https://doi.org/10.3390/nano10091635.
[255] K. Deng, Q. Chen, L. Li, Modification engineering in SnO_2 electron transport layer toward perovskite solar cells: efficiency and stability, Adv. Funct. Mater. 30 (2020) 2004209, https://doi.org/10.1002/adfm.202004209.
[256] Y. Chen, H. Zhou, Defect chemistry in high-efficiency and stable perovskite solar cells, J. Appl. Phys. 128 (2020) 060903, https://doi.org/10.1063/5.0012384.
[257] Y. Tian, L. Tao, C. Chen, H. Lu, H. Li, X. Yang, M. Cheng, Facile synthesized fluorine substituted benzothiadiazole based dopant-free hole transport material for high efficiency perovskite solar cell, Dyes. Pigm. 184 (2021) 108786, https://doi.org/10.1016/j.dyepig.2020.108786.
[258] M. Zheng, Y. Miao, A.A. Syed, C. Chen, X. Yang, L. Ding, H. Li, M. Cheng, Spatial configuration engineering of perylenediimide-based non-fullerene electron transport materials for efficient inverted perovskite solar cells, J. Energy Chem. 56 (2021) 374–382, https://doi.org/10.1016/j.jechem.2020.08.012.
[259] H. Guo, H. Zhang, J. Yang, W. Gong, H. Chen, H. Wang, X. Liu, F. Hao, X. Niu, Y. Zhao, Lanthanum-doped strontium stannate for efficient electron-transport layers in planar perovskite solar cells, ACS. Appl. Energy Mater. 3 (2020) 6889–6896, https://doi.org/10.1021/acsaem.0c00978.
[260] K. Gkini, N. Balis, M. Papadakis, A. Verykios, M.-C. Skoulikidou, C. Drivas, S. Kennou, M. Golomb, A. Walsh, A.G. Coutsolelos, M. Vasilopoulou, P. Falaras, Manganese porphyrin interface engineering in perovskite solar cells, ACS. Appl. Energy Mater. 3 (2020) 7353–7363, https://doi.org/10.1021/acsaem.0c00710.

[261] X. Zhang, W. Yang, J. Qi, Y. Hu, Preparing ambient-processed perovskite solar cells with better electronic properties via preheating assisted one-step deposition method, Nanoscale Res. Lett. 15 (2020) 178, https://doi.org/10.1186/s11671-020-03407-9.
[262] Y. Yu, F. Zhang, H. Yu, Self-healing perovskite solar cells, Sol. Energy 209 (2020) 408–414, https://doi.org/10.1016/j.solener.2020.09.018.
[263] F. Bella, E.D. Ozzello, A. Sacco, S. Bianco, R. Bongiovanni, Polymer electrolytes for dye-sensitized solar cells prepared by photopolymerization of PEG-based oligomers, Int. J. Hydrogen. Energy 39 (2014) 3036–3045, https://doi.org/10.1016/j.ijhydene.2013.06.110.
[264] F. Bella, A. Chiappone, J. Nair, G. Meligrana, C. Gerbaldi, Effect of different green cellulosic matrices on the performance of polymeric dye-sensitized solar cells, Chem. Eng. Trans. 41 (2014) 211–216, https://doi.org/10.3303/CET1441036.
[265] D. Pugliese, A. Lamberti, F. Bella, A. Sacco, S. Bianco, E. Tresso, TiO_2 nanotubes as flexible photoanode for back-illuminated dye-sensitized solar cells with hemi-squaraine organic dye and iodine-free transparent electrolyte, Org. Electron. 15 (2014) 3715–3722, https://doi.org/10.1016/j.orgel.2014.10.018.
[266] S. Martinet, C. Bourbon, M. Amuntencei, D. Peralta, L. Simonin, M. Rey-Chapuis, S. Patoux, Application of the methodology of design of experiments to the development of Li-ion battery active materials, in: Proc. 224th ECS Meet, San Francisco, USA, 2013, https://doi.org/10.1149/MA2013-02/12/899 paper no. 899.
[267] S. Martinet, C. Bourbon, M. Amuntencei, C. Chabrol, D. Tomasi, M. Rey, S. Patoux, Design of experiment methodology to improve the energy density of lithiated metal phosphates, Solid. State Ion. 268 (2014) 247–251, https://doi.org/10.1016/j.ssi.2014.06.016.
[268] J. Guo, F. Gao, D. Li, X. Luo, Y. Sun, X. Wang, Z. Ran, Q. Wu, S. Li, Novel strategy of constructing hollow Ga_2O_3@N-CQDs as a self-healing anode material for lithium-ion batteries, ACS Sustainable Chem. Eng. 8 (2020) 13692–13700, https://doi.org/10.1021/acssuschemeng.0c03756.
[269] J.H. Teo, F. Strauss, Đ. Tripković, S. Schweidler, Y. Ma, M. Bianchini, J. Janek, T. Brezesinski, Design-of-experiments-guided optimization of slurry-cast cathodes for solid-state batteries, Cell Rep. Phys. Sci. 2 (2021) 100465, https://doi.org/10.1016/j.xcrp.2021.100465.
[270] O. Rynne, M. Dubarry, C. Molson, D. Lepage, A. Prébé, D. Aymé-Perrot, D. Rochefort, M. Dollé, Designs of experiments for beginners—a quick start guide for application to electrode formulation, Batteries. (Basel) 5 (2019) 72, https://doi.org/10.3390/batteries5040072.
[271] Y. Kerdja, M. Chandesris, S. Martinet, Microscopy imaging based numerical model of Li-ion batteries electrode: a parametric study through a design of experiment approach, J. Power. Sources. 507 (2021) 230250, https://doi.org/10.1016/j.jpowsour.2021.230250.
[272] J.-S. Kim, D.-C. Lee, J.-J. Lee, C.-W. Kim, Optimization for maximum specific energy density of a lithium-ion battery using progressive quadratic response surface method and design of experiments, Sci. Rep. 10 (2021) 15586, https://doi.org/10.1038/s41598-020-72442-4.
[273] L. Li, T. Yang, Z. Li, Parameter optimization and yield prediction of cathode coating separation process for direct recycling of end-of-life lithium-ion batteries, RSC. Adv. 11 (2021) 24132–24136, https://doi.org/10.1039/D1RA04086C.
[274] A. Awarke, S. Lauer, S. Pischinger, M. Wittler, Percolation–tunneling modeling for the study of the electric conductivity in $LiFePO_4$ based Li-ion battery cathodes, J. Power. Sources. 196 (2011) 405–411, https://doi.org/10.1016/j.jpowsour.2010.07.048.
[275] F. Bella, A.B. Muñoz-García, F. Colò, G. Meligrana, A. Lamberti, M. Destro, M. Pavone, C. Gerbaldi, Combined structural, chemometric, and electrochemical investigation of vertically aligned TiO_2 nanotubes for Na-ion batteries, ACS. Omega 3 (2018) 8440–8450, https://doi.org/10.1021/acsomega.8b01117.
[276] R.K. Nekouei, F. Rashchi, A.A. Amadeh, Using design of experiments in synthesis of ultra-fine copper particles by electrolysis, Powder. Technol. 237 (2013) 165–171, https://doi.org/10.1016/j.powtec.2013.01.032.
[277] A. Chebil, V. Mazzaracchio, S. Cinti, F. Arduini, C. Dridi, Facile development of cost effective and greener all solid-state supercapacitor on paper substrate, J. Energy Storage 33 (2021) 102107, https://doi.org/10.1016/j.est.2020.102107.
[278] P. Du, Y. Dong, Y. Dong, X. Wang, H. Zhang, Fabrication of uniform MnO_2 layer-modified activated carbon cloth for high-performance flexible quasi-solid-state asymmetric supercapacitor, J. Mater. Sci. 57 (2022) 3497–3512, https://doi.org/10.1007/s10853-021-06728-x.
[279] X. Wu, J. Liu, C. Guo, Z.Z. Shi, Z. Zou, W. Sun, C.M. Li, Living cell-based ultrahigh-supercapacitive behaviours, J. Mater. Chem. A 10 (2022) 1241–1247, https://doi.org/10.1039/D1TA09818G.
[280] W. Zong, Y. Ouyang, Y.-E. Miao, T. Liu, F. Lai, Recent advances and perspectives of 3D printed micro-supercapacitors: from design to smart integrated devices, Chem. Commun. 58 (2022) 2075–2095, https://doi.org/10.1039/D1CC05544E.
[281] E. Thirugnanasambandam, G. Shanmugam, B. Selvaraj, A newly synthesized copper redox couple electrolyte with activated carbon electrode from *Samanea saman* wood tissue for flexible supercapacitor, Energy Fuels 36 (2022) 2228–2238, https://doi.org/10.1021/acs.energyfuels.1c04330.
[282] J. Yin, J. Li, L. Wang, B. Cai, X. Yang, X. Li, W. Lü, Integrated photoelectrochromic supercapacitor for applications in energy storage and smart windows, J. Energy Storage 51 (2022) 104460, https://doi.org/10.1016/j.est.2022.104460.
[283] L. Cui, H. Xu, Y. An, M. Xu, Z. Lei, X. Jin, N, S co-doped lignin-based carbon microsphere functionalized graphene hydrogel with "sphere-in-layer" interconnection as electrode materials for supercapacitor and molecularly imprinted electrochemical sensors, Adv. Powder. Technol. 33 (2022) 103571, https://doi.org/10.1016/j.apt.2022.103571.
[284] M. Wu, X. Zhao, J. Gao, J. Guo, J. Xiao, R. Chen, Multifunctional boron-doped carbon fiber electrodes synthesized by electrospinning for supercapacitors, dye-sensitized solar cells, and photocapacitors, Surf. Interfaces. 31 (2022) 101983, https://doi.org/10.1016/j.surfin.2022.101983.
[285] Z. Song, J. Wu, L. Sun, T. Zhu, C. Deng, X. Wang, G. Li, Y. Du, Q. Chen, W. Sun, L. Fan, H. Chen, J. Lin, Z. Lan, Photocapacitor integrating perovskite solar cell and symmetrical supercapacitor generating a conversion storage efficiency over 20%, Nano Energy 100 (2022) 107501 https://doi.org/10.1016/j.nanoen.2022.107501.
[286] T. Berestok, C. Diestel, N. Ortlieb, S.W. Glunz, A. Fischer, A monolithic silicon-mesoporous carbon photosupercapacitor with high overall photoconversion efficiency, Adv. Mater. Technol. 7 (2022) 2200237, https://doi.org/10.1002/admt.202200237.
[287] F. Schmitz, N. Lago, L. Fagiolari, J. Burkhart, A. Cester, A. Polo, M. Prato, G. Meneghesso, S. Gross, F. Bella, F. Lamberti, T. Gatti, High open-circuit voltage $Cs_2AgBiBr_6$ carbon-based perovskite solar cells via green processing of ultrasonic spray-coated carbon electrodes from waste tire sources, ChemSusChem. 15 (2022) e202201590, https://doi.org/10.1002/cssc.202201590.
[288] S. Siccardi, J. Amici, S. Colombi, J.T. Carvalho, D. Versaci, E. Quartarone, L. Pereira, F. Bella, C. Francia, S. Bodoardo, UV-cured self-healing gel polymer electrolyte toward safer room temperature lithium metal batteries, Electrochim. Acta 433 (2022) 141265, https://doi.org/10.1016/j.electacta.2022.141265.
[289] L. Fagiolari, D. Versaci, F. Di Berardino, J. Amici, C. Francia, S. Bodoardo, F. Bella, An exploratory study of MoS_2 as anode material for potassium batteries, Batteries (Basel) 8 (2022) 242, https://doi.org/10.3390/batteries8110242.
[290] R. Colombo, N. Garino, D. Versaci, J. Amici, M.L. Para, E. Quartarone, C. Francia, F. Bella, S. Bodoardo, Designing a double-coated cathode with high entropy oxides by microwave-assisted hydrothermal synthesis for highly stable Li–S batteries, J. Mater. Sci. 57 (2022) 15690–15704, https://doi.org/10.1007/s10853-022-07625-7.
[291] M. Eisa, D. Ragauskaitė, S. Adhikari, F. Bella, J. Baltrusaitis, Role and responsibility of sustainable chemistry and engineering in providing safe and sufficient nitrogen fertilizer supply at turbulent times, ACS Sustainable Chem. Eng. 10 (2022) 8997–9001, https://doi.org/10.1021/acssuschemeng.2c03972.
[292] S. Trano, F. Corsini, G. Pascuzzi, E. Giove, L. Fagiolari, J. Amici, C. Francia, S. Turri, S. Bodoardo, G. Griffini, F. Bella, Lignin as polymer electrolyte precursor for stable and sustainable potassium batteries, ChemSusChem. 15 (2022) e202200294, https://doi.org/10.1002/cssc.202200294.
[293] F. Elizalde, J. Amici, S. Trano, G. Vozzolo, R. Aguirresarobe, D. Versaci, S. Bodoardo, D. Mecerreyes, H. Sardon, F. Bella, Self-healable dynamic poly(urea-urethane) gel electrolyte for lithium batteries, J. Mater. Chem. A 10 (2022) 12588–12596, https://doi.org/10.1039/D2TA02239G.
[294] M. Alidoost, A. Mangini, F. Caldera, A. Anceschi, J. Amici, D. Versaci, L. Fagiolari, F. Trotta, C. Francia, F. Bella, S. Bodoardo, Micro-mesoporous carbons from cyclodextrin nanosponges enabling high-capacity silicon anodes and sulfur cathodes for lithiated Si-S batteries, Chem. Eur. J. 28 (2022) e202104201, https://doi.org/10.1002/chem.202104201.
[295] E. Manarin, F. Corsini, S. Trano, L. Fagiolari, J. Amici, C. Francia, S. Bodoardo, S. Turri, F. Bella, G. Griffini, Cardanol-derived epoxy resins as biobased gel polymer electrolytes for potassium-ion conduction, ACS. Appl. Polym. Mater. 4 (2022) 3855–3865, https://doi.org/10.1021/acsapm.2c00335.
[296] M.A.A. Mohd Abdah, M. Mokhtar, T.K. Lee, K. Sopian, N.A. Dzulkurnain, A. Ahmad, Y. Sulaiman, F. Bella, M.S. Su'ait, Synthesis and electrochemical characterizations of poly(3,4-ethylenedioxythiophene)/manganese oxide coated on porous carbon nanofibers as a potential anode for lithium-ion batteries, Energy Rep. 7 (2021) 8677–8687, https://doi.org/10.1016/j.egyr.2021.10.110.
[297] L. Lavagna, G. Syrrokostas, L. Fagiolari, J. Amici, C. Francia, S. Bodoardo, G. Leftheriotis, F. Bella, Platinum-free photoelectrochromic devices working with copper-based electrolytes for ultrastable smart windows, J. Mater. Chem. A 9 (2021) 19687–19691, https://doi.org/10.1039/D1TA03544D.
[298] C. Baiano, E. Schiavo, C. Gerbaldi, F. Bella, G. Meligrana, G. Talarico, P. Maddalena, M. Pavone, A.B. Muñoz-García, Role of surface defects in CO_2 adsorption and activation on $CuFeO_2$ delafossite oxide, Mol. Catal. 496 (2020) 111181, https://doi.org/10.1016/j.mcat.2020.111181.
[299] A. Carella, R. Centore, F. Borbone, M. Toscanesi, M. Trifuoggi, F. Bella, C. Gerbaldi, S. Galliano, E. Schiavo, A. Massaro, A.B. Muñoz-García, M. Pavone, Tuning optical and electronic properties in novel carbazole photosensitizers for p-type dye-sensitized solar cells, Electrochim. Acta 292 (2018) 805–816, https://doi.org/10.1016/j.electacta.2018.09.204.
[300] F. Bella, A. Verna, C. Gerbaldi, Patterning dye-sensitized solar cell photoanodes through a polymeric approach: a perspective, Mater. Sci. Semicond. Process. 73 (2018) 92–98, https://doi.org/10.1016/j.mssp.2017.07.030.
[301] D. Pintossi, G. Iannaccone, A. Colombo, F. Bella, M. Välimäki, K.-L. Väisänen, J. Hast, M. Levi, C. Gerbaldi, C. Dragonetti, S. Turri, G. Griffini, Luminescent downshifting by photo-induced sol-gel hybrid coatings: accessing multifunctionality on flexible organic photovoltaics via ambient temperature material processing, Adv. Electron. Mater. 2 (2016) 1600288, https://doi.org/10.1002/aelm.201600288.
[302] M. Gerosa, A. Sacco, A. Scalia, F. Bella, A. Chiodoni, M. Quaglio, E. Tresso, S. Bianco, Toward totally flexible dye-sensitized solar cells based on titanium grids and polymeric electrolyte, IEEE J. Photovoltaics 6 (2016) 498–505, https://doi.org/10.1109/JPHOTOV.2016.2514702.
[303] F. Bella, A. Sacco, G. Massaglia, A. Chiodoni, C.F. Pirri, M. Quaglio, Dispelling clichés at the nanoscale: the true effect of polymer electrolytes on the performance of dye-sensitized solar cells, Nanoscale 7 (2015) 12010–12017, https://doi.org/10.1039/C5NR02286J.

[304] A. Sacco, F. Bella, S. De La Pierre, M. Castellino, S. Bianco, R. Bongiovanni, C. F. Pirri, Electrodes/electrolyte interfaces in the presence of a surface-modified photopolymer electrolyte: application in dye-sensitized solar cells, Chemphyschem. 16 (2015) 960–969, https://doi.org/10.1002/cphc.201402891.
[305] F. Bella, A. Sacco, D. Pugliese, M. Laurenti, S. Bianco, Additives and salts for dye-sensitized solar cells electrolytes: what is the best choice? J. Power. Sources. 264 (2014) 333–343, https://doi.org/10.1016/j.jpowsour.2014.04.088.
[306] M. Imperiyka, A. Ahmad, S.A. Hanifah, F. Bella, A UV-prepared linear polymer electrolyte membrane for dye-sensitized solar cells, Physica B 450 (2014) 151–154, https://doi.org/10.1016/j.physb.2014.05.053.
[307] L.A. Kumar, M. Kathiresan, S. Alwarappan, F. Bella, A.M. Stephan, Fast charging of lithium-ion batteries by the effective formulation of nonaqueous liquid electrolytes, J. Phys. Chem. C 129 (2025) 9980–9991, https://doi.org/10.1021/acs.jpcc.5c00374.
[308] S. Domenici, R. Speranza, F. Bella, A. Lamberti, T. Gatti, A sustainable hydrogel-based dye-sensitized solar cell coupled to an integrated supercapacitor for direct indoor light-energy storage, Sol. RRL. 9 (2025) 2400838, https://doi.org/10.1002/solr.202400838.
[309] G. Pascuzzi, S. Trano, C. Francia, S. Turri, F. Bella, G. Griffini, Elucidating the interplay between structure and electrochemical behavior in lignin-based polymer electrolytes for potassium batteries, Battery Energy 4 (2025) e70002, https://doi.org/10.1002/bte2.70002.
[310] F. Elizalde, S. Trano, J. Ayestarán, X.L. de Pariza, R. Aguirresarobe, C. Francia, D. Mecerreyes, H. Sardon, F. Bella, A light-mediated, 3D-printable, and self-healable polymer electrolyte for lithium batteries, Adv. Funct. Mater. 35 (2025) 2419034, https://doi.org/10.1002/adfm.202419034.
[311] E. Ravesio, G. Montinaro, G. Mincuzzi, M. Negozio, D. Versaci, V. Gartiser, A.H. A. Lutey, F. Bella, S. Bodoardo, Ultrashort pulsed laser texturing of current collector for Si/C Li-ion anodes: characterization of electrochemical performance and evolution of interface morphology, J. Energy Storage 109 (2025) 115226, https://doi.org/10.1016/j.est.2024.115226.
[312] B. Bertoncini, A. Taddeucci, S. Trano, S. Raviolo, I. Valdrighi, F.M. Vivaldi, V. Mattoli, F. Bella, M. Carlotti, A multipotent precursor approach for the preparation of high-molecular weight conjugated polymers with redox active units, Small. Methods 9 (2025) 2500488, https://doi.org/10.1002/smtd.202500488.
[313] P. Prete, S. Trano, P. Zaccagnini, L. Fagiolari, J. Amici, A. Lamberti, A. Proto, F. Bella, R. Cucciniello, Glycerol carbonate and solketal carbonate as circular economy bricks for supercapacitors and potassium batteries, ChemSusChem. 17 (2024) e202401636, https://doi.org/10.1002/cssc.202401636.
[314] D. Versaci, R. Colombo, G. Montinaro, M. Buga, N.Cortes Felix, G. Evans, F. Bella, J. Amici, C. Francia, S. Bodoardo, Tailoring cathode materials: a comprehensive study on LNMO/LFP blending for next generation lithium-ion batteries, J. Power. Sources. 613 (2024) 234955, https://doi.org/10.1016/j.jpowsour.2024.234955.
[315] H. Darjazi, M. Falco, F. Colò, L. Balducci, G. Piana, F. Bella, G. Meligrana, F. Nobili, G.A. Elia, C. Gerbaldi, Electrolytes for sodium ion batteries: the current transition from liquid to solid and hybrid systems, Adv. Mater. 36 (2024) 2313572, https://doi.org/10.1002/adma.202313572.
[316] N. Pirrone, S. Garcia-Ballesteros, S. Hernández, F. Bella, Membrane/electrolyte interplay on ammonia motion inside a flow-cell for electrochemical nitrogen and nitrate reduction, Electrochim. Acta 493 (2024) 144415, https://doi.org/10.1016/j.electacta.2024.144415.
[317] A. Benigno, S. Raviolo, S. Trano, S. Domenici, M. Castellino, C. Francia, D. Gaspar, L. Pereira, F. Bella, From biomass to battery: lignin-derived carbons achieving unprecedented high capacity retention in potassium batteries, Chem. Eng. J. 528 (2026) 172142, https://doi.org/10.1016/j.cej.2025.172142.
[318] A. Mangini, A. Garbujo, P. Biasi, V. Testa, M.C. Bruzzoniti, L. Rivoira, S. Garcia-Ballesteros, F. Bella, Debunking pitfalls of Li–N_2 cells for ammonia electroproduction: is this setup affordable to prove nitro-fixation before lithium plating? ACS Electrochem 1 (2025) 2866–2877, https://doi.org/10.1021/acselectrochem.5c00402.
[319] A. Mangini, L. Fagiolari, A. Sacchetti, A. Garbujo, P. Biasi, F. Bella, Lithium-mediated nitrogen reduction for ammonia synthesis: reviewing the gap between continuous electrolytic cells and stepwise processes through galvanic Li–N_2 cells, Adv. Energy Mater. 14 (2024) 2400076, https://doi.org/10.1002/aenm.202400076.
[320] S. Sathya, C. Soosaimanickam, F. Bella, D.J. Yoo, A.M. Stephan, Cycling performance of SiO_x-Si-C composite anode with different blend ratios of PAA-CMC as binder for lithium sulfur batteries, J. Polym. Res. 31 (2024) 205, https://doi.org/10.1007/s10965-024-04005-4.
[321] F. Boll, M. Fadda, M. Happel, M. Crisci, A. Athanassiou, B. Smarsly, F. Bella, F. Lamberti, G. Perotto, T. Gatti, Multicomponent synergistic contribution in nanoengineered nanofibers for flexible energy storage, ACS. Appl. Energy Mater. 7 (2024) 4733–4744, https://doi.org/10.1021/acsaem.4c00417.
[322] D. Dessantis, P. Di Prima, D. Versaci, M. Santarelli, F. Bella, V. Kolotygin, P. López-Aranguren, J. Amici, Investigating sulfide-based all solid-state cells performance through P2D modelling, Chem. Eng. J. Adv. 18 (2024) 100610, https://doi.org/10.1016/j.ceja.2024.100610.
[323] E. Maruccia, S. Galliano, E. Schiavo, N. Garino, A.Y. Segura Zarate, A.B. Muñoz-García, M. Pavone, C. Gerbaldi, C. Barolo, V. Cauda, F. Bella, Exploring zinc oxide morphologies for aqueous solar cells by a photoelectrochemical, computational, and multivariate approach, Energy Adv. 3 (2024) 1062–1072, https://doi.org/10.1039/D4YA00010B.
[324] F. Schmitz, R. Bhatia, J. Burkhart, P. Schweitzer, M. Allione, J. Gallego, P. Piotrowski, J. Cajzl, P. Paszke, G.M. Das, D.A. Pawlak, F. Bella, D. Schlettwein, F. Lamberti, S. Meloni, T. Gatti, Improved hole extraction and band alignment via interface modification in hole transport material-free Ag/Bi double perovskite solar cells, Sol. RRL. 8 (2024) 2300965, https://doi.org/10.1002/solr.202300965.
[325] G. Gianola, R. Speranza, F. Bella, A. Lamberti, Homo-tandem-bifacial dye-sensitized solar cell: a new paradigm to boost photoconversion efficiency above limit, Sol. Energy 265 (2023) 112116, https://doi.org/10.1016/j.solener.2023.112116.
[326] R. Colombo, D. Versaci, J. Amici, F. Bella, M.L. Para, N. Garino, M. Laurenti, S. Bodoardo, C. Francia, Reduced graphene oxide embedded with ZnS nanoparticles as catalytic cathodic material for Li-S batteries, Nanomaterials 13 (2023) 2149, https://doi.org/10.3390/nano13142149.
[327] M. Bonomo, A.Y. Segura Zarate, L. Fagiolari, A. Damin, S. Galliano, C. Gerbaldi, F. Bella, C. Barolo, Unreported resistance in charge transport limits the photoconversion efficiency of aqueous dye-sensitised solar cells: an electrochemical impedance spectroscopy study, Mater. Today Sustainability. 21 (2023) 100271, https://doi.org/10.1016/j.mtsust.2022.100271.
[328] M. Gandolfo, J. Amici, L. Fagiolari, C. Francia, S. Bodoardo, F. Bella, Designing photocured macromolecular matrices for stable potassium batteries, Sustainable Mater. Technol. 34 (2022) e00504, https://doi.org/10.1016/j.susmat.2022.e00504.
[329] Y. Lu, M. Maftouni, T. Yang, P. Zheng, D. Young, Z.J. Kong, Z. Li, A novel disassembly process of end-of-life lithium-ion batteries enhanced by online sensing and machine learning techniques, J. Intell. Manuf. 34 (2023) 2463–2475, https://doi.org/10.1007/s10845-022-01936-x.
[330] H. Sun, R. Dixon, Development of cooling strategy for an air cooled lithium-ion battery pack, J. Power. Sources. 272 (2014) 404–414, https://doi.org/10.1016/j.jpowsour.2014.08.107.
[331] A.P. Schmidt, M. Bitzer, Á.W. Imre, L. Guzzella, Experiment-driven electrochemical modeling and systematic parameterization for a lithium-ion battery cell, J. Power. Sources. 195 (2010) 5071–5080, https://doi.org/10.1016/j.jpowsour.2010.02.029.
[332] Y. Xie, H. Guo, W. Li, Y. Zhang, B. Chen, K. Zhang, Improving battery thermal behavior and consistency by optimizing structure and working parameter, Appl. Therm. Eng. 196 (2021) 117281, https://doi.org/10.1016/j.applthermaleng.2021.117281.
[333] M. Masih-Tehrani, M. Hairi-Yazdi, V. Esfahanian, Power distribution development and optimization of hybrid energy storage system, Int. J. Automot. Eng. 4 (2014) 675–684.
[334] C. Hametner, S. Jakubek, State of charge estimation for lithium ion cells: design of experiments, nonlinear identification and fuzzy observer design, J. Power. Sources. 238 (2013) 413–421, https://doi.org/10.1016/j.jpowsour.2013.04.040.
[335] J.M. Amanor-Boadu, A. Guiseppi-Elie, Improved performance of Li-ion polymer batteries through improved pulse charging algorithm, Appl. Sci. 10 (2020) 895, https://doi.org/10.3390/app10030895.
[336] B. Stumper, J. Dhom, L. Schlosser, D. Schreiner, A. Mayr, R. Daub, Modeling of the lithium calendering process for direct contact prelithiation of lithium-ion batteries, Procedia CIRP. 107 (2022) 984–990, https://doi.org/10.1016/j.procir.2022.05.096.
[337] A. Gabryelczyk, S. Ivanov, A. Bund, G. Lota, Taguchi method in experimental procedures focused on corrosion process of positive current collector in lithium-ion batteries, Electrochim. Acta 360 (2020) 137011, https://doi.org/10.1016/j.electacta.2020.137011.
[338] J.-J. Lee, J.-S. Kim, H.-K. Chang, D.-C. Lee, C.-W. Kim, The effect of tab attachment positions and cell aspect ratio on temperature difference in large-format LIBs using design of experiments, Energies. (Basel) 14 (2021) 116, https://doi.org/10.3390/en14010116.
[339] L.A. Román-Ramírez, G. Apachitei, M. Faraji-Niri, M. Lain, W.D. Widanage, J. Marco, Understanding the effect of coating-drying operating variables on electrode physical and electrochemical properties of lithium-ion batteries, J. Power. Sources. 516 (2021) 230689, https://doi.org/10.1016/j.jpowsour.2021.230689.
[340] A. Verma, P. Saikia, D. Rakshit, Unification of intensive and extensive properties of the passive cooling system under a single envelope for the thermal management of Li-ion batteries, J. Energy Storage 50 (2022) 104184, https://doi.org/10.1016/j.est.2022.104184.
[341] O. Delbeke, H. Laget, S. Hollevoet, L. Vandevelde, J. Mertens, A comprehensive and time efficient characterisation of redox flow batteries through design of experiments, J. Energy Storage 50 (2022) 104574, https://doi.org/10.1016/j.est.2022.104574.
[342] G. Chen, J. Huang, J. Gu, S. Peng, X. Xiang, K. Chen, X. Yang, L. Guan, X. Jiang, L. Hou, Highly tough supramolecular double network hydrogel electrolytes for an artificial flexible and low-temperature tolerant sensor, J. Mater. Chem. A 8 (2020) 6776–6784, https://doi.org/10.1039/D0TA00002G.
[343] X.-S. Zhang, C.-Y. Yan, T.-H. Wu, L.-F. Li, J.-H. Guo, C.-Z. Yao, Fabrication of $CsPbBrI_2$ quantum dots and its photodetector performance, Acta Photonica Sin 49 (2020) 0123002, https://doi.org/10.3788/gzxb20204901.0123002.
[344] S. Aiassa, R. Terracciano, S. Carrara, D. Demarchi, Biosensors for bimolecular computing: a review and future perspectives, Bionanoscience 10 (2020) 554–563, https://doi.org/10.1007/s12668-020-00764-8.
[345] Z. Duan, J. Ning, M. Chen, Y. Xiong, W. Yang, F. Xiao, S.V. Kershaw, N. Zhao, S. Xiao, A.L. Rogach, Broad-band photodetectors based on copper indium diselenide quantum dots in a methylammonium lead iodide perovskite matrix, ACS. Appl. Mater. Interfaces. 12 (2020) 35201–35210, https://doi.org/10.1021/acsami.0c06837.
[346] X. Wang, L. Yu, Q. Kang, L. Chen, Y. Jin, G. Zou, D. Shen, Enhancing electrochemiluminescence of $FAPbBr_3$ nanocrystals by using carbon nanotubes

and TiO_2 nanoparticles as conductivity and co-reaction accelerator for dopamine determination, Electrochim. Acta 360 (2020) 136992, https://doi.org/10.1016/j.electacta.2020.136992.

[347] J. Valdes-García, L.D. Rosales-Vázquez, I.J. Bazany-Rodríguez, A. Dorazco-González, Recent advances in luminescent recognition and chemosensing of iodide in water, Chem. Asian J. 15 (2020) 2925–2938, https://doi.org/10.1002/asia.202000758.

[348] Q. Yu, Y. Zhao, L. Huang, J. Sun, D. Jin, Y. Shu, Q. Xu, X.-Y. Hu, A flexible rGO electrode: a new platform for the direct voltammetric detection of salicylic acid, Anal. Methods 12 (2020) 3892–3900, https://doi.org/10.1039/D0AY00112K.

[349] Y. Zheng, L. Wang, L. Zhao, D. Wang, H. Xu, K. Wang, W. Han, A flexible humidity sensor based on natural biocompatible silk fibroin films, Adv. Mater. Technol. 6 (2021) 2001053, https://doi.org/10.1002/admt.202001053.

[350] C. Trigona, Living sensors: the greenest paradigm in instrumentation and measurements, IEEe Instrum. Meas. Mag. 26 (2023) 35–41, https://doi.org/10.1109/MIM.2023.10034956.

[351] J. Min, J. Tu, C. Xu, H. Lukas, S. Shin, Y. Yang, S.A. Solomon, D. Mukasa, W. Gao, Skin-interfaced wearable sweat sensors for precision medicine, Chem. Rev. 123 (2023) 5049–5138, https://doi.org/10.1021/acs.chemrev.2c00823.